Nuclear Fusion Project Semi-annual Report of the Association KfK/EURATOM

October 1988 – March 1989

Projekt Kernfusion

Kernforschungszentrum Karlsruhe
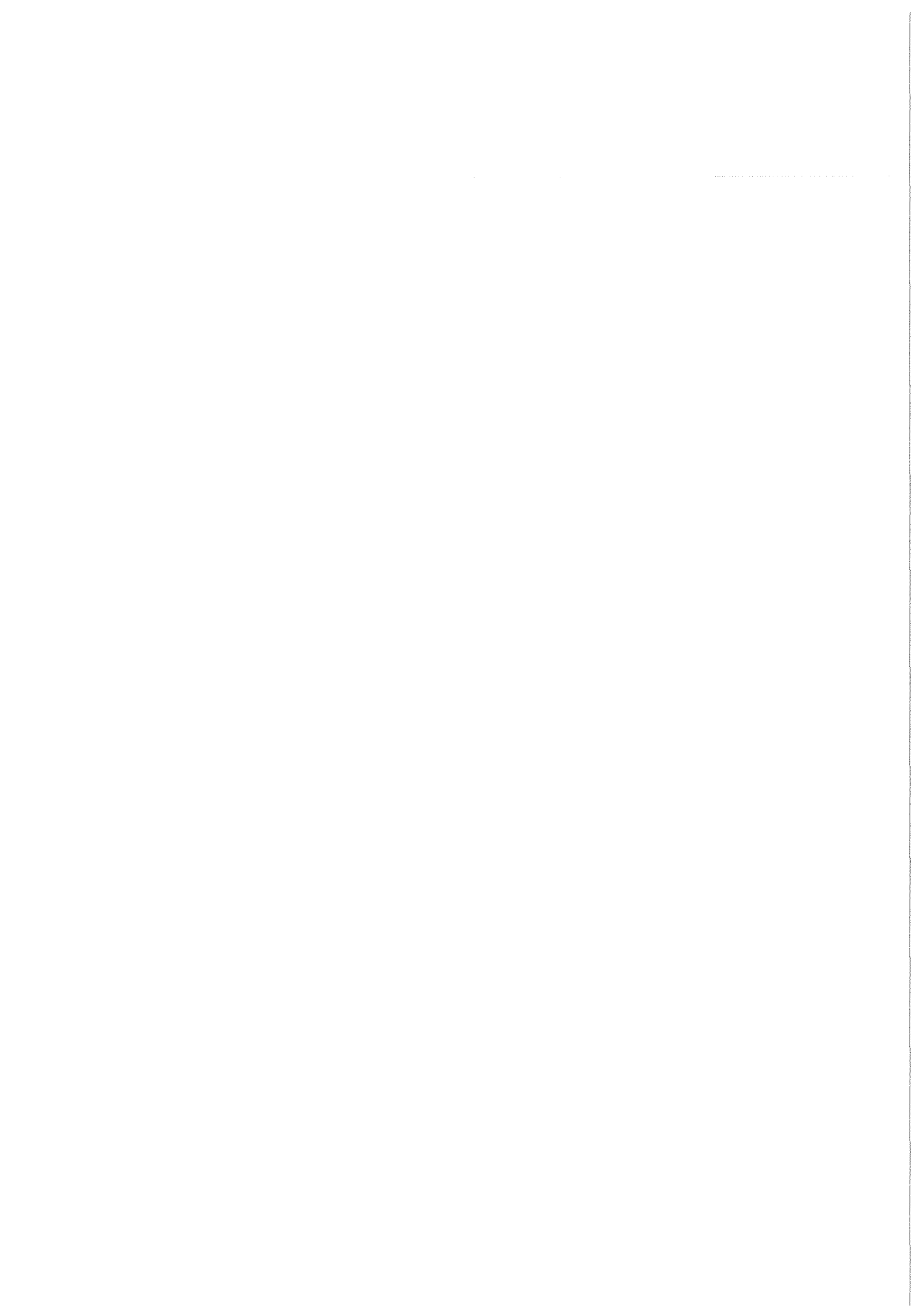
Nuclear Fusion Project
Semi-annual Report of the
Association KfK/EURATOM

October 1988 - March 1989

compiled by
G. Kast

Kernforschungszentrum Karlsruhe

Contents

B 1 Blanket Design Studies

Two design concepts are studied at KfK: a helium cooled ceramic blanket and a blanket with Pb-17Li eutectic as breeder material and coolant.

Both concepts should be DEMO-relevant and design studies are being conducted to adapt the concepts to DEMO conditions. In parallel test objects for NET are developed.

1. Helium-cooled Ceramic Breeder Blanket

The concept of the outboard blanket with canister-shaped elements is being investigated with regard to its potential under DEMO conditions. In this context a helium cooled first wall of martensitic steel 1.4914 without a protective layer of graphite bricks was designed and optimized. Helium flow is passing through bores arranged toroidally in the wall. Temperature as well as linear elastic stress calculations were carried out with a view to optimize static wall load (s. Fig. 1).

At the same time, a helium cooled DEMO blanket as well as a test blanket element for NET were designed. Experiments were carried out with regard to the possibility of soldering stainless steel cooling tubes and beryllium plates. First results obtained are very encouraging.
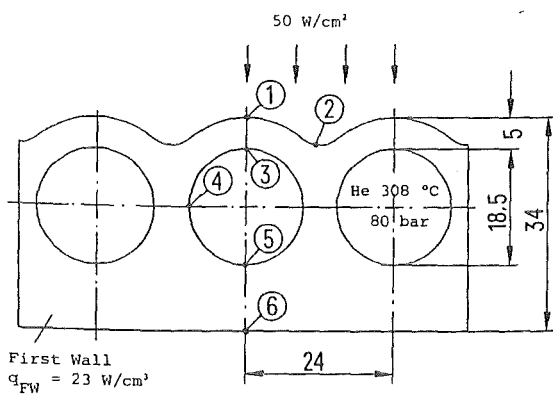
Point	Temperature /°C/	von Mises stress /MPa/	
		primary	primary + secondary
1	569	15	201
2	511	9	406
3	461	16	60
4	364	37	217
5	381	17	248
6	442	8	123

Fig 1: Helium cooled first wall: Temperature and equivalent stresses

Preliminary design investigations have been carried out also of the helium cooling, helium purge flow and helium purification systems for the NET test object. These investigations are being performed in collaboration with INTERATOM. Fig. 2 shows horizontal sections of the cooling system A, the purification system B, and the purge flow system C.

Detailed calculations of temperatures, pressure drops and local tritium inventories in the blankets are being performed for the NET II and DEMO boundary conditions by means of ad-hoc developed codes.

Staff:
L. Boccaccini
E. Bojarsky
M. Dalle Donne
U. Fischer
M. Küchle
P. Norajitra
G. Reimann
H. Reiser
G. Sordon

2. Liquid Metal-Cooled Blanket

The development of the liqud metal self-cooled blanket has been continued with the design of a NET test blanket and the external cooling and tritium extraction loops.

One of the torus plugs, which were planned for the access to remote handling facilities, has been modified to a removable test blanket. This is about 0.7 m wide and 2.5 m high relative to the first wall.

The external loops, connected to this test blanket, are the Pb-17Li loop, the intermediate NaK loop and the water cooling loop. In the first loop the tritium and heat produced in the blanket are transported with the Pb-17 Li flow to the first heat exchanger. Here the heat is conducted through the pipe wall and the tritium flow is permeated through the same pipe wall to the NaK of the intermediate loop. The main NaK flow is circulated by a magnetic pump to the second heat exchanger where the heat is transferred to the water loop and to the central cooling system. A bypass flow of the NaK loop is led to a tritium extraction system, where NaK tritid is precipitated in cold traps. From the cold trap tritium is later released by draining and evacuating the cold trap and heating to about 400 °C. The trapping of the tritium and the release is done daily.

The intermediate NaK loop is an effective barrier against tritium losses to the water loop. This is based on the fact that the tritium partial pressure can be kept low in the NaK flow by cold trapping of tritid and by the fact that the tritium solubility in NaK is much higher as in Pb-17Li.

The first layout of the loops and the design in cooperation with Interatom has been made. The arrangement of the components in the NET building has been discussed with the NET team.

INTERATOM
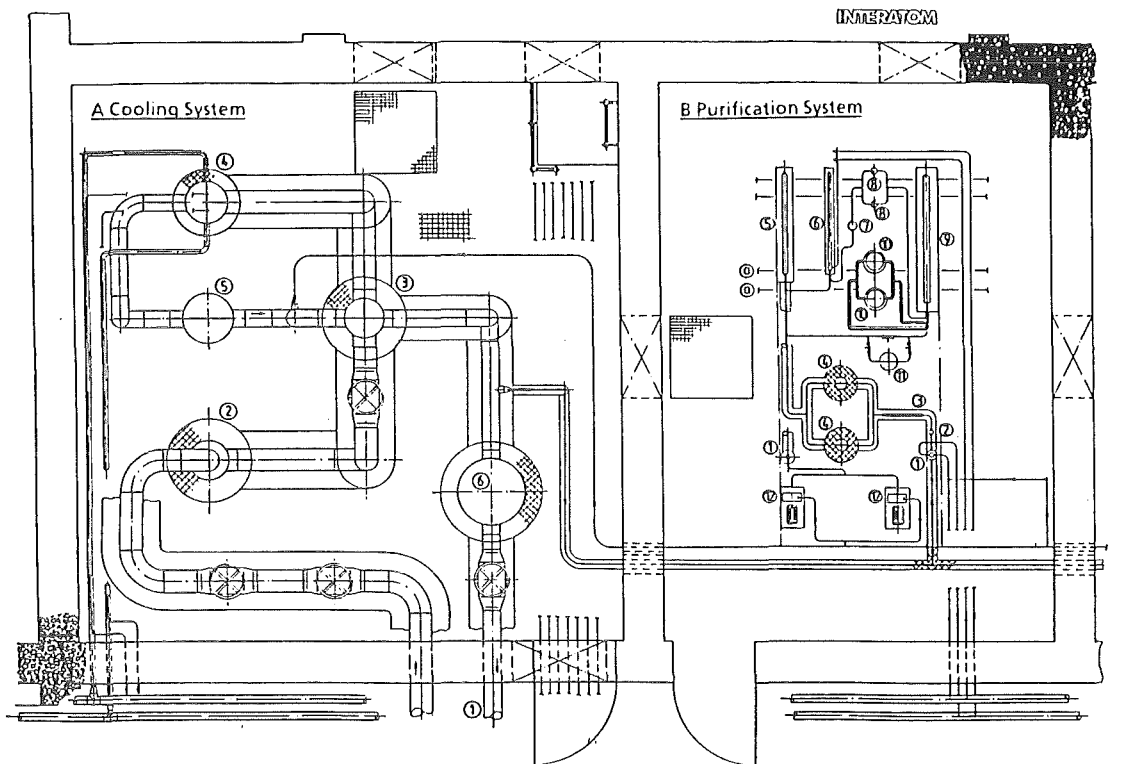
A Cooling System

1 to the outboard blanket
2 dust filter
3 recuperative heat exchanger
4 helium/water heat exchanger
5 blower
6 electrical heater

B Purification System

1 helium/water heat exchanger
2 filter
3 electrical heater
4 CuO-catalyst
5 recuperative heat exchanger
6 helium/water heat exchanger
7 water separator
8 room temperature adsorber
9 recuperative heat exchanger
10 low temperature adsorber
11 hydrogen getter
12 blower

C Purge Gas System

1 to the outboard blanket 5 canisters
2 helium/water heat exchanger
3 room temperature adsorber
4 electrical heater
5 permeation filter
6 hydrogen getter
7 recuperative heat exchanger
8 low temperature adsorber
9 blower
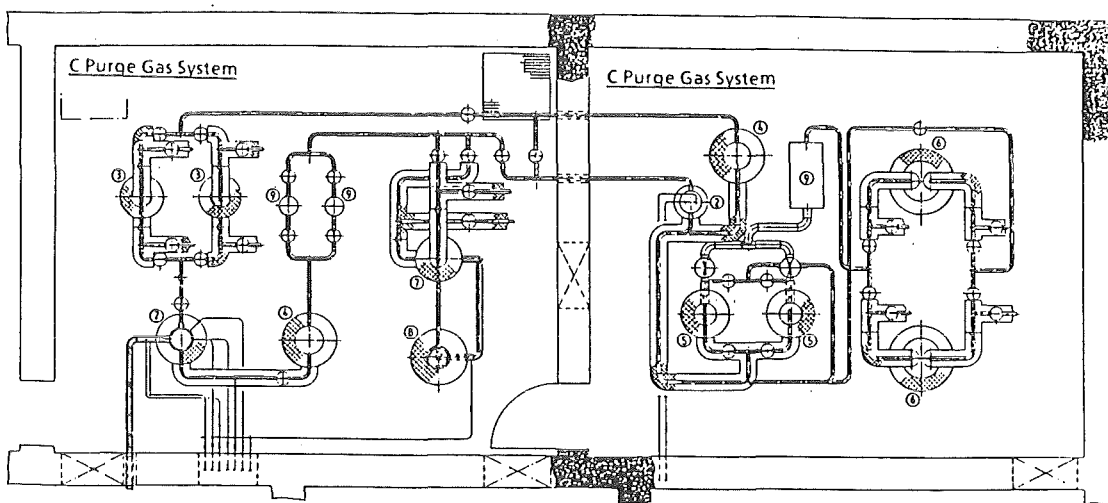
Fig. 2   Helium Cooled Canister Blanket-Peripheral Circuits of NET TEST OBJECT

One basic prerequisite for realization of a self-cooled blanket is the reduction of MHD pressure losses. They are created by electric currents induced in the fluid and short-circuited over the steel structures. To disconnect the electrical short-circuit through the steel structure the blanket under development will be equipped with flow channel inserts (FCI). An FCI is a laminated element. Two steel sheets at the outside separated by a ceramic layer. The ceramic is bounded to both steel sheets. The FCI are loosely fitted into the flow channels. They cover parts of the flow channel surface. At the edges the two outer sheets of the FCI are welded together to prevent the ceramic layer to be attacked by the liquid metal. The avoidance of an electrical short-circuit by the load carrying wall by an FCI can be seen in Fig. 3. The electrical short circuit is only possible by the very thin (0.5 to 1 mm) inner steel sheet of the FCI.

The development of FCI's has been continued together with industry (MBB). The investigation of various fabrication methods was completed. The method selected contains the following fabrication procedure.
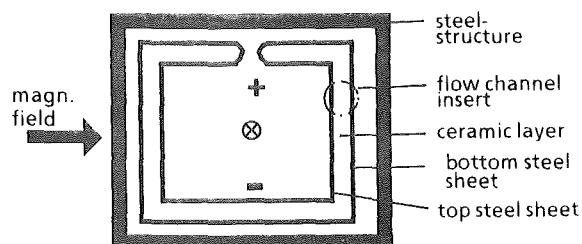
Fig. 3: Schematic of a flow channel insert

- cutting of top (inner) and bottom (outer) sheets of the FCI
- shaping of the two sheets
- sand blasting of the two sheets
- coating of inner side of the bottom sheet with a bonding material (NiCrAl) by plasma spraying
- coating of the bonding material with a ceramic layer by plasma spraying (Al_2O_3 with additives)
- coating of the ceramic with a metallic layer by plasma spraying (Ni, Cu)
- coating of the inner side of the top sheet with Ni or Cu
- assembling of coated bottom and top sheets
- diffusion welding in a pneumatic isostatic hot press process
- welding of the top and bottom sheets at all edges

The optimization of the fabrication procedure has been continued. Numerous tension tests show a tensile strength of the laminated elements between 10 to 25 MPa. This strength is in the range of the ultimate strength of plasma sprayed ceramic layers which indicates a good bonding at the various interfaces of the element. Fig. 4 shows a photo micrograph of a laminated element. It is intended to complete the development of fabrication methods within this year and to start with out-of-pile testing of FCI.
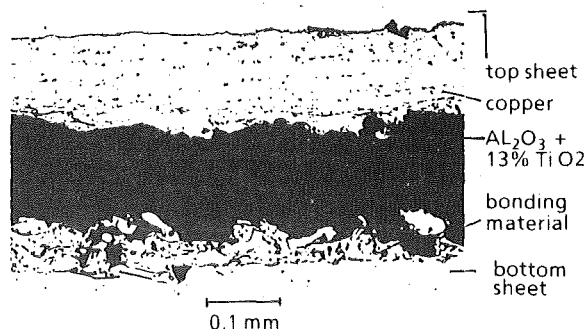
Fig. 4: Photomicrograph of a flow channel insert

Staff:
K. Arheidt
H.J. Brinkmann
V. Casal
G. Eisele
U. Fischer
H. John
S. Malang
D. Rackel
J. Reimann
K. Rust
H. Schneider

B 2   Development of Computational Tools for Neutronics

At KfK both the development of new calculational methods for fusion neutronics and the evaluation of relevant nuclear data are under work. Special emphasis is put on the critical application of the processed nuclear data in integral benchmark experiments. In this way both the nuclear data as the applied transport programmes can be checked.

A general anisotropic neutron transport code system that is suitable for fusion neutronics has been developed at KfK during the past years. While the one-dimensional transport module ANTRA1 is in frequent use for analyzing integral benchmark experiments (see below), the two-dimensional module ANTRA2 presently is checked by applying it to a 14 MeV neutron experiment in two-dimensional cylindrical geometry. In this experiment the angular neutron flux distributions on the surface of a beryllium slab have been measured and analyzed. The recalculation of the measured angular energy spectra is a very sensitive test for the newly developed transport programme ANTRA2. As an example, Fig. 5 shows preliminary results for a beryllium slab thickness of 5 cm at a polar angle of 41.8^0.

For analyzing the 14 MeV neutron multiplication of beryllium a detailed study has been started last year. This study is performed on the basis of the double-differential neutron cross-section data (DDX) on the European Fusion File EFF-1 and it's consistent use in the ANTRA1 transport code. At present only incomplete experimental data are available for checking the beryllium data in an integral benchmark. The 14-MeV neutron experiment performed at the Kurchatov Institute Moscow presently is the most complete and the most reliable one. There the total leakage multiplication has been measured by an integral method for spherical beryllium shells of different thicknesses (1.5-8 cm); the measured multiplication factors agree very well with the calculated ones (see Table 1).

For a beryllium spherical shell of 5 cm thickness, the energy spectrum of the leaking neutrons also has been measured; satisfactory agreement can be obtained with the calculated neutron spectra based on the EFF-1 cross-section data (Fig. 6). This rather good agreement reflects well into the data given in Table 2, where the neutron spectrum has been assembled in four coarse energy intervals: only in the energy region between 0.35 and .7 MeV, where the experimental uncertainty is rather high, there is a larger discrepancy.

A further remarkable result is contained in fig. 2: it is obvious that the ANTRA1-calculation agrees with a Monte-Carlo-calculation (MCNP code) and a conventional S_N-calculation in P_5-approximation (ONETRAN-code) using the same basic nuclear data in a completely different way. With respect to the ANTRA1/ONETRAN agreement this behaviour can be traced back to the fact that the angular distributions of the scattered neutrons on the file are given in the Legendre representation in the centre-of-mass system in a somewhat rough approximation (fits of rather smooth experimental data). For the EFF-2 file a completely new ^{9}Be-evaluation is being performed, which takes into account the many particle kinematics of all reaction channels of the system $n + ^9$Be and thus necessitates the tabular representation of the correlated angle-energy distributions in the laboratory system. Actually the ANTRA1/2 programme and the associated DDX-processing code is adapted to such a data representation that is most adequate to describe the physical processes. Thus it is expected that ANTRA1-calculations will show improvements over ONETRAN-calculations with EFF-2 ^{9}Be-data.

For the generation of conventional group constants from the basic nuclear data files the NJOY-code is in use at KfK. In 1988 a new reference version, NJOY-87.0, became available and has been implemented on the KfK computer system IBM3090/SIEMENS 7890. As in the former KfK-version, all corrections and modifications have been introduced into NJOY-87.0. This refers for instance to an error in the calculation of the total photon KERMA-factors and the completion of a part of a programme that calculates photon production matrices using angular distributions of the secondary photons that are given as tabulated functions of the cosine of the scattering angle on the data file. The original versions of NJOY-6/83 and NJOY-87.0 only could process photon angular distributions in the Legendre representation. Presently the latest version of the code, NJOY-87 (KfK) is being used to generate a nuclear data library of pointwise neutron cross-sections for different temperatures from the EFF/JEF-files. This point data library will form the basis for the calculation of group constants for different group structures and weighting spectra.

Staff:
I. Broeders
U. Fischer
B. Krieg
H. Küsters
A. Schwenk-Ferrero
E. Wiegner

Angular (41.8 deg) energy spectrum of a Be (5 cm)-slab
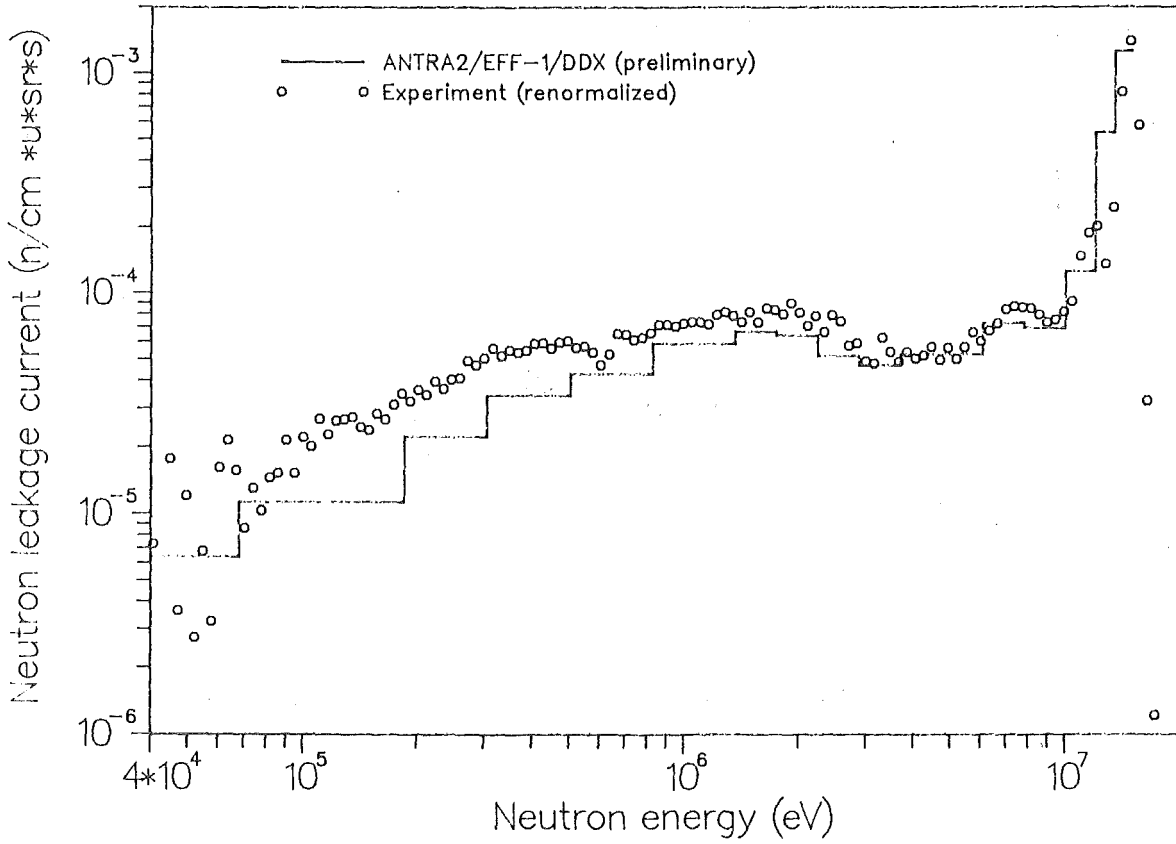
Fig. 5   Angular energy spectrum of neutrons leaking a 5 cm thick Be-slab at a polar angle of 41.8⁰ (14 MeV neutron source)

shell thick-ness [cm]	neutron leakage multiplication	
	experiment	ANTRA1 (EFF-1/DDX)
1.5	1.14 ± .036	1.10
5.0	1.365 ± .04	1.359
8.0	1.525 ± .043	1.547

Table 1:   Neutron leakage multiplication factors for spherical
beryllium shells with a central 14 MeV neutron source

MOSCOW BE-SPHERE EXPERIMENT
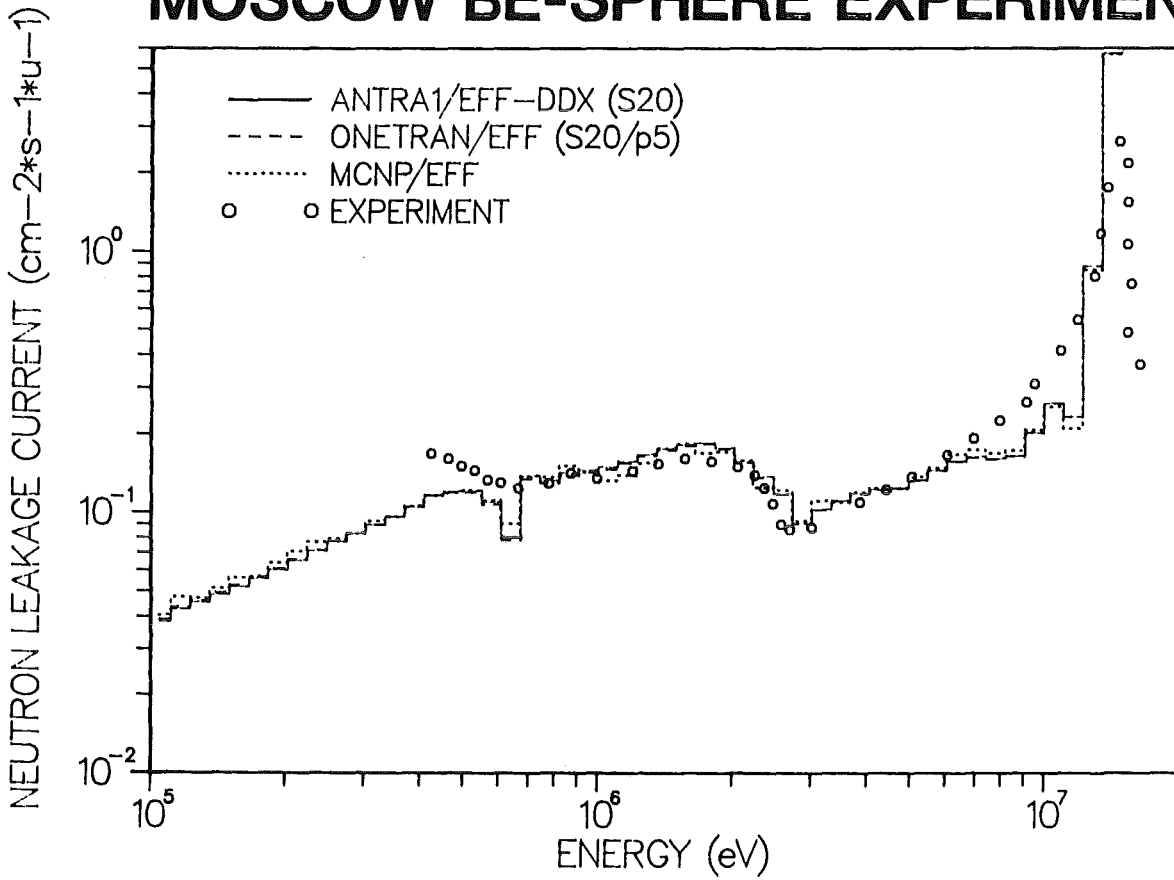
Fig. 6   Energy spectrum of neutrons leaking a 5 cm thick spherical Be-shell (central 14 MeV neutron source)

Energy intervals $E_i - E_{i+1}$ [MeV]	partial neutron multiplication	
	experiment	ANTRA1 (EFF-1/DDX)
0.35 - 0.7	0.096 ± .005	0.081
0.7 - 3	0.20 ± .01	0.215
3 - 10	0.19 ± .01	0.175
10 - 15	0.69 ± .03	0.697

Table 2:   Partial leakage multiplication factors for the 5 cm thick beryllium spherical shell

B 6   Corrosion of Structural Materials in Flowing Pb-17Li

Dynamic corrosion tests in the PICOLO loop were continued in order to generate data for the self-cooled liquid metal blanket. The completing last run at 500°C was started in January 1989 and finished after ~1000 hours duration in February 1989. The corrosion effects were evaluated by weight and diameter controls, metallographic examinations will be performed with selected specimens.

Staff:

Ch. Adelhelm

H.U. Borgstedt

G. Drechsler

G. Frees

D. Linder

Z. Perić

G. Streib

Publications:

1.   S. Malang, K. Arheidt, L. Barleon, H.U. Borgstedt, V. Casal, U. Fischer, W. Link, J. Reimann, K. Rust, G. Schmidt, Fusion Technology 14 (1988) 1343-56

Fig. 7:   Fatigue life of steel X 18 CrMoVNb 12 1 (1.4914, Manet) at 550°C in air resp. argon atmosphere and in stagnant Pb-17Li melt.

B 6.3   Fatigue of Structural Material in Pb-17Li

The lcf tests of the heat-treated specimens of the martensitic steel X 18 CrMoVNb 121 (1.4914, Manet) (21 mm gauge length, 8.8 mm minimal diameter, hour-glass shape) were related to recently performed reference tests in air the results of which were nearly identical with results of tests in argon gas (with $p_{O_2} \sim 10^{-4}$ bar). The stagnant molten Pb-17Li has a beneficial effect on the fatigue life of the steel. The difference was found to be largest at high strain amplitudes ($\Delta \varepsilon t \geq 0.01$), the effect decreases at lower strain amplitudes. A pre-corrosion of the material in stagnant liquid Pb-17Li causes a gradual reduction of the fatigue life as reported earlier (see semi-annual report KfK 4488, page 7).

The data which have been gained in this test series are shown in Fig. 7. Evaluation of the test results and metallurgical studies of the specimens are under the way.

Staff:

H.U. Borgstedt

M. Grundmann

Z. Perić

B. Seith

B 9   Tritium Extraction from Liquid Pb-17Li by the Use of Solid Getters

Several methods were proposed to extract tritium from liquid Pb-17Li blanket material. Task B9 will study the use of solid getters.

While the facility TRITEX (1) is now in the start-up phase, the investigation of deuterium transport by Pb-17Li in a thermal convection loop continues (2). In parallel, studies of the compatibilities of materials with static molten Pb-17Li are performed. Besides getter metals some possible structural metals were investigated (3). Figure 8 shows a test stand with three capsules.
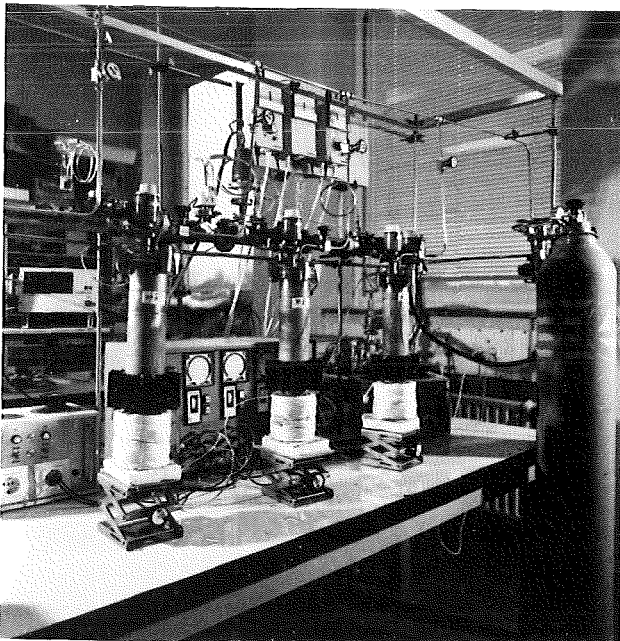
Fig. 8: Teststand for compatibility studies

For some blanket concepts with Pb-17Li, beryllium is proposed as a neutron multiplier. This metal was therefore used in capsule tests.

All preparation was done in an argon atmosphere with less than 1 ppm oxygen. 50 to 60 grams of Pb-17Li were used in Mo-crucibles, the sample sheets fixed by Mo-stripes. Degassing and annealing of samples and capsules was done at 700°C at 10^{-5} mbar. Any contact between the samples and the Mo-crucible was avoided. Otherwise problems occurred because of reactions between the sample and molybdenum below the Pb-17Li surface. The covergas in the capsules was purified Ar-6.0.

After an experiment the capsules were opened in a glove box and the samples removed from the Pb-17Li. All the Pb-17Li was dissolved, using a special extraction technique with nearly the stoichiometric amount of nitric acid. Dissolved

materials were determined by ICP-AES analysis. Remaining Pb-17Li in the Mo-crucibles was dissolved in acetic acid-H_2O_2, the samples cleaned by an electrolytic method and prepared for metallographic and microprobe investigations.

Results

Fig. 9 shows the results. At a temperature of 450°C the amount of dissolved beryllium was very low even after 4500 hours exposure time. A constant dissolution rate was found at a temperature of 500°C. Pretreatment of the samples for a longer time at 450°C had no influence on the results. No saturation of the Pb-17Li by Be was found within 3400 hours exposure time. In Table 3 dissolution rates of different metals are compared with this of beryllium. It can be seen that Be is more stable than the ferritic steel 1.4922. Of the investigated metals, only molybdenum and vanadium are more stable.
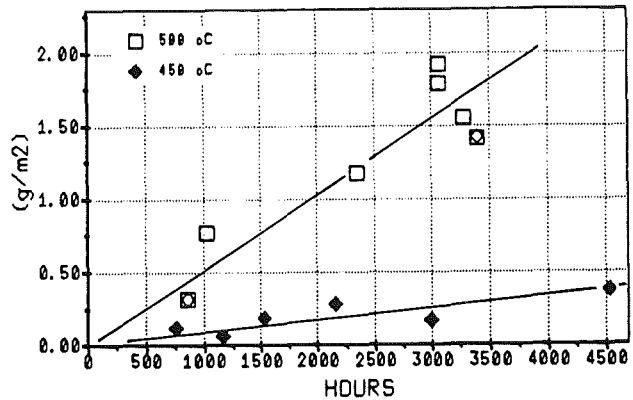
Fig. 9 : Dissolution of beryllium by static Pb-17Li

It may be concluded from the results that beryllium can be used in direct contact with the liquid eutectic. However experiments with flowing Pb-17Li and under non-isothermal conditions would be required to predict real corrosion rates and mass transfer effects for a reactor blanket.

	$g/m^2 \cdot d$
Mo	< 0.001
V	0.0056
1.4922	0.052
Be	0.014
Ti	0.22
Zr	1.2

Table 3:   Dissolution rates of metals in static Pb-17Li at 500°C.

- 9 -

References:

(1)   H. Feuerstein, J. Nucl. Mat. 155-157 (1988) 520

(2)   Task B9 in KfK 4488, EUR 11392EN (1988)

(3)   H. Gräbner, J. Nucl. Mat. 155-157 (1988) 702

Staff:
J. Beyer
H. Feuerstein
H.Gräbner
S. Horn
J. Oschinski

B 11 - 16   Development of Ceramic Breeder Materials

The KfK contribution concentrates on the Li-Silicates and includes all the steps necessary to achieve a product to be used in the helium-cooled blanket design. The development starts with fabrication and characterization of pellets and pebbles. Physical, mechanical and chemical properties are measured before and after irradiation. The irradiation program makes use of several reactors within the European and the Beatrix Cooperation. Lithium-Orthosilicate has been proven to be the most promising candidate for the NET reference ceramic breeder material.

1.   Fabrication and Characterization of Breeder Materials (B11, B12)

The preparation and characterization of lithium containing monosilicates, especially Li_4SiO_4, and lithium metazirconate, Li_2ZrO_3, are under development to be used as breeder materials within the European Fusion Program (Task B11 and B12). Samples of disks with cylindrical shape were prepared from lithium orthosilicate and metazirconate powders to be irradiated within the international experiment SIBELIUS, which is of special interest for the compatibility behavior with beryllium. Concerning the observed fast tritium release with $Li_{4-3x}Al_xSiO_4$ mixed crystals at low temperatures, solid solutions of Li_4SiO_4-Mg_2SiO_4 were prepared for comparison to the aluminium doped silicate material.

Characterization of Ceramic Breeder Materials

The joint French-German irradiation experiment LILA/LISA 1 will start mid February in the SILOE reactor of Grenoble. It has been equipped from the German side with three kinds of pellets made of pure lithium orthosilicate, lithium orthosilicate doped with aluminium, and lithium metazirconate. The two kinds of orthosilicate pellets had a density of about 93 % of the theoretical density. In contrast to all other samples fabricated up to now they did not show any measurable open porosity. In accordance to this result, the specific surface area was below the lower limit of the measurement equipment (Table 4).

The density of the metazirconate pellets was about 81 % of the theoretical density. The open porosity determined by means of mercury intrusion porosimetry was about 10 % of the pellet volume and had effective channel diameters between 60 and 460 nm. The measurement, using a helium pycnometer, demonstrated that a relatively large amount of open porosity existed below the lower limit of the mercury intrusion porosimeter of about 3 nm in diameter. The specific surface area was below 1 m²/g (Table 4).

Besides specific surface area, open porosity seems to play an important role for tritium release. This conclusion can be drawn from a comparison of the tritium release data of the various samples in the two experiments LISA 2 (SILOE reactor at Grenoble) and TRIDEX 3 (DIDO reactor at Jülich).

Table 4:   Density and structure data of three specimens of the experiment LILA/LISA 1

Specimen	OSi	OSi(Al)	MZr
He-pycn. density (g/cm³)	2.18	2.16	3.96
Hg-poros. density (g/cm³) (% th.d.)	2.21 92.5	2.22 92.9	3.34 80.5
Open porosity He-pycn. (%) Hg-poros. (%)	< 1 < 1	< 1 < 1	15.7 10.3
Specific surface area (m²/g)	< 0.2	< 0.2	0.78
Effective channel diameters (nm)	---	---	60 - 460

OSi Li_4SiO_4 (theor. density   2.38 g/cm³)
OSi(Sl) $Li_{3.7}Al_{0.1}SiO_4$ (theor. density   ~ 2.39 g/cm³)
                        (estimated)
MZr Li_2ZrO_3 (theor. density   4.15 g/cm³)

Table 5 summarizes values of open porosity (determined by means of helium pycnometer and mercury porosimeter) and specific surface area of various Li_4SiO_4 samples from some irradiation experiments.

Preparation of Ceramic Breeder Materials

The compatibility behavior of Li_4SiO_4, $LiAlO_2$, Li_2ZrO_3 and Li_2O as well as the 316 L and 1.4914 types of stainless steel with beryllium is foreseen to be tested in the international irradiation experiment SIBELIUS. For this experiment and for additional investigation of the out-of-pile compatibility behavior 50 disks of 8 mm in diameter and 1.5 mm in height were prepared from lithium orthosilicate and metazirconate powders by sintering to the specified shape. Some of the disks got a central hole of 0.8 to 0.9 mm in diameter for assembling of thermocouples. In addition this, a smaller amount of Li_4SiO_4 pebbles are also foreseen to be tested within this experiement.

The tritium release of aluminium doped lithium orthosilicate ($Li_{3.7}AL_{0.1}SiO_4$) was observed to be very fast at low temperatures (about 92 % at 300 °C), which is an essential result of an irradiation experiment performed in the FR 3 reactor at Jülich. It is suggested, that magnesium doped

Table 5: Structure data of various Li_4SiO_4 samples of some irradiation experiements

| Experiment | Con-figuration | open porosity | | Specific surface area |
		He pycn. (%)	Hg poros. (%)	(m²/g)
LISA 2	pellet	8.4	1.0	0.2
LISA 2	sintered granulates	~ 9	2.1	2.1
LISA 2	molten spheres	~ 7	0.8	5.9
TRIDEX 3	pellet	< 1	< 1	< 0.2
TRIDEX 3	sintered granulates	19.7	20.5	0.4
TRIDEX 3	molten spheres	6.7	2.9	2.3
LILA/LISA 1	pellet	< 1	< 1	< 0.2
LILA/LISA 1	pellet (Al doped)	< 1	< 1	< 0.2
EXOTIC 5	sintered granulates	17.9	19.1	< 0.2

orthosilicate could $(Li_{4-2x}Mg_xSiO_4)$ lead to comparable results. Therefore, the preparation of Li_4SiO_4-Mg_2SiO_4 mixed crystals was carried out using the preparation method in alcoholic suspension similar to those of the preparation techniques already described in detail. We obtained a sinterable mono-phase ceramic material of the composition $Li_{3.8}Mg_{0.1}SiO_4$. A first short-time irradiation experiment is under development.

Publications:

T. Kurasawa, H. Watanabe, E. Roth, D. Vollath:
In-pile tritium release behaviour from lithium aluminate and lithium orthosilicate of the VOM-23 experiment
J. of Nucl Mater 155-257 (1988) 544-548

H. Elbel:
Open pore structure analysis of lithium bearing ceramics
J. Nucl. Mater. 155-175 (1988) 480

W. Breitung, H. Elbel, J. Lebkücher, G. Schumacher, H. Werle:
Out-of-pile tritium extraction from lithium silicate
J. Nucl. Mater. 155-157 (1988) 507

H. Werle, W. Breitung, M. Briec, R.G. Clemmer, H. Elbel, H.E. Häfner, J. Masson, G. Schumacher, H. Wedemeyer:
The LISA-2 experiment: In-situ tritium release from lithium orthosilicate (Li_4SiO_4)
J. Nucl. Mater. 155-157 (1988) 538

G.W. Hollenberg, C. Alvani, B. Rasneur, H.Elbel, H. Wedemeyer, D.E. Walker, T. Takahashi, K. Noda, A. Akiyma:
The FUBR-1B experiment in BEATRIX-1: Design and materials characterization
J. Nucl. Mat. 155-157 (1988) 563

Staff:

B. Dörzapf
H. Elbel
E. Günther
R. Hanselmann
J. Heger
W. Laub
H. Nagel
R. Scherwinsky
D. Vollath
H. Wedemeyer
M. Wittmann
Ch. Adelhelm
S. Winkler
H. Werle

2. Measurement of Physical, Mechanical and Chemical Properties (B 13)

Constitution

The experimental investigation of the Li_2O-ZrO_2 phase relations was continued in the lithium-rich region between Li_2O and Li_2ZrO_3. In the literature there was some confusion about the stoichiometry of the compounds in this region. The own results confirmed the existence of the compounds Li_8ZrO_6 and $Li_6Zr_2O_7$, whereas no phase of a composition Li_4ZrO_4 was found in the temperature range above 500 °C up to the melting region. Between Li_2O and Li_8ZrO_6 a eutectic was found at 1100 °C, the eutectic composition lying between 10 and 15 mole-% ZrO_2. The polymorphism of Li_8ZrO_6 was confirmed, but the transition was observed by DTA at a lower temperature, instead of 660 °C reported in the literature. $Li_6Zr_2O_7$ has probably an incongruent melting point at 1290 °C.

Staff:
G. Schlickeiser
A. Skokan

Physical and Mechanical Properties

Investigations of the thermophysical properties of Li_4SiO_4 of different origin showed a non-defined behaviour concerning the thermal conductivity. Data of the thermal conductivity

given in previous reports cannot be ascribed to the compound Li_4SiO_4 alone, but are also due to extrinsic parameters. The storage time of Li_4SiO_4 samples seems to have a strong influence. The room temperature value of the thermal diffusivity of Li_4SiO_4 decreased with time to reach ~ 0.004 cm^2/sec, which is far below all other values known from own measurements and literature data. In the next time the thermal transport behaviour of Li_4SiO_4 will be studied in more detail.

A compilation of mechanical properties data of ceramic breeder materials (Li_2O, $LiAlO_2$, Li_4SiO_4, Li_2SiO_3, Li_2ZrO_3) was made within the scope of an IEA campaign for the International Fusion Materials Handbook. Sufficient data and parameter correlations could be given for the elastic properties in general, and for the ultimate strength of $LiAlO_2$ and Li_4SiO_4 at room temperature. There is still insufficient supply of ultimate strength data at elevated temperature. Correlating the various creep results appears problematic as such. Finally, the data base for Li_2ZrO_3 was found to be rather scarce.

On request of ENEA (Casaccia) a pellet batch of ENEA-LiAlO₂ (about 80 % TD) was examined concerning elastic properties and ultimate compressive strength. The mean values determined were: E = 59 GPa, v = 0.23, σ_c = 277 MPa (Weibull modulus: 12.4).

Staff:
M. Blumhofer
W. Dienst
G. Haase
B. Schulz
H. Zimmermann

Physicochemical Properties of Lithium Silicates

Among the criteria used for an evaluation of ceramic materials such as lithium silicates proposed for tritium breeding in fusion the hydrogen solubility, which itself depends upon bulk and surface material properties, is of importance. The surface characteristics are mainly determined by the history of the ceramics, i.e. method of synthesis, exposure to air or other atmosphere, etc.
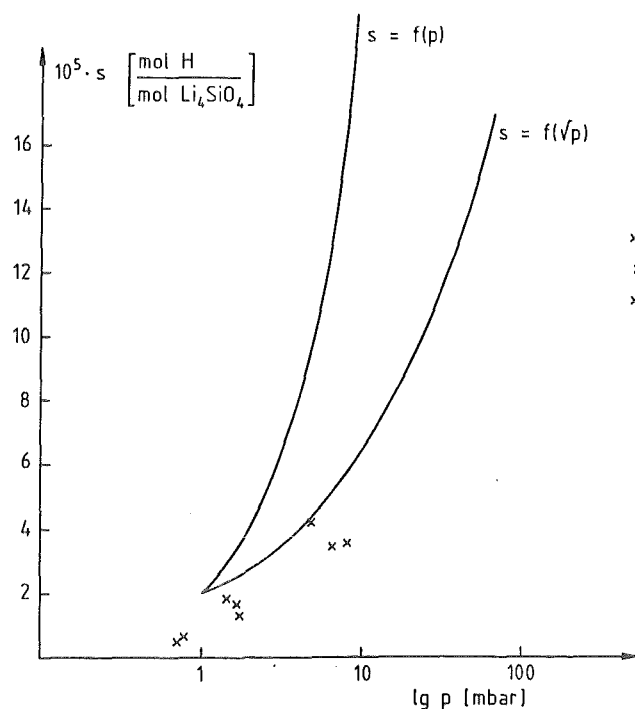
Fig. 10

That lithium silicates interact with atmospheric components is apparent from thermogravimetric measurements. Upon heating a significant weight loss takes place which can be attributed to the release of water and/or carbon dioxide (see Table 6). The presence of carbonate was confirmed by differential thermal analysis as well as by an XPS investigation, employing Li_2CO_3 as a reference material. The XPS surface analysis suggests a correlation between the lithium carbonate surface concentration and the lithium content of the sample. Since the C 1s photopeak is drastically

Material	Synthesized from	ρLi (m/cm³)	Weight loss %	surface conc, in atom %	
				Li silic.	Li carb.
Li_4SiO_4	$LiOH/CH_3OH/SiO_2$	0.55	30.8	3	97
Li_2SiO_3	$LiOH / SiO_2$	0.35	1.0	79	21
$Li_2Si_2O_5$	Li_2CO_3 / SiO_2	0.23	n.d.	98	2

Table 6: Characterization of lithium silicate powders

reduced during argon sputtering it is concluded that carbonates are concentrated on the surface.

In a number of runs the solubility of hydrogen in 30 g Li_3SiO_4 was examined employing a gas volumetric technique. To obtain a very dry sample the lithium ceramic pellets were dried at 900°C under high vacuum over a period of one day. Whereas in previous experiments on the hydrogen solubility in lithium metasilicate emphasis was placed on the influence of temperature , this work concentrated on the pressure dependance. As illustrated in Fig. 10, the solubility increase with pressure is much lower than, that expected from a simple Sievert's or Henry law (both shown in the figure as solid lines). The experimental solubilities (x) can be considered as upper values with respect to an estimation of the tritium inventory due to physically dissolved tritium.

Staff:
M. Glugla
R. Kaufmann
R.-D. Penzhorn
K.H. Simon

3. Irradiation Testing of Ceramic Breeder Materials (B 15 and B 15.3)

In assessing the performance of solid breeders, tritium release is an important aspect. KfK concentrates on lithium silicates, especially, orthosilicate, and metazirconate. In addition to in-pile tests (B16), tritium release is studied in out-of-pile annealing experiments.

The influence of purge gas chemistry on tritium release kinetics and on the type of released tritium species (water, gas) has been studied systematically. In agreement with in-pile observations it was found that addition of H_2 (Fig. 11) and H_2O accelerates, whereas O_2 retards tritium release. Both, the release kinetics and the type of detected tritium species depend strongly on the material surrounding the samples (oxigen potential): with a copper furnace kinetics is slow and more than 90 % of the tritium is water, with stainless steel kinetics is fast and the detected tritium is below 400 °C water, but above 500 °C gas (Fig. 11). The investigations indicate that tritium release from orthosilicate is controlled by desorption, from metasilicate and metazirconate by diffusion + desorption. Because generally several desorption processes are involved, it is very difficult to determine the order of the reactions.

An international intercomparison irradiation of breeding ceramic specimens entitled COMPLIMENT (Comparison of Lithium Materials Damage Effects by Fast Neutrons and 6Li(n,α)T-Reactions) coordinated by the KfK Institute for Materials and Solid State Research III (IMF III) is on the way. The irradiation experiment ELIMA 2 in the fast flux (behind a cadmium screen in the HFR/Petten) has been already finished after a duration of 177 FPD. The corresponding experiment DELICE 03 in the thermal flux of

the OSIRIS reactor will be finished in march 1989 after about 80 FPD. Beginning of PIE work at KfK is foreseen for the second half of 1989.

Staff:
W. Breitung
T. Eberle
H. Elbel
H.E. Häfner
K. Heckert
J. Lebkücher
M. Möschke
K. Philipp
H.-J. Ritzhaupt-Kleissl
G. Schumacher
H. Werle

4. Tritium Recovery from Ceramic Breeder Material (B 16)

Tritium recovery from ceramic breeder material is important in assessing the performance of breeder blankets. The behaviour of lithium silicates, especially orthosilicate, and of metazirconate is studied by KfK in the LISA-series of in-pile tests performed in the SILOE reactor at CEN Grenoble.

Results of the last test (LISA 2, finished December 1987) for various orthosilicate samples have been discussed in the previous semi-annual report. The next test (LILA/LISA) is a common CEN/KfK experiment and will start March 1989. Samples of aluminate, doped aluminate and metazirconate from CEN and of orthosilicate, Al-doped orthosilicate and metazirconate from KfK will be studied. One important goal of this test is to select the most promising metazirconate for the Be-ceramic SILOE in-pile interaction test SIBELIUS planned to start July 1989.

Staff:
H. Elbel
H.E. Häfner
H. Werle
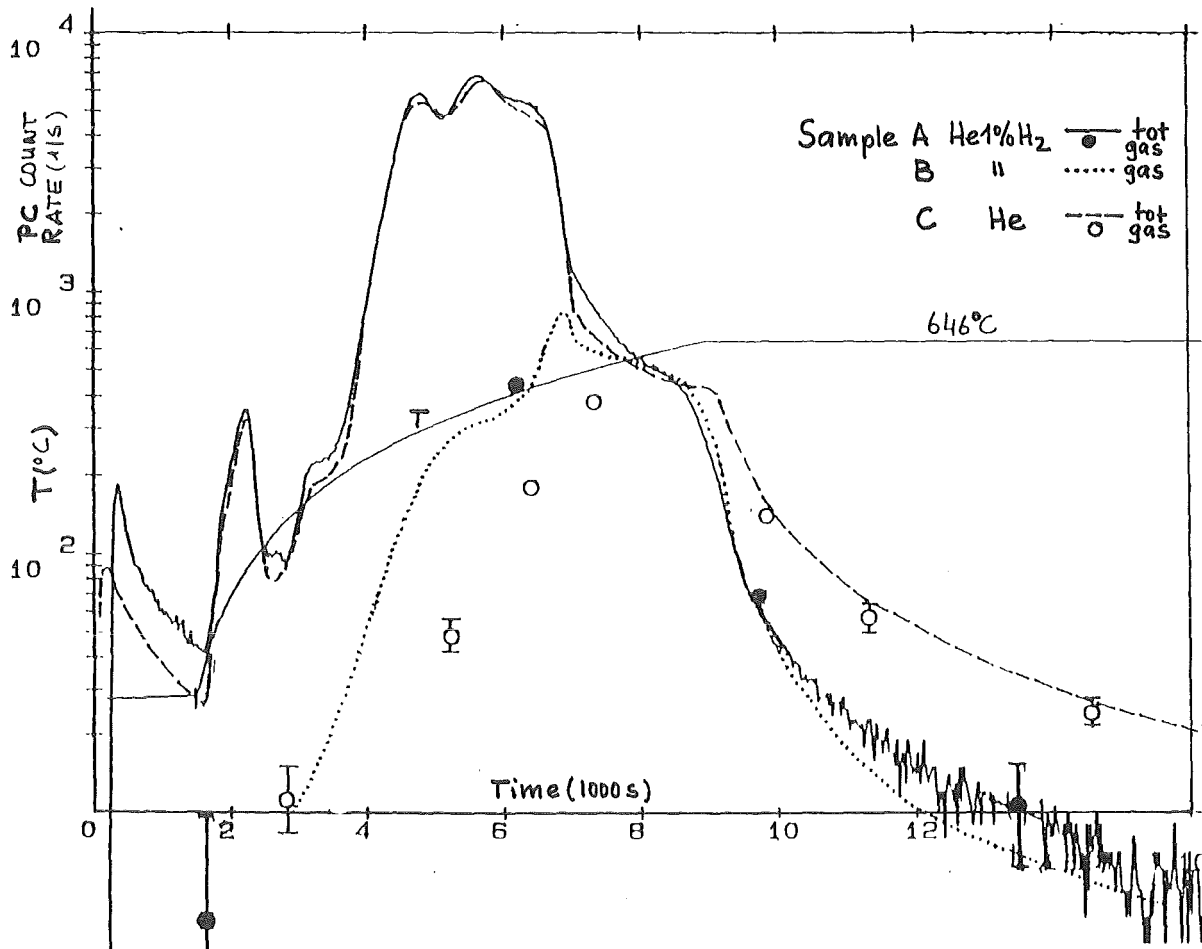
Fig. 11: Influence of H_2 in purge gas on total (tot) and gaseous (gas) tritium release (PC countrate). Three samples of 0.5 mm ⊘ Li_4SiO_4-spheres (type Schott 86, Ventron) were annealed with 5°C/min (T Temperatutre) in a stainless steel furnace

M 3 Development of High Field Composite Conductors

Staff:

W. Barth	B. Lott
M. Beckenbach	G. Nöther
M. Brünner	A. Nyilas
P. Duelli	H. Orschulko
R. Flükiger	H. Raber
S. Förster	T. Schneider
W. Goldacher	W. Specking
A. Kling	S. Stumpf
M. Klemm	P. Turowski

The new high field test facility (10 kA/100 kN at $B \leq 13$ T) for NET TF conductors has been successfully tested under full axial load for the first time. This facility will be used for the characterisation of the KfK concept of NET TF conductors at a subsize scale (approximatively 1:18). In addition, it will be also used for testing other conductors concepts developed by other laboratories for the NET team. A contract for a test programme on ABB and LMI cables has been signed between NET and ITP. The present high field facility is actually worldwide the only one allowing the measurement of axial stress effects on I_c of conductor of the dimensions ~20x10 mm².

So far, several Nb_3Sn flat cables with and without Cu stabilization have been tested up to 8 kA. The critical current of these cables consisting of 31 strands corresponds approximately to the short sample values, indicating that no degradation of I_c took place during the cabling process. The variation of I_c with strain exhibits a flat maximum at ~0.3 - 0.4%, which is comparable to the behaviour for single strands.

In order to measure the effect of the strong transverse compressive forces acting on a fusion magnet under full load, an appropriate modification of the test rig for NET subsize conductors was decided, which is actually under work.

A particular test facility to be used in the HOMER magnet system was realized. The critical currents of coils consisting of one Nb_3Sn flat cable layer can now be tested up to 11.5 T under the combined effect of Lorentz and mechanical forces. Tensile or compressive forces can be applied hydraulically on the superconducting windings. An important feature of this device is the precise measurement of the induced strains. Several strain gauges have been placed, in order to take into account possible inhomogeneities of the strain at different points of the winding.

Unexpected difficulties were encountered during the reaction heat treatment of Nb_3Sn cables. Three flat cables with different configurations were wound to pancakes and reacted for 64 h at 700°C in a vacuum tight stainless steel container specially developed for this purpose. Using intermediate stainless steel and graphite foils between the flat cables, together with a tight adjustment of the structure, the tolerances after the reaction heat treatment could decisively be reduced. On a cable length of 10 m, a variation in width between 12.45 and 12.49 mm (± 20 μm) was observed, while the corresponding variation in thickness was ± 5 μm (from 1.995 to 2.015 mm). The precise knowledge and control of these tolerances after the reaction heat treatment is a necessary condition for the realization of NET-TF conductors by means of the "react and wind" technique.

M 4   Superconducting Poloidal Field Coil Development

The aim of task M 4 is to develop and test a superconducting poloidal model coil relevant for Tore Supra and NET and to simulate in the test similar load conditions. The model coil of 3 m Ø is designed to be operated in the KfK-TOSKA test facility in 1990. Both tasks M 4 and M 8 are joint efforts of KfK and CEA.

Conductor fabrication

The progress in the completition of the Polo conductor for the Polo model coil sticked by the enclosure of the round cable in the protection tube. Adjustments of the set of rollers of the tube folding device and optimization of welding parameters combined with a controlled start and stop led finally to a considerable improvement of the quality of the weld seam. Not only empty tubes but also a test cable enclosed in the protection tube was manufactured in a length of about 100 m. The compaction of the protection tube for fixture of the subcables were performed by a die and swaging machine in the same line. All four pieces of the cable of the model coil of 150 m length each were manufactured.

The fixture of the subcables by wrapping of two steel tapes and compaction by a swaging machine is under development as well as another production method of the cable jacket by extrusion and but welding. This alternative manufacturing methods were started to get a normal basis for cost assessments.

Basic investigations

Experiments performed for the investigation of the stability of subcable joint (Fig. 12) were evaluated. A calculation model was developed by which the stability limit of a subcable joint was determined if the geometry and the transition resistances were known.

The stability experiment of the full size cable with CuNi wrapped subcables was finished. A detailed analysis is still running. The results can be summarized as the following:

a)   The stability of the cable is in the upper current region considerably lower than expected from the strand and subcable stability measurements.

b)   The possibility of a current redistribution between the subcables (for parallel current feeding in) did not increase the stability.

c)   The strands and single subcables had in the upper current range a much higher stability limit.

d)   Only a slight differences were found for cooling by liquid He (1 bar) and supercritical helium (4 bar) as expected from single strand tests and theory.
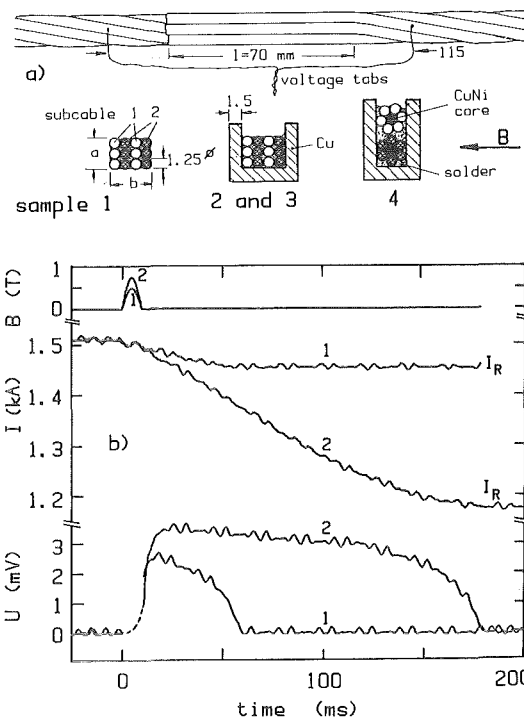
Fig. 12:   Three different types of subcable joints and the typical behaviour during a pulse of a transverse field

Item a) - c) need further evaluation. A preliminary explanation is the following: The contact resistances between the subcables have a considerable scattering. These resistances determine the losses of the cable. This means that the losses are locally very different and can induce normal region. The stability is determined by the smallest transition resistance between the subcables above the recovery current. The extrapolation of the stability limit from strand measurements to the cable gave to high values. This result is very important for such type of cables. For the actual case the stability limit is still sufficient to withstand the requirements of a plasma disruption at 15 kA like specified in Tore Supra.

A test series was started in the high voltage laboratory to investigate the mechanical degradation of insulation materials by mean of measurement and analysis of the activity of partial discharges.

Construction of the model coil

A detailed design of the model coil is being finished. For the basic components (radial-, axial-break, measuring feedthrough) prototypes were built and successfully tested. Series testing of 27 axial breaks is running. 12 axial breaks were already tested. The leak rate were less than 10^{-7} mbar l/s. The prototype of the midpoint connection is being under construction. The soldering of the subcable joints was excersized under the later boundary conditions. Some

improvements were necessary to get a sufficient filling of the solder between the wires.

A design change in the end terminations brought a release in the required parts and the prototype testing.

A high voltage instrumentation cable (46 kV test voltage) was developed. Some improvements were necessary. Three modified cable types are being manufactured.

As soon as the conductor will be available the winding of the pancake of the model coil can be started.

Modification of the TOSKA Facility

The cryogenic installation for the testing of the model coil was completed. The test loop used for the two phase experiment was modified. It can be used now for simulation of the model coil in the cryogenic system. The cryogenic control and instrumentation was installed, calibrated and taken into operation. The computer system was prepared for the data acquisition of this test. The cooldown for a test of cryogenic system is being in progress.

The 22 kA and 23 kV vapour cooled lead design is now complete. The cold end of the vapour cooled lead and the joint to the coil termination is now cooled by supercritical helium. One part of this gas runs through the heat exchanger of vapour cooled lead (~1.5 gr/s) while other part (~4.5 gr/s) is returned cold to the coldbox. A design change was necessary in the coil terminals to match the tolerances needed for the lateral thermal contraction of the coil. This led to a simplification of the coil terminal. Experiments for an optimization of the soldering parameters were performed for the manufacturing of the heat exchanger. Pressure drop measurements are running in a 53 cm long pice of the heat exchanger.

The agreement between the calculations and the measurements is excellent which confirms that the assumptions are a very good approximation for the description of the sophisticated heat transfer (Fig. 13).

Publication:

C. Schmidt, Stability of poloidal field coil conductors and subcable results, Proc. 12th ICEC Southampton, GB, July 12-15, 1988.
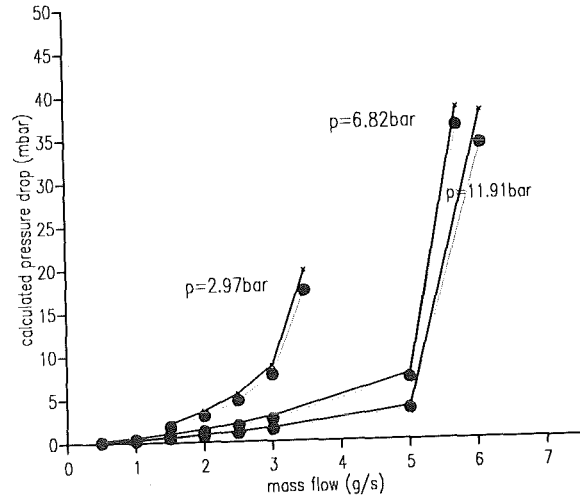
Fig. 13: The pressure drop versus mass flow. The comparison of the measured (dotted line) and the calculated (solid line) pressure drop of the heat exchanger of the vapour cooled current lead.

Staff:

H. Bayer	L. Schappals
I. Donner	G. Schenk
P. Duelli	C. Schmidt
S. Förster	K. Schweickert
P. Gruber	E. Specht
T. Hardy	H.-J. Spiegel
W. Heep	J. Seibert
R. Heller	F. Süß
U. Jeske	M. Süßer
D. Li	A. Ulbricht
G. Nöther	A. Vogt
A. Nyilas	D. Weigert
M. Oehmann	F. Wüchner
U. Padligur	V. Zwecker
K. Rietzschel	

M 8   Design and Construction of a Poloidal Field Coil for TORE SUPRA as NET-Prototype Coil

The objective of the task is the development and test of an Equilibrium Field Coil (EF Coil) with parameters relevant for NET. The reliable operation of a superconducting PF-coil shall be demonstrated in a real tokamak environment with the rapid field variations due to start up, plasma position control and disruptions. The development has to confirm the coil construction process proposed for NET on a fairly large scale.

For this purpose, the upper ring coil "E_h" of TORE SUPRA will be replaced by a superconducting coil "EHS". Design and construction will be based on the results of the already running task M 4.

The task of the design and construction of the TORE SUPRA coil was transferred to CEA Cadarache in joint agreement. KfK will assist with its experience in the development and test of the polo model coil. It will contribute to the high voltage components and to conductor related questions.

The TORE SUPRA EHS coil was approved by the FTSC in November 1988. A joint work shop CEA/KfK was held in Cadarache at February 22/23, 89. The status and results of the model coil (M 4) and the design of the TORE SUPRA coil were exchanged. The developed basic components (axial and radial insulation breaks, feed throughs) can immediately or slightly modified applied for the "EHS" coil. A key question for the realization of the EHS coil are the conductor costs which exceed presently the funding limits. Alternative manufacturing methods for the protection tube and the jacket are being under development. Results will be available in the mid of the year.

Staff:
S. Förster
U. Jeske
G. Schenk
C. Schmidt
A. Ulbricht

M 9 Structural Materials Fatigue Characterization at 4 K

Before starting with the cryogenic fatigue crack growth rate tests the materials 4 K tensile behaviour were subject of the current investigations in the reporting period. These tensile investigations are necessary to make an assessment for materials structural performance. The tested materials were the selected austenitic stainless steel plate materials (1.4429, 1.4306 and 1.4435) in bulk and welded configuration. The standard 5 mm ∅ tensile specimens were machined in T-L and L-T orientations. The L-T orientation of the welded plate materials covered the transverse weld metal, bulk metal and the fusion (HAZ) zone. Whereas the specimens of T-L orientation consists of ~100% weld metal phase in longitudinal direction. All tests were carried out in the 4 K cryogenic rig. This rig allows to determine the tensile data of four individual specimens in one run after cool down to 4 K. The displacements during the loading were recorded by extensometers (clip gage technique) specially developed for cryogenic use. These extensometers were attached to the specimens directly using a stiff unidirectional working clamp technique. The sensitivity of the readings (resolution <1 µm, error at 4 K <±1% and linearity <±0.3%) allowed to determine the total stress vs. strain properties of each material up to fracture. The Table 7 gives the 4 K results of these three materials. An analysis of the stress vs. strain plots of these tests revealed that the serrations occuring during the loading could be used to gain informations about the structural performance of the materials under test. The extensometers with a gage length of 16 mm were placed during these tests in the middle of the specimens reduced section (30 mm total length), which allowed free ends of 7 mm reduced section in upper and lower portion of the specimens. This system gave the possibility to classify the rapid serrated unloadings as events which happens outside or inside the gage length. The serration occured inside the gage length were coupled with registered discrete displacements with step lengths of up to 100 µm. The Figures 14 and 15 show the original records of the welded materials (1.4429) stress vs. strain behaviour at 4 K. The serration events of the weld metal (Fig. 14) show an uniform statistical unloading distribution along the reduced section. Whereas the bulk/weld metal test (L-T) given in Fig. 15 show very clearly that the majority of the unloadings occur within the gage length. Here the fusion boundary (HAZ) seems to be the key controlling element for the serration occurance, which in turn is dislocation related. On the other hand we see also that the onset of the serrations for the transverse L-T orientation are shifted towards smaller strain values ~1,7 strain (L-T) compared to ~6,5% strain (T-L)). The accumulation of the serrations at the vicinity of the fusion boundary makes the fusion boundary the key controlling element for the fracture. Responsible for this phenomena is the stiffness change between the weld and bulk material phases. The higher yield strength and the somewhat lower Young's modulus of the weld metal determines the earlier serration starting and the accumulation of the serrations in a small area.

Table 8 gives the recorded onset positions of the serration at 4 K. The bulk materials 1.4429 (plate and forging) and the weld metals of the materials 1.4429, 1.4306 and 1.4435 have their serration onsets well above 6% strain. Whereas the bulk metal 1.4306 and the weld transverse orientations for all three materials have significant lower onset positions with respect to strain.

Out of these findings we can conclude that for 4 K structural applications only the material 1.4429 should be recommended. The low yield strengths of the materials 1.4306 and 1.4435 coupled with earlier onsets of the serrations makes their structural use doubtful. For the material 1.4429 the weld transverse orientation (L-T) is the weakest structural link and the design should be concentrated to remove this regime from high stress fields.
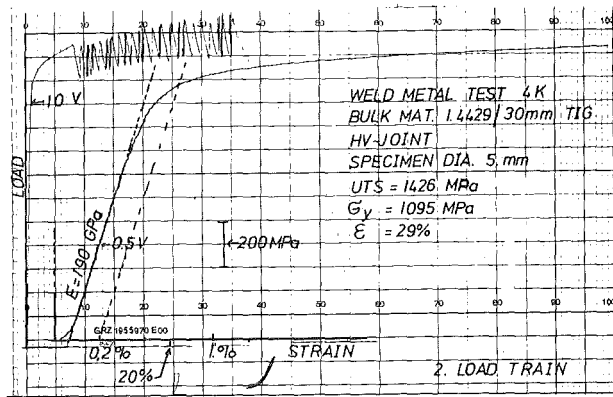
Fig. 14: 4 K stress vs. strain record of the weld metal (T-L)
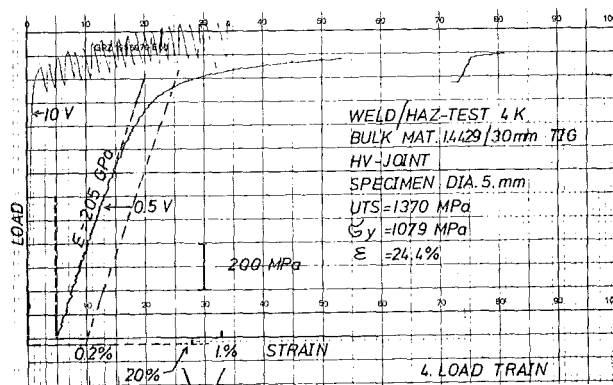
Fig. 15: 4 K stress vs. strain record of the weld/bulk and HAZ configuration

Staff:

A. Nyilas

H.P. Raber

- 20 -

Alloy	Mechanical Properties		Bulk material		Weld material (weld wire alloy 1.4429)	
			T - L	L - T	Weld centerline T - L	Weld transverse L - T
1.4429 plate	σ_y	MPa	932 , 926	988 , 988	1085 , 1095	1069 , 1079
	UTS	MPa	1507 , 1527	1527 , 1538	1416 , 1426	1360 , 1370
	EL	%	42 , 41	40 , 36	33 , 26	23 , 29
	RA	%	54 , 54	50 , 41	30 , 29	28 , 24
	E	GPa	204 , 205	203 , 206	170 , 190	205 , 205
1.4429 forging	σ_y	MPa	906 , 948	1038 , 1040	-	-
	UTS	MPa	1426 , 1497	1446 , 1441		
	EL	%	38 , 41	33 , 31		
	RA	%	50 , 54	42 , 42		
	E	GPa	203 , 204	205 , 204		
1.4306	σ_y	MPa	410 , 428	468 , 460	1049 , 1049	621 , 800
	UTS	MPa	1578 , 1619	1589 , 1537	1355 , 1395	1344 , 1324
	EL	%	43 , 47	46 , 44	28 , 41	32 , 31
	RA	%	54 , 51	51 , 51	23 , 29	45 , 29
	E	GPa	204 , 205	196 , 208	202 , 206	206 , 193
1.4435	σ_y	MPa	626 , 646	652 , -	1049 , 1049	825 , 855
	UTS	MPa	1334 , 1314	1314 , -	1355 , 1344	1324 , 1242
	EL	%	50 , 47	47 , -	28 , 26	33 , 25
	RA	%	59 , 62	51 , -	18 , 22	26 , 19
	E	GPa	197 , 207	206 , -	183 , 197	200 , 194

Table 7:   4 K weld and bulk metal tensile properties of selected stainless steels for cryogenic use

Alloy	Bulk material		Weld material (weld wire alloy 1.4429)	
	T - L	L - T	Weld centerline T - L	Weld transverse L - T
1.4429 plate	8.1 ; 8.1	9.1 ; 7.9	6.6 ; 6.5	1.7 ; 1.6
1.4429 forging	6.5 ; 6.3	9.4 ; 10	-	-
1.4306	2.2 ; 2.4	1.3 ; 1.5	3.4 ; 5.2	0.4 ; 0.6
1.4435	3.9 ; 4.1	4.0 ; -	6.9 ; 6.6	0.7 ; 0.7

Table 8:   Onset of serrations given in % strain

M 12 Low Electrical Conductivity Structural Development

Carbon fibre composites with polymeric matrices, having relatively high resistance against radioactive irradiation, have been investigated with respect to their degradation characteristics under cyclic, thermal and mechanical loads.

Composites with a polyetheretherketone (PEEK) showed nearly no formation of cracks at thermal loading from RT to LN_2 temperatures. Tensile threshold fatigue loading causes little crack formation. Only at the end of fatigue life a strong increase of crack density occurs. (see Fig. 16)

The Young's modulus degrades only less than 10% within the fatigue life rather independently of load amplitude. This is true for unidirectional and cross plied fibre arrangements.

These investigations will be continued under pure shear loads. A torsion-tension machine is in operation.

Staff:
V. Ahlborn
G. Hartwig
S. Knaak
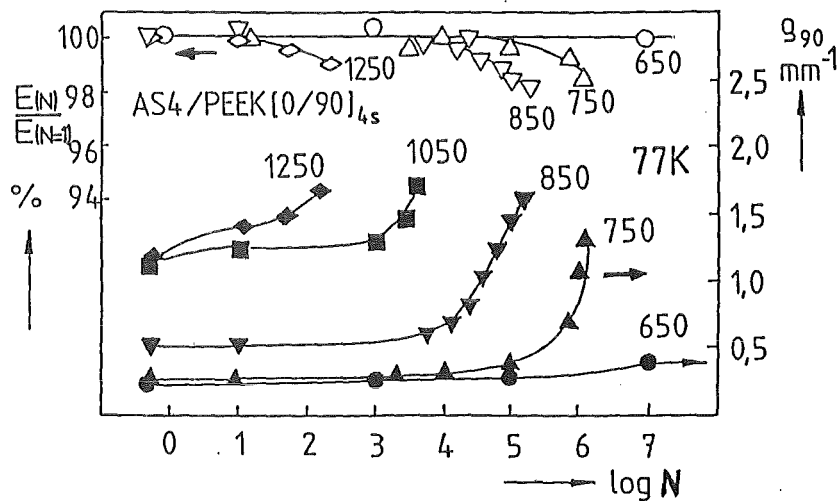
Fig. 16: Relative change of the Young's modulus and the crack density p versus load cycles. The parameter is the load amplitude (in MPa))

MAT 1.6 Development and Qualification of MANET 1

An instrumented notch impact bending device for miniature V-notch specimens of the dimensions 3x4x27 mm and 5x5x55 mm resp., has been developed and tested.

Staff:
B. Dafferner
H. Kempe
E. Materna-Morris
W. Meyer
L. Schäfer

MAT 1.9   Pre- and Post-Irradiation Fatigue Properties of 1.4914 Martensic Steel

Thermal cycling of large components is a serious problem for the designer. The structure considered in the present case is the first wall of a fusion reactor. Its surface, in the present design concept, will be subjected to radiation heating from the plasma facing side which may lead to severe thermal stresses. Due to the discontinuous operational mode thermal cycling will generate oscillating temperature gradients. These, depending on the loading conditions, will cause elastic or elasto-plastic reversed deformation giving rise to thermal fatigue which at present is considered as the most detrimental lifetime phenomenon for the structure considered. The investigations of MAT 1.9 are devoted to this problem.

The studies to be reported within MAT 1.9 are:

-   The influence of mean strain upon isothermal low-cycle fatigue-behaviour of MANET 1.

-   Preliminary installation of 5 facilities for thermal fatigue

-   Thermal fatigue of AISI 316 L with a ΔT between 350 and 550°C.

1.   Isothermal Fatigue

Three different loading conditions had been distinguished to study the influence of mean strain ε_m upon low-cycle fatigue-behaviour of MANET 1.

In Fig. 17 strain is plotted as function of time.

1. Symmetrical loading with $\pm \Delta\varepsilon_t/2$ (zero mean strain, (top)).

2. Negative strain with $-\Delta\varepsilon_t$ (compressive mean strain, (bottom, left)).

3) Positive strain with $+\Delta\varepsilon_t$ (tensile mean strain, (bottom, right)).

The investigations had been performed at 250, 450 and 650°C with a total strain range of 0.5% and a strain rate of 3×10^{-3}/s.

Results for these conditions are given in Fig. 18. Each point represents a mean value of two tests. Compared to values at zero mean strain, the numbers of cycles to fracture N_f result
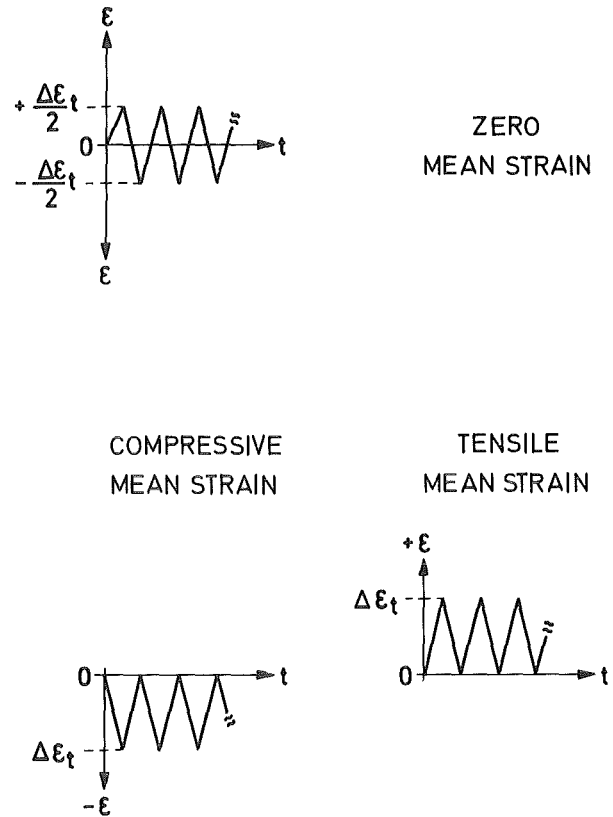
Fig. 17: Strain as function of time for different loading conditions.

in somewhat lower values for compressive mean strain ($\varepsilon_m = -0.25\%$) whereas the N_f-values are slightly higher for tensile mean strain experiments ($\varepsilon_m = +0.25\%$) in the examined temperature range.

Although the variations in N_f-values, at a given temperature, are small for all unsymmetric loading conditions, considerable differences in maximum tensile stress and compressive stress can be found depending upon the loading condition used. Fig. 19 represents these correlations for 450°C. Concerning tensile mean strain for instance ($\varepsilon_m = +0.25\%$), a decrease of maximum tensile stress with increasing number of cycles can be observed, whereas for compressive mean strain ($\varepsilon_m = -0.25\%$) the maximum tensile stress increases.

For maximum compressive stresses just the opposite behaviour occurs.
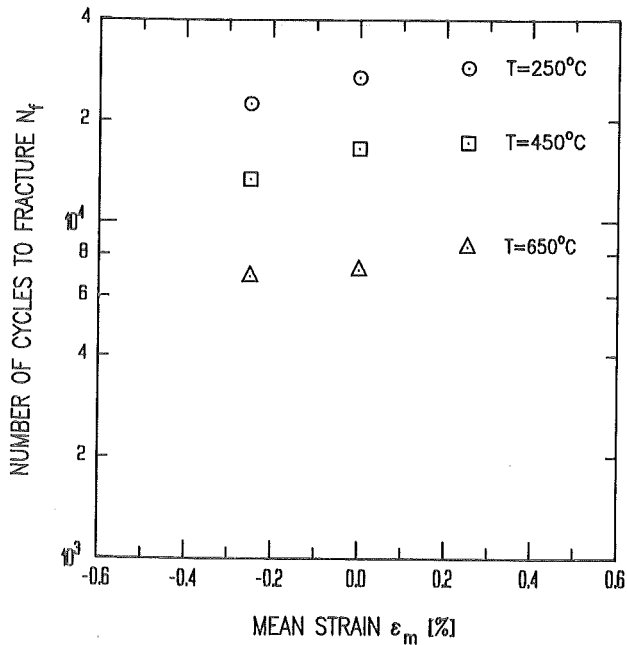
Fig. 18: Influence of mean strain upon number of cycles to fracture for MANET 1 in the temperature range 250 - 650°C.
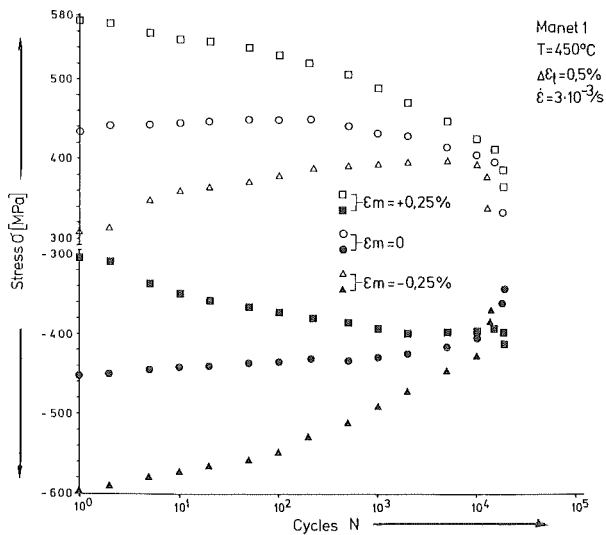
Fig. 19: Maximum tensile and compressive stress as function of cycles for three loading conditions.

2. Temperature cycling experiments

2.1 Preliminary installation of 5 facilities

Five test rigs, consisting of a heating device, a load frame and the data acquisition system - containing also the load and strain transducer feeding electronics - are preliminarily installed since the end of 1988. An acceptance test program was successfully completed.

2.2 Thermal fatigue of AISI 316 L

The aim of these experiments was, to generate a first data set of thermally cycled AISI 316 L and beside that to increase the accuracy and reproducibility of the test procedure.

The test conditions were such to allow comparison with data from literature. The temperature/time loading profile was saw-tooth like with variable T_{max} between 550°C and 750°C and $T_{min} = 200°C$, leading to a variable ΔT between 350°C and 550°C. Frequencies between 0.5 and 0.3 cpm (8.3 to 5.3×10^{-3}/sec) were equal for the heating and the cooling phase, resp. and led to a constant rate of 5.8 K/s. The specimen was clamped at $T = 375°C$. The test started into the cooling phase and accordingly the first cycle occured in tension.

The deformation was controlled by an overall strain amplitude (thermal and mechanical) and therefore the stress range $\Delta\sigma$ as well as the mechanical strain range $\Delta\varepsilon_t$ changed with the number of cycles.

In Fig. 20 results from thermomechanical cycling
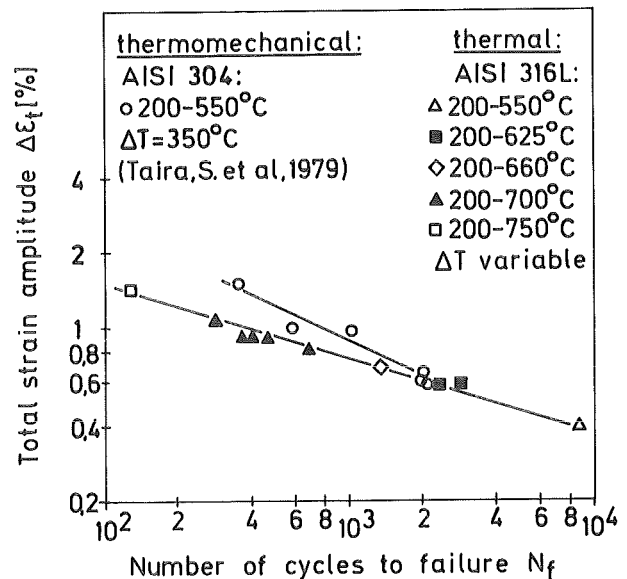
Fig. 20: $\Delta\varepsilon_t$ versus N_f-diagram.

experiments conducted on AISI 304 (1) are shown together with the own results on AISI 316 L in a $\Delta\varepsilon_t$ vers. N_f-diagram. For $\Delta\varepsilon_t$ the steady state values were taken.

At similar mechanical strain range ($\Delta\varepsilon_t \geq 0.7\%$) samples under thermal cycling failed at lower N_f-values then those under thermomechanical cycling.

2.3 Microstructural observations

Electron scanning microscopy was used to examine the fracture surface of failed specimens. Typically striation lines are observed. Crack initiation occured in most cases on nonmetallic inclusions or impurities. Above $T_{max} = 700°C$ a mixed damage structure consisted of striations and dimples.

Staff:
W. Baumgärtner
M. Boček
C. Petersen
D. Rodrian
W. Scheibe
R. Schmitt
H. Schneider
W. Schweiger

2.4 Thermal fatigue of AISI 316L under multiaxial stresses

The cyclic thermal loading of the first wall in a fusion reactor causes cyclic multiaxial stress states. These cyclic stresses may initiate cracks and failure of the structure. To understand crack initiation and propagation caused by such thermocyclic loads and to investigate, if there is another damage than under equivalent isothermal loading, experiments were performed under multiaxial cyclic thermal stresses. The specimens were watercooled tubes, comparable to the first wall. In these specimens a biaxial stress state arises by heating from the outside. For the first comparison isothermal tests with uniaxial stresses were carried out, too.

The equipment for thermal fatigue testing is a newly developed set up. Tubular specimens with a diameter of 60 mm, a wall thickness of 3.5 mm and a heated length of 150 mm are used. By induction heating the outer surface temperature rises from 100°C to 375°C within 2.2 s. For cooling, deionized water is streaming through the tube. Free thermal expansion of the specimen is possible. The temperature gradients in the wall, caused by the rapid heating, produce cyclic thermal stresses. Fig. 21 shows the schematic set up.

The temperature distribution in the wall of the tube was calculated with the help of temperature measurements on the surfaces and an assumption about the volumetric distribution of the heat induction. Then, the periodic strains in the wall were calculated for elastic and for a simple plastic
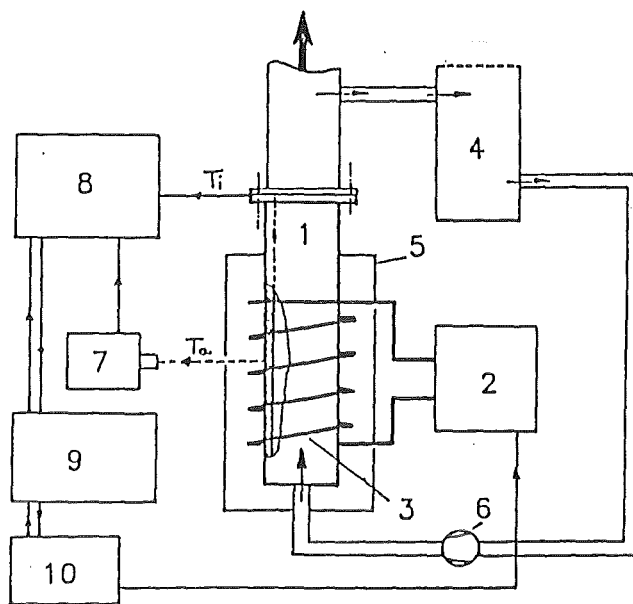
Fig. 21: Schematic sketch of the experimental set up for thermal fatigue tests.
① Specimen, ② HF-generator, ③ Induction coil, ④ Water supply, ⑤ FARADAY cage, ⑥ Pump, ⑦ Pyrometer, ⑧ Data acquisition, ⑨ Computer (HP 9816), ⑩ Generator controller.

material response. Fig. 22 shows the calculated strains in the plastic case.
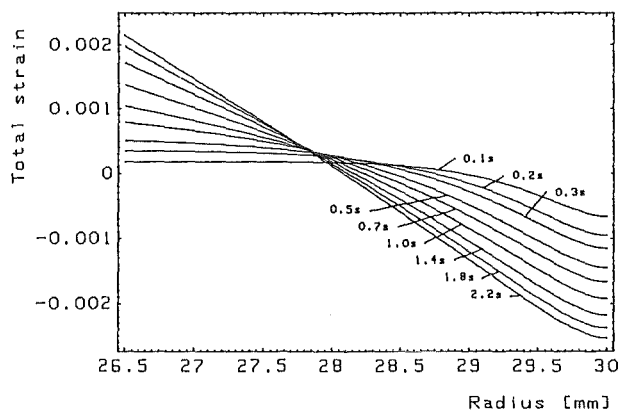
Fig. 22: Calculated principal strain in the tube as a function of the radius for different times after the beginning of the heating.

The strains lead to crack initiation after about 30 000 cycles and to failure by wall penetrating cracks after 100 000 cycles. During the test, crack initiation and growth of the inner surface is observed and measured by an endoscope. Fig. 23 shows the popagation of some cracks in dependance of the number of thermal cycles. After finishing the test, cracks with different surface length are opened mechanically to find

the relationship between crack length and crack depth. Additional metallographic examinations are performed. The failure of the tubes caused by wall-penetrating cracks is shown in Fig. 24 for the calculated maximum strain component. For comparison the measured failure of specimen under uniaxial isothermal loads is plotted, too. The first comparison shows that the failure occurs earlier in the thermal fatigue tests. Yet it isn't clear if this is caused by the thermal loading or by the multiaxial stress state.

Staff:
T. Fett
W. Hartlieb
J. Neumann
B. Schinke
E. Wiens
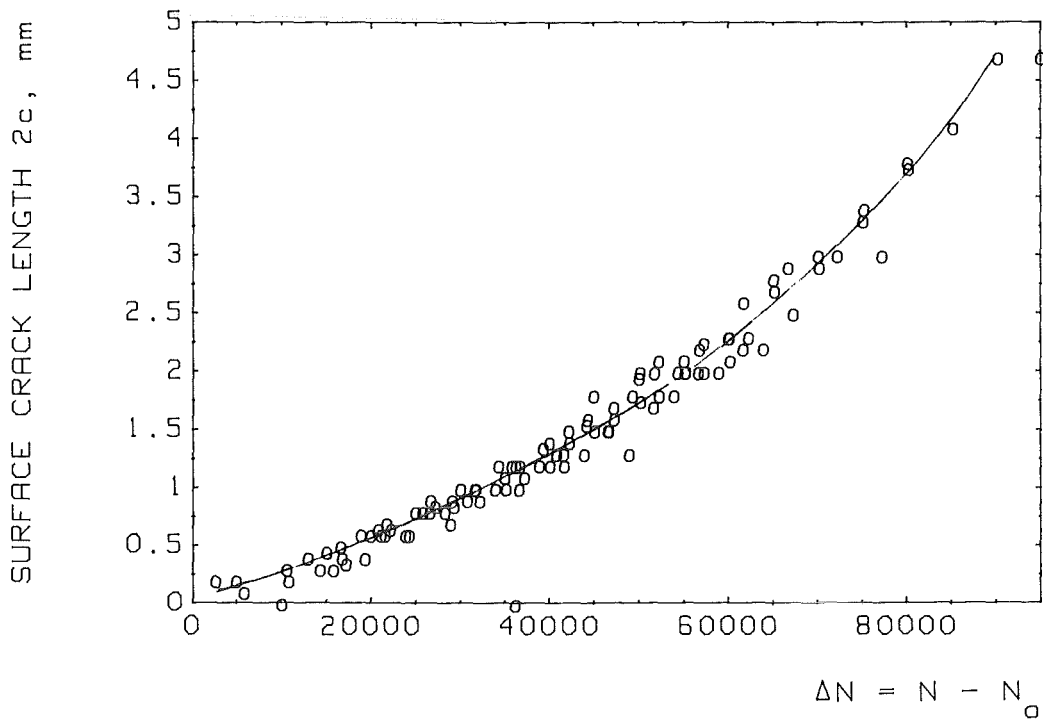
Fig. 23:   Crack propagation as a function of thermal cycles. ($N_o \approx 30.000$ = Number of cycles to crack initiation)
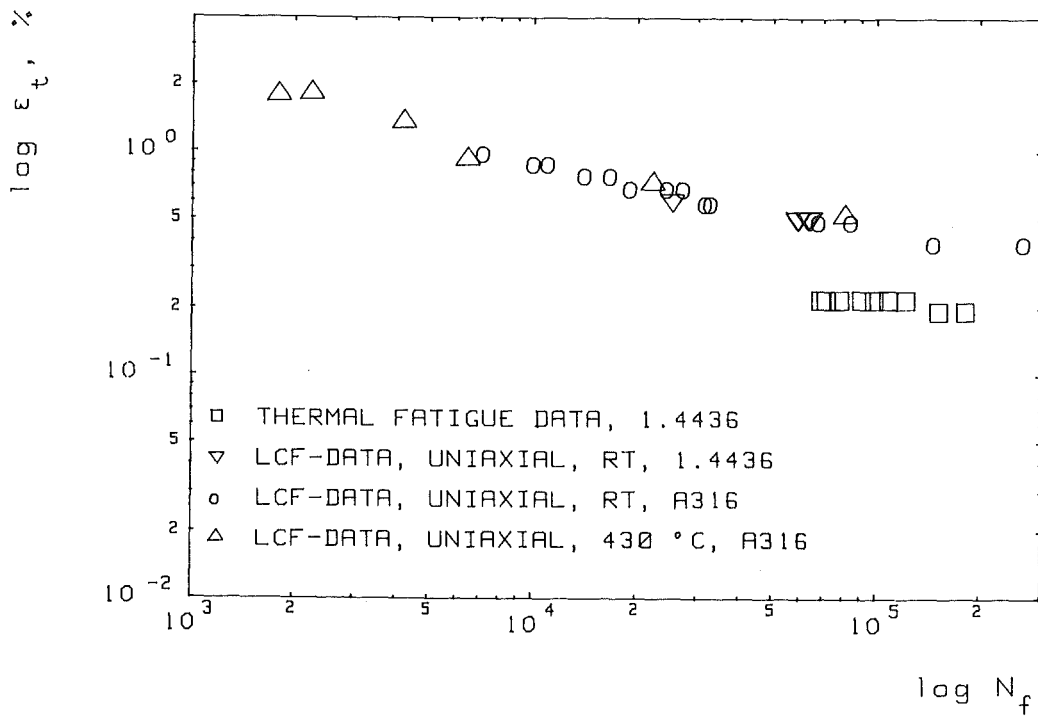
Fig. 24:   Cycles to failure N_f of specimens under thermal multiaxial and isothermal uniaxial fatigue as a function of the cyclic range of the maximum principal strain ε_t.

MAT 2.2 In-Pile Creep-Fatigue Testing of Type 1.4914 Steel

It is intended to study the in-reactor deformation and fracture behaviour of the candidate structural ferritic/martensitic material MANET (DIN 1.4914) in the central position of the KNK II reactor. The samples are capsules made from tubing which are loaded by pressurizing with gas; the temperature is controlled from outside. Foreseen is a cyclic loading scheme with pressures varying between 10 and 450 bar maximum and temperatures between 475 and 550 °C.

The pressure supply device has been finished by the end of 1988 and has successfully been tested out-of-pile. The most important part of the pressurizing installation is the closed loop for pressurizing/depressurizing with a multistage compressor and electrically operated valves. Eight samples can be handled in parallel. A simplified schemat of the whole device is shown for one sample in Fig. 25. The processor
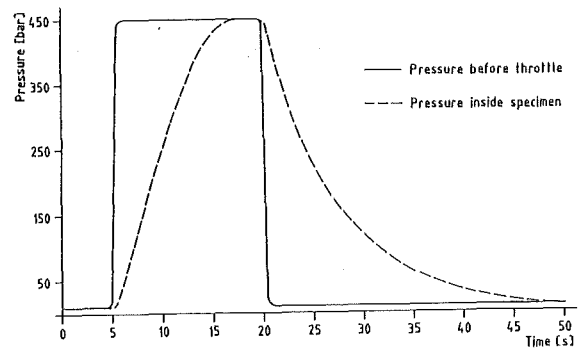
Fig. 26: Measured pressure curves

Staff:
K. Ehrlich
H. Lehning
G. Reimann
L. Schmidt
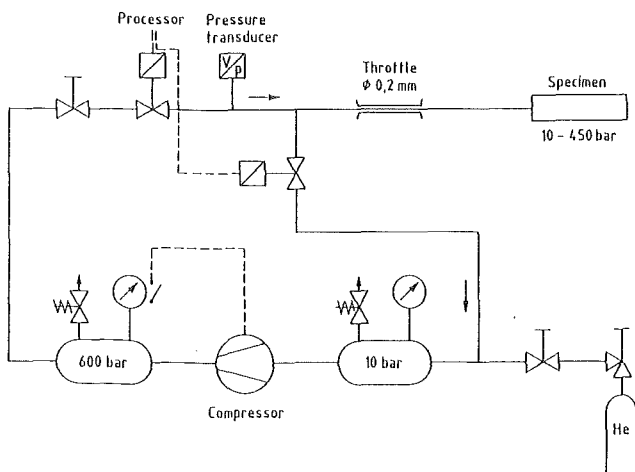
Fig. 25: Schematic drawing of the pressure supply circuit

which controlles the temperature has been modified to include handling of the pressurizing part as well in its program.

The loading of the sample is determined by the throttle setting in the pressure line. The actually achieved stresses of a capsule have been determined with a special rig in which the sample is replaced by a pressure transducer. A stress ramp is introduced in the sample by an appropiate way of handling the pressure valves; an actually measured pressure curve is shown in Fig. 26. The time for the increasing stress ramp is 15 sec - independent of the absolute amount of pressures. The same is true for the time of the decreasing stress ramp, wich amounts to 30 sec. If all eight samples are cycled to 450 bar then a holding time of approximately 200 sec is required before repressurisation because of the limiting capacity of the compressor. In this case a cycling rate of 15/h can be achieved for all samples.

MAT 6/MAT 13   Ceramics for First Wall Protection and for RF Windows

SiC qualities of industrial manufacturers are to be tested concerning the durability of tiles to protect the first wall against plasma instabilities and disruptions. Insulator materials (like Al_2O_3, $MgAl_2O_4$, AlN) are to be selected with regard to their resistance to thermal crack formation by dielectric loss in RF-windows. These windows shall be applied to separate wave guides for ECR heating from the plasma vacuum.

The final laboratory tests on SiC specimens concern the resistance of small tiles for first wall protection to cracking under steady-state heat flux. Fig. 27 shows a cracked tile. The dimensions of the head-part are about 25 x 25 x 10 mm^3, and the tail is shaped to fit two cooling tubes. The front side was heated by a 50 kW acetylene/oxygen gas burner. The heat transfer was calibrated with a copper tile equipped with thermocouples. Preliminary test results on tiles of three different qualities (one HIP- and two S-SiC) showed that about 1 of 5 tiles can fail at a heat load of 165 W/cm^2. The temperature drop in the tiles was from about 1800 to 1000 °C.
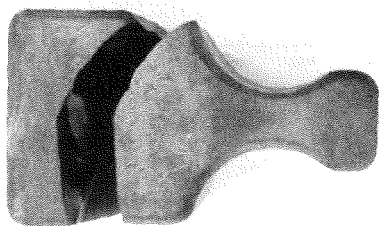
Fig. 27:   SSiC tile cracked under steady-state heat flux of 185 W/cm^2 at the front side (on the left).

Post-irradiation examination of irradiated specimens has been started in the period under review. Samples of HIP-SiC and of different qualities of AlN and Al_2O_3 were irradiated up to 0.8 dpa in LAMPF (Los Alamos) which is a spallation neutron source. The irradiation temperature was ≤ 400 °C. The volume changes under irradiation were relatively small compared to the results of fission reactor irradiations to the same dpa level. The mean ultimate bending strengths appeared unchanged, but the Weibull moduli of HIP-SiC and HIP-AlN had decreased under irradiation. The irradiation of BIO-Al_2O_3 samples to about 8 dpa at 550 °C in OSIRIS (Saclay) resulted in the volume change expected and in a considerable decrease of mean UBS and Weibull modulus, from 322 MPa and 9.8 to 214 MPa and 6.1.

The investigations on the thermophysical properties of non-irradiated window materials to establish proper data sets on AlN, $MgAl_2O_4$, Al_2O_3 and Al_2O_3-ZrO_2 are mostly finished (x in the following table):

Material	Specific heat	Thermal expansion	Thermal conductivity
Al_2O_3	X	X	X
Al_2O_3-ZrO_2	X		X
$MgAl_2O_4$	X		X
AlN	X	X	X

For completion the thermal expansion of the $MgAl_2O_4$-spinel will be determined. To study the possible influence of powder preparation and compaction, measurements of the thermal conductivity of AlN-samples prepared at KfK will be undertaken. The investigation of the thermophysical behaviour of single crystal $MgAl_2O_4$ will be related directly to the study of the influence of irradiation on the thermophysical properties of this material.

The specific heat of AlN (Shapal) was determined in a Perkin-Elmer DSC (Fig. 28) and is compared to data shown in the Touloukian Series of "Thermophysical Properties of Matter". We used our data for extrapolation up to 1300 K in order to calculate the thermal conductivity of this compound from thermal diffusivity. The standard deviation of the data is 1 %.
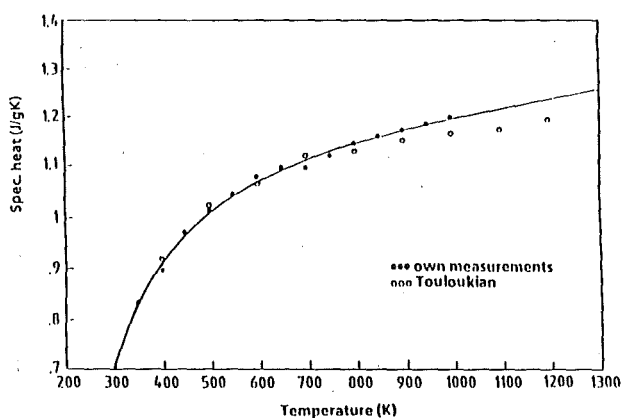
Fig. 28:   Specific heat of AlN (Shapal).

The thermal expansion of AlN (Shapal) and Al_2O_3 (Sapphire, Hemex quality) was determined with a Difference Dilatometer with excellent results. Fig. 29 and 30 show the thermal expansion as function of temperature. The standard deviation of $\Delta l/l$ is $0.04 \cdot 10^{-3}$.

The thermal conductivity of AlN (Shapal) is the highest of all candidate window materials (Fig. 31). Together with its low thermal expansion (see Fig. 29) this should result in an excellent thermoshock behaviour with regard to thermophysical properties. The thermal conductivity of Al_2O_3-ZrO_2 (Fig. 32) is slightly lower than that of alumina. An interpretation of the influence of ZrO_2 cannot be given up to now for two reasons: data of the thermal conductivity of non-stabilized zirconia are not available, and a chemical analysis for the
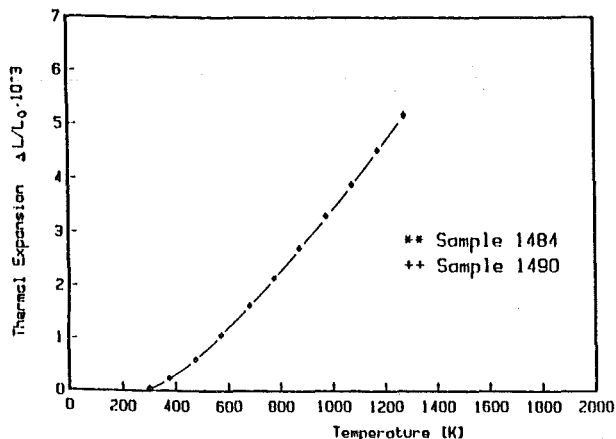
Fig. 29:   Thermal expansion of AlN (Shapal).
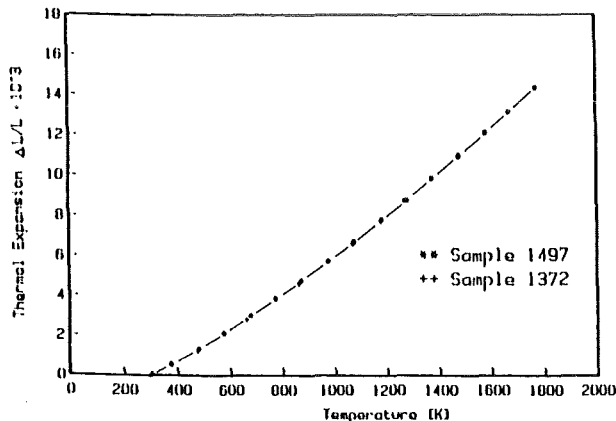
Fig. 30:   Thermal expansion of Al_2O_3 (sapphire, 0001-direction).
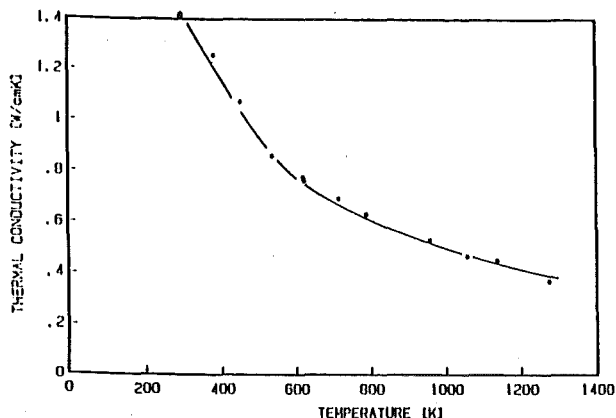
Fig. 31:   Thermal conductivity of AlN (Shapal).

true composition is necessary to relate measured densities to theoretical densities and thus to porosity. The thermal conductivity measurement on $MgAl_2O_4$ (first results in the previous report) is completed, as shown in Fig. 33. It shows an unusually broad band of measured values, thus reflecting the fact that the spinel up to now was the most problematic material. A standard deviation of 7 % has to be taken into account.
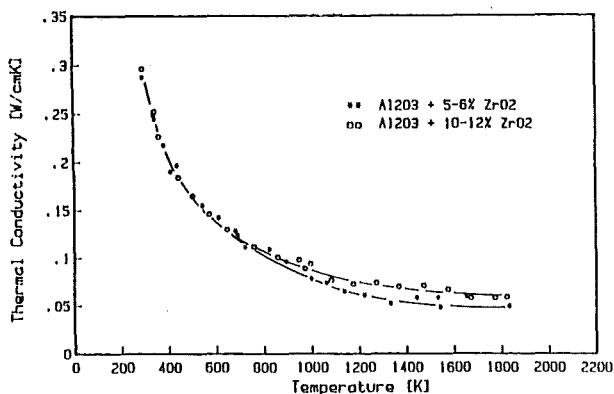
Fig. 32:   Thermal conducitivity of Al_2O_3-ZrO_2.
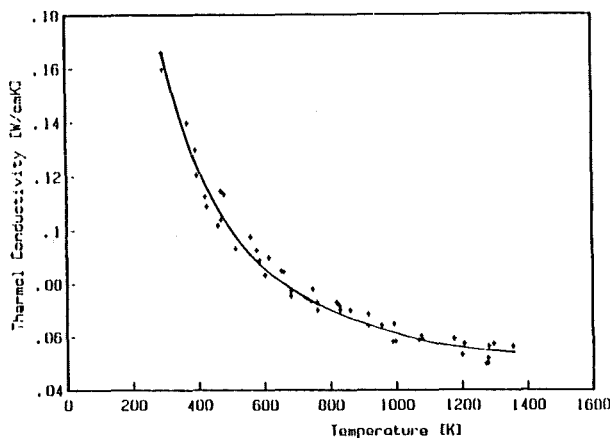
Fig. 33:   Final results on the thermal conductivity of polycrystalline $MgAl_2O_4$.
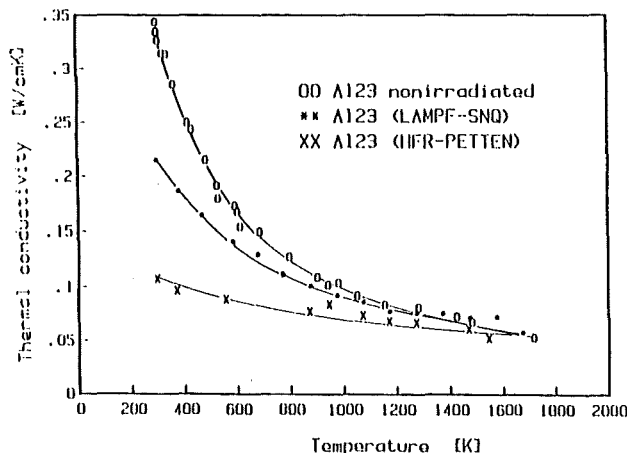
Fig. 34 :   Thermal conductivity of irradiated and non-irradiated AL 23.

At the end of 1988 the second laser flash apparatus was installed and now is especially used for irradiated samples. First results of AL 23 (Al_2O_3) irradiated in LAMPF-SNS are compared with non-irradiated AL23 and with data obtained from an irradiation in HFR (Petten), Fig. 34. The irradiation conditions were:

HFR-Petten: $2.6 \cdot 10^{20}$ n/cm² (E > 0.1 MeV), T ≤ 475 K

LAMPF-SNS: $5 \cdot 10^{20}$ n/cm² (spallation neutrons), T = 550 - 700 K

The main result is the significantly smaller decrease of the thermal conductivity of AL 23 irradiated in LAMPF-SNS, despite the fact that the neutron fluence is doubled compared to that in HFR (Petten). The irradiation temperatures are somewhat different, but a significant effect of the higher temperature in the LAMPF irradiation concerning recombination effects is not expected. Thus it seems that spallation neutrons produce a lower rate of irradiation damage, insofar as thermal transport behaviour in alumina is discussed.

The equipment for dielectric measurements on insulator materials at 143 - 146 GHz is available for routine operation at room temperature. Studies for the extension to variable temperatures (70 - 500 K) were started. A cryostat system has been designed and ordered for construction. For reference, dielectric data at 300 - 700 K were measured at 10 - 1000 kHz in a recently developed measuring cell. The loss tangent of sapphire was always less than 10^{-3}.

Staff:
M. Blumhofer
W. Dienst
G. Gausmann
Ch. Gosgnach
G. Haase
R. Heidinger
B. Schulz
S. Winkler
H. Zimmermann

MAT 9.2   Investigation of Fatigue under Dual-Beam Irradiation

The Dual Beam Facility of KfK, where alpha-particles (104 MeV) and protons (15-40) are focussed onto a target, was developed as a research tool for materials within the European Technology Programme. This Dual Beam Technique allows the simulation of fusion neutrons by the systematic variation of hydrogen, helium and damage production in thick metal and ceramic specimens as well as Tokamak relevant thermal cycling and mechanical loadings like low cycle fatigue in proposed first wall materials.

1.   Development of the Irradiation Facility

In order to achieve a homogeneous beam density profile, a X,Y-scanning magnet was installed at the 104 MeV alpha-particle beam. Depending on the mode (sinus, triangle, saw-tooth) and the angle of deflection, the scanning frequency can be adjusted up to about 30 Hz. This relatively high frequency avoids fluctuations of temperature within the irradiated specimens. Fig. 35 shows the homogeneity of the beam
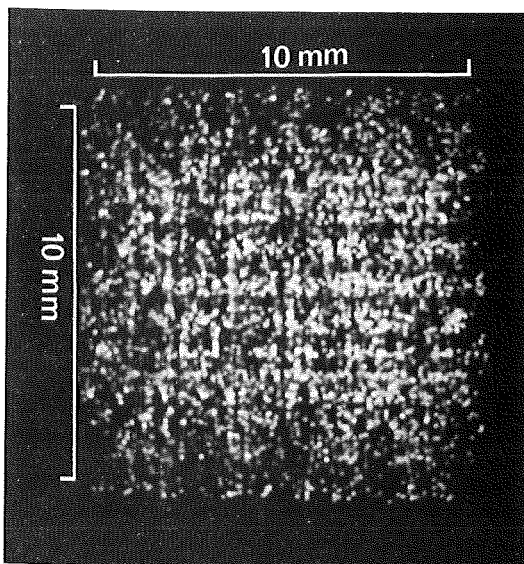
Fig. 35:   beam density distribution of the α-particle beam at the specimen surface.

density distribution within an area of 1 cm². This X,Y-scanning magnet is now successfully in operation and a second one will be built for the proton beam.

The endurance machine (ZWICK 1474) for in-beam low cycle fatigue experiments has been delivered and some Dual Beam specific options were tested during an inspection phase. Now the extensive constructions of the vacuum irradiation chamber with all the beam diagnostic modules, the heating and cooling systems as well as the instrumentation for temperature and strain control are on the way.

2.   Specimen development for In-Beam Low Cycle Fatigue

Whereas H-GRIM-specimens are suitable for many applications, they have to be replaced in future In-Beam-LCF-experiments for various reasons. The necessity to develop a new specimen geometry follows from the knowledge that cylindrical specimens would have to be rotated very costly during the In-Beam-LCF-experiment in order to achieve homogeneous temperature and irradiation conditions. The specimen devised for the non-rotating version has a square cross section, a constant wall thickness within the irradiated gauge length (Fig. 36) and can be fabricated
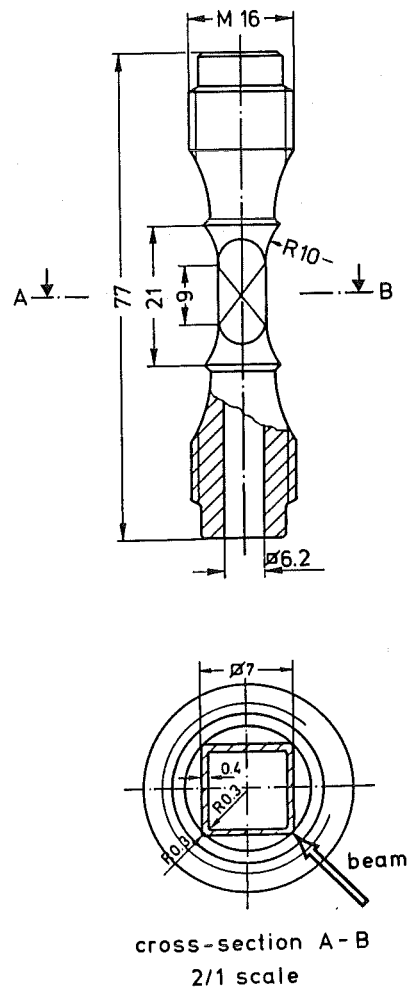
Fig. 36:   Specimen geometry with a square cross section for in-beam-LCF-experiments.

with a roughness of 8-10 μm. The main features of this hollow (H-SQUARE) specimen are:

> good homogeneity of the temperature, implantation and damage profiles without losing the efficient in-wall helium gas cooling.

- Sufficient maintenance of a uniaxial stress distribution as finite element calculations, performed at IMF IV, have shown (N3 this volume).

- Allmost all specimens made of MANET fail at temperatures between 450 and 550°C in the centre of the gauge lenth and their deformation stability is ensured up to local strains of at least 0.9%. This guarantees that all first wall loadings discussed for NET can be investigated.

- The strain amplitudes and the numbers of cycles to failure are all within a small scatter band (Fig. 37). As a
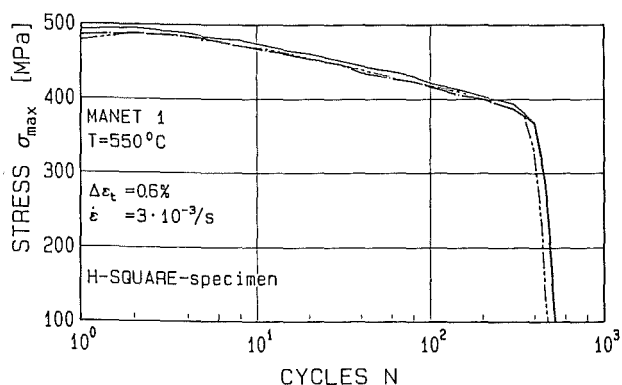
Fig. 37: Three hollow-square LCF-specimens tested at the same conditions showing high reproducibility.

result of this also small irradiation effects should be observed easily.

- Fractographic SEM investigations of LCF-tested specimens show homogeneously distributed crack initiation at large precipitates and crack propagation perpendicular to the applied stress along oscillation bands (Fig. 38). These bands also show that the main crack moves within about 200 cycles through the wall of 400 µm thickness.

- Calculations have shown that the H-SQUARE specimen has a well defined, sufficiently constant strain within the irradiated deformation volume even if the strain controlling extensiometers are pinned 10.5 mm away from the centre of the gauge length. Therefore it is possible with this type of specimen to generate material specific fatigue properties usually measured with solid cylindrical specimens.

3. Postirradiation Low Cycle Fatigue

To investigate the effect of helium and damage on the low cycle fatigue behaviour at different temperatures, LCF specimens (H-GRIM-geometry) made of MANET 1 were irradiated between 300°C and 600°C with helium contents up
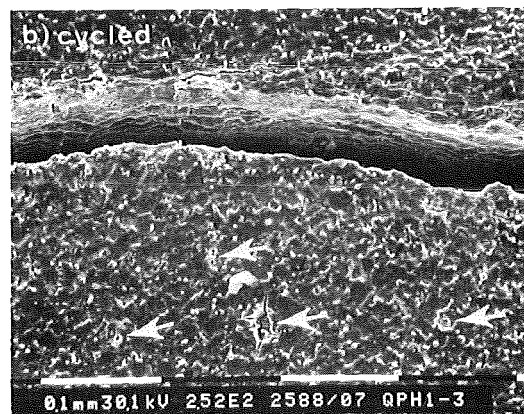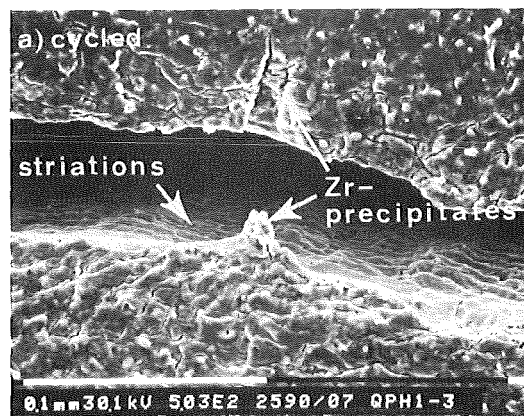
Fig. 38: Zr-precipitates (arrows) near the surface initiate fatigue cracking in MANET 1.

to 200 appm and damage levels up to 1.2 dpa. Strain controlled LCF-tests done at the same conditions show (Fig. 39) that specimens with low He contents irradiated at 450°C tend to increase slightly the number of cycles to failure N_f mainly due to a decrease of the dislocation density, whereas a reduction of N_f is observed in helium-implanted specimens. 65 appm He corresponds to about 70% of the total amount of helium in a first wall (NET 1). The other specimens irradiated at the Dual-Beam-Facility are going to be LCF-tested in the hot cells at test temperatures equal to the irradiation temperature. Parallel to the mechanical tests
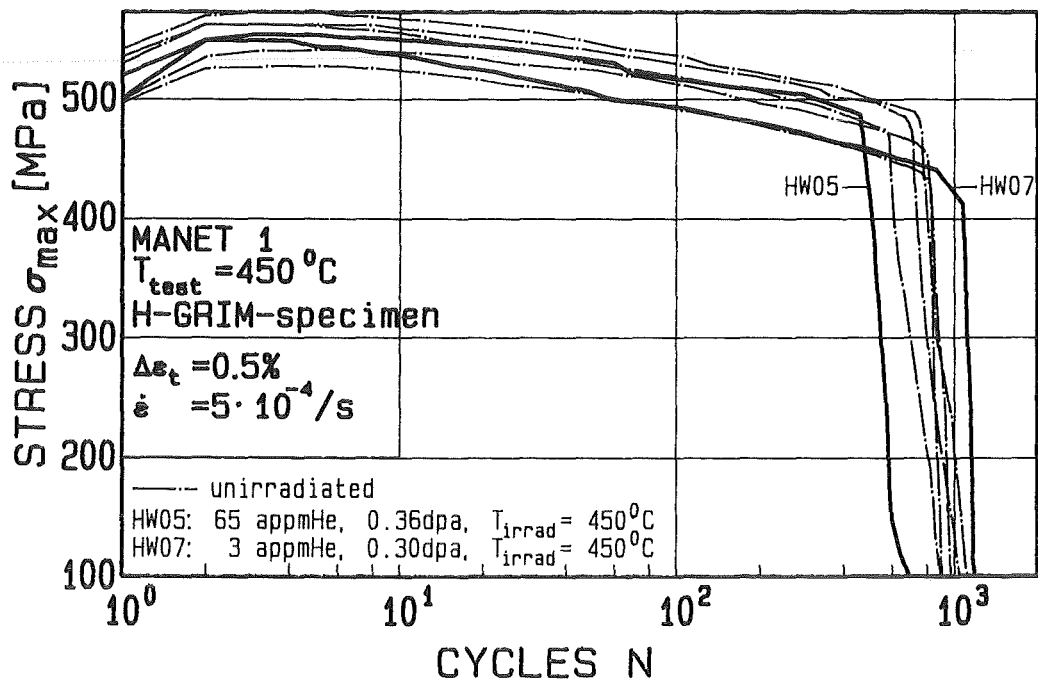
Fig. 39: Maximum tensile stress vs. number of cycles for unirradiated, irradiated and helium-implanted LCF-specimens.

specimen preparation for the transmission electron microscope was developed further to investigate also cylindrical geometries without damaging the microstructure.

Staff:

S. Baumgärtner

G. Bürkle

R. Lindau

A. Möslang

D. Preininger

G. Przykutta

Publications:

[1]   D. Preininger, A. Möslang, K. Ehrlich and R. Lindau

Jahrestagung Kerntechnik '88, May 17-19, 1988, p.691;
ISSN0720-9207

[2]   Patent DE-05 3705 295, 1988

MAT 18   Development of Low Activation Ferritic-Martensitic Steels

First wall and blanket structures of fusion machines will become radioactive during operation what renders more difficult maintenance, recycling or waste disposal. To reduce these problems it is necessary to avoid the presence of certain alloying elements exhibiting unfavourable activation properties. Research efforts underway at KfK on Ce, Ta and Hf bearing chromium steels have been described in recent semi-annual reports (KfK-reports 4165, 4399, 4418 and 4488).

New results have been obtained on the tensile properties between RT and 700°C of the two heats C857 (Ta-Hf) and C 858 (Ce-Ta). After hardening from 1075°C the specimens were tempered 2h at 600, 700 or 750°C. As an example, Fig. 40

The tensile and yield strength data of C857 and C858 are 20-25% below those of the Manet heat whereas the ductility data of these three alloys are rather similar.

Staff:
K. Anderko
M. Schirra
W. Schweiger

Fig. 40:   Tensile properties

shows tensile (R_m) and yield strength (R_{p0.2}) as well as uniform (Ag) and total elongation (A) and reduction in area (Z) of the specimens tempered at 700°C. Also plotted are corresponding data of Manet and of two other heats of the same alloy type (12% Cr + Mo, V, N).

N 1 Design Study of Plasma Facing Components

First Wall Testing

A test program is planned at KfK for testing first wall (FW) sections in order to:

1. Provide an experimental basis to improve confidence in the prediction of thermal fatigue life by:

   (a) Validation of computational methods for

   - thermo-mechanical analysis

   - crack initiation by cyclic plastic deformations

   - fatigue crack propagation

   in complicated geometries.

   (b) Life time determination including

   - observation during life

   - study of failure modes for prototype FW sections under representative thermo-mechanical conditions.

2. Compare integral behaviour of different FW concepts including protection

   The test specimens will be tested under mechanical boundary conditions and thermal loads as close as possible to those of NET.

   The specimen will be positioned in a vacuum chamber; it will be actively cooled with water and will be heated by thermal radiation in a cyclic manner.

Pretesting of the radiative heater as a crucial part of the test apparatus is being continued. Different types of graphite namely carbon fiber composites, finegrained graphite, and graphite laminate of different manufacturers have been tested as resistance heaters in a water-cooled vacuum chamber. Test goal is the qualification of a heater material and a heater geometry for at least 5000 power cycles, corresponding to approximately one week of operation. A typical cycle consists of 60 - 90 s of full power heating (burn time) which increases the temperature of the heater up to a level of 2100 or 2200°C and of a similar time span of near zero power (dwell time) which lets the temperature of the heater drop by about 1000 K. In the tests the heat flux at the heater was in the order of 70 W/cm^2 of the effective heater surface and may be increased if necessary. Up to now three heaters out of a total number of six tested were successful with more than 6000 cycles without failure, their temperature maxima were measured slightly above 2200°C. At the end of each test different degrees of graphite erosion in local areas with the highest temperatures were observed resulting in a somewhat nonuniform heat flux distribution. It seems

that this erosion and its consequences could be strongly reduced by lowering the maximum temperature to about 2100°C. At this time it is concluded from the pretest that graphite should make a suitable heater for the FW test apparatus. Nevertheless the pretest will be continued for more details.

In addition to the heater pretests, an examination of the measurement technique has been carried out. The cyclic thermomechanical behaviour of the test specimens will be controlled by thermocouples and strain gauges. The number of both measuring devices has been determined.

Both measurement techniques will cause local disturbances of the original temperature field and consequently of resulting stress-strain fields and the displacements.

In order to determine the magnitude of the uncertainty inherent in measurement, the temperature field has been calculated by using FEM. Parameters of this investigations are the diameter of the installed TC's, and the position at the point of measurement. Furthermore, calibration tests of instrumented specimen are under way in order to reduce the uncertainties of the resulting heat transfer coefficients. Again by help of the FE-method, the influence of strain gauges inside the coolout tubes has been considered. The heat insulating effect of the adhesive tape will locally disturb the temperature field and, therefore, affect thermal strains, which is the quantity to be measured.

For the main test facility for First Wall Testing at Karlsruhe (FIWATKA) design and procurement of the components are in progress and some components are delivered. The time schedule asks for the facility to be available for testing early in 1990.

Staff:
E. Diegele
E. Eggert
G. Hofmann
B. Schinke
G. Schweinfurther

Divertor Testing

The main design issues for the NET divertor are the high heat flux, the physical and chemical erosion, and the surface damage from plasma disruptions. Current divertor concepts consist of a metallic heat sink structure protected by a heat and erosion resistent surface material. In this douplex structure the major thermomechanical concerns are material compatibility, perfect bonding, temperature limits, and cycling shear stresses due to differential thermal expansion. Preparations for the two year testing program on the thermomechanical behavior of candidate divertor materials by use of a plasma flame as a heat source under NET contract (task PDT 2.1) are nearly complete. This involves fabrication of the rotating sample holder and the plasma gun swivel

mechanism including the programmable drive unit. All components are expected to be delivered and assembled during March 89, so that testing of the monolayer type samples is scheduled to commence in April 89.

Definition of a 300 kW divertor test facility (DIVA) with an electron beam gun as a heat source was pursued and documented in a program draft to be discussed with the NET team. The three year programm covers the design, construction, functional testing, and calibration of DIVA, which must be capable of subsequent thermomechanical and thermalhydraulic testing of representative divertor mock-ups for NET in a flexible way. A crucial question with commerically available electron beam guns of this size is an adequate beam control with respect to focusing and scanning frequency limits and the feasibility of simulating plasma sweeping at the divertor plates. Pretests with an existing electron beam gun at Leybold AG are initiated to answer these questions.

As a contribution to the divertor design an eccentric swirl promoter is proposed as a means to optimize divertor thermalhydraulics. The problem is as follows. The heat flux at parallel circular divertor coolant channels is strongly non-uniform in both circumferential and longitudinal direction, and large portions of the divertor plate receive little heat. Therefore an effective thermalhydraulic layout of the component calls for high flow velocities where needed and low flow velocities elsewhere. The eccentric swirl promoter (Figure 41) promises to meet these goals. It consists of an
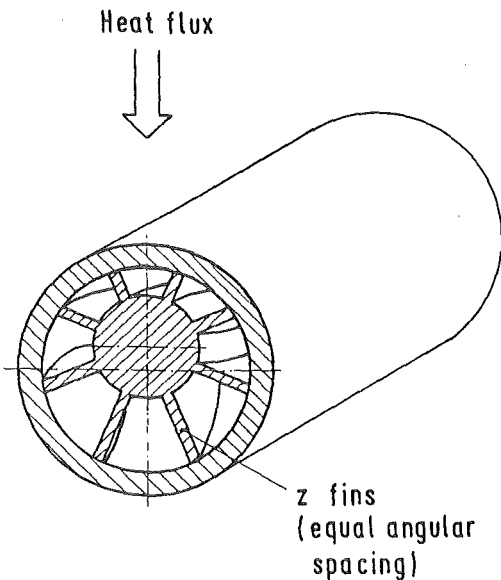
Figure 41: Eccentric Swirl Promoter

eccentrically finned and twisted rod which is insered into the circular coolant channel. This configuration forms small sub-channels (i.e. high velocity) at the heated side and large sub-channels at the opposite side. The flow resistance in each sub-channel and, hence, the mass flow rates are equal as long as the total channel length is a multiple of the twist pitch.

In order to estimate the effectiveness of the eccentric swirl concept a simple thermalhydraulic model has been developed based on empirical correlations for the pressure drop, critical heat flux, and heat transfer coefficient. The application of the model to typical divertor coolant configurations shows the large benefit of the eccentric swirl promoter with respect to flow velocity, mass flow rate, pressure drop, pumping power, and feed line diamter (Table 9). The basis for the comparison

	Design Variant		
	tube with twisted tape	plate with plain chan-nels	tube with eccen-tric swirl
Input:			
Channel diameter, cm	1.4	0.6	1.8
Number of channels[a]	24	48	24
Critical heat flux, MW/m^2	26	26	26
Results:			
Max. flow velocity, m/s	11.4	10.3	2.5
Mass flow rate[a], kg/s	39	14	4.5
Pressure drop, bar/m	1.75	2.1	0.3
Total pressure drop[a], bar	3.5	~ 3.1	~ 0.45
Pumping power[a], kW	13.7	4.3	0.2
Feed line dia[b], cm	13	7.7	4.4
Temperature rise, K	5	13.7	42
Heat transfer coeff. W/(cm^{2}K)	4.9	5	2

[a] per 1/48 divertor sector
[b] at flow velocity of 3 m/s

Table 9: Estimated thermohydraulic characteristics of three divertor cooling concepts

is to obtain the same critical heat flux for all of the three configurations. The heat transfer coefficient, on the other hand, will be penalized. The scheme needs experimental verfication in both thermalhydraulics and technological aspects, e.g., fabrication, fin shape, crevices at the tips of the fins, etc.

Staff:
G. Class
K. Kleefeldt
K. Schramm
E. Stratmanns
E. Wolf

N 3 Development of Procedures and Tools for Structural Design Evaluation

The objective of the investigation is to gain knowledge of computational tools for lifetime assessment in highly loaded components. During the previous period, attention has been focused to

· analyses of inelastic strain fields

· lifetime prediction of ceramic windows.

In low cycle fatigue (LCF) tests usually two quantities are measured, i.e. the total elongation across a gauge length and the total force on the specimen. Some test samples, e.g. GRIM specimens, hollow GRIM specimens (H-GRIM) are of varying wall thickness which leads to axially nonuniform stress and strain fields. Damage of samples is mainly controlled by strains. LCF-results which are obtained from different types of specimen can be compared on the basis of maximum local strains.

A procedure has been developed how to calculate these local inelastic strain fields from the gobally measured variables (force and elongation). The procedure includes cyclic softening and hardening of the material. The method has been applied to GRIM and H-GRIM specimens with different geometries. Additionally, the FE-method is used to calculate cyclic plastic strains for hollow samples, i.e. H-GRIM and H-SQUARE specimens.

The temperature gradients in the microwave window cause thermal stresses and especially in case of ceramic windows the tensile stresses are the decisive factor for the lifetimes. Formulae for the calculation of temperatures and thermal stresses due to dielectric losses are developed. These calculations are the basis for lifetime evaluations for different candidate materials and for an optimization of the design of the window.

In a first step the two candidate materials AlN and Al_2O_3 were compared with respect to temperatures and stresses [1]. The power and geometric data are W = 200 kW, R = 3.5 cm, l = 0.3 cm, v = 150 GHz (Mode TE_{03}), and the physical properties for the "design-point" are summarized in Table 10. By use of these data concrete temperature and stress calculations can be performed. The stationary temperature distributions for Al_2O_3 and AlN are plotted in Fig. 42 for both disc surfaces. The tangential thermal stresses are represented in Fig. 43. From both figures the superiority of the AlN is obvious, since the temperatures are by a factor of about 2 less than for the.Al_2O_3. The maximum stresses are reduced by a factor of 4.

		Al_2O_3	AlN
tan δ		$5 \cdot 10^{-4}$	$5 \cdot 10^{-4}$
ε		10.0	8.27
λ	W/cmK	0.15	1.0
E	GPa	370	310
α	$1 \cdot 10^{-6}$/K	7.6	4.4

Table 10: Physical properties of the candidate materials
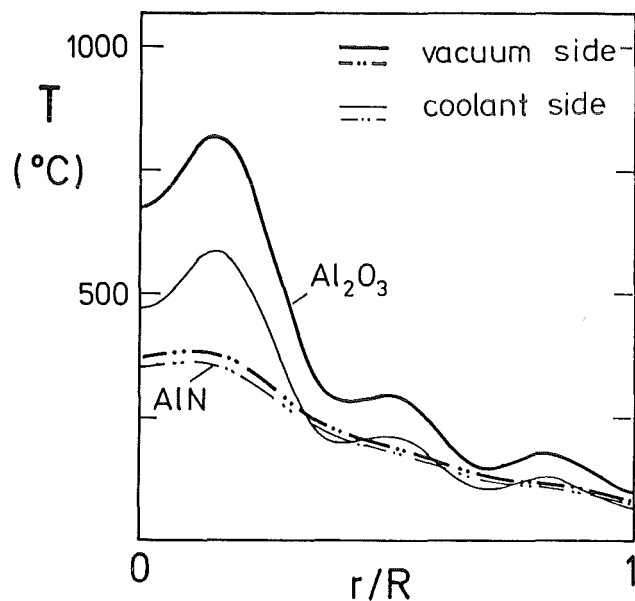
Fig. 42 Temperature distributions in the HF-window (Mode: TE_{03})
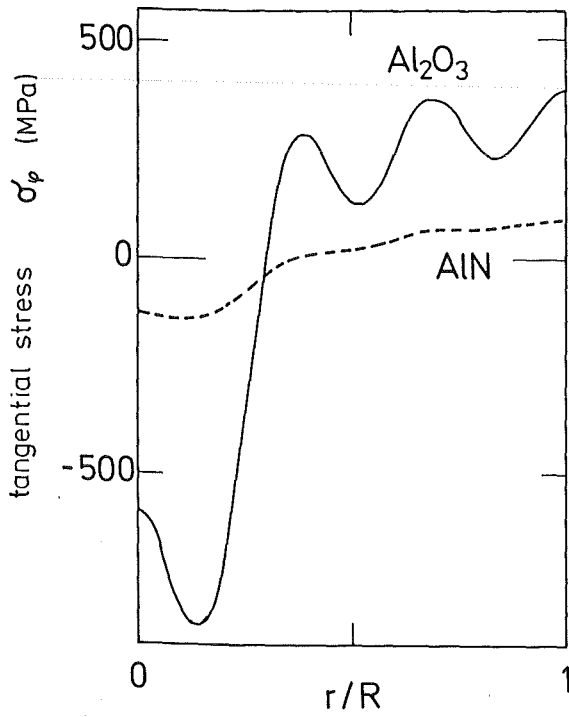
Fig. 43   Tangential stress distributions
(Mode: TE$_{03}$)

Staff:

E. Diegele

T. Fett

D. Munz

Reference:

[1]   T. Fett, D. Munz, "Lifetime predictions for ceramic windows in fusion reactors", 15.SOFT, Uetrecht, 1988.

RM 1   Background Studies on Remote Maintenance

Within the framework of this project, development work is carried out on remotely operated connections to be used in NET. This remote connecting techniques includes connections of all pipes, electric cables, vacuum and cryogenic lines, and also remote cutting and welding.

In the period under review the following main activities were carried out:

1.   Qualification of Electrical Connectors

Work has been started in the frame of a NET contract with the review of the NET-report 201/85. In reviewing this report it was recognized that additional information on remotely operated connectors can be obtained from the design work carried out for fission projects, from results of experimental work at KfK and from extensive inquires on fusion-related experiments. With the additional information it will be possible to produce the first data sheets for standard types in the 2nd quarter of 1989.

In parallel efforts have been put into the investigation of the different types of the screw-version of connectors. This type shows a high potential for further applications and it can be adapted to the remote handling equipment and to the NET environmental conditions.

2.   Qualification of Mechanical Pipe Connectors

A number of pipe connectors for water, vacuum and liquid metal has been selected. The remote handling qualification test of relevant connectors has been started with the KfK types of connectors and the bolted flange connection of the JET-type.

In the test rig FLATEST (Figure 44) the investigation of the soft iron material as a gasket material for liquid metal pipe connections has been continued. The test results will be presented in a first report mid 1989.

A new type of a clamping ring pipe connections has been designed and fabricated. The new type is designed for pipes of > 250 mm diameter.

3.   Qualification of Fluid Connectors

Under this sub-task KfK will indentify the range of fluid connectors to be used as the standard for NET. These connectors will be used for coupling water and pneumatic lines. An inquiry about the state of the art regarding remotely operable fluid connectors and the review of the NET applications has been started.

4.   Qualification of Welded Connections
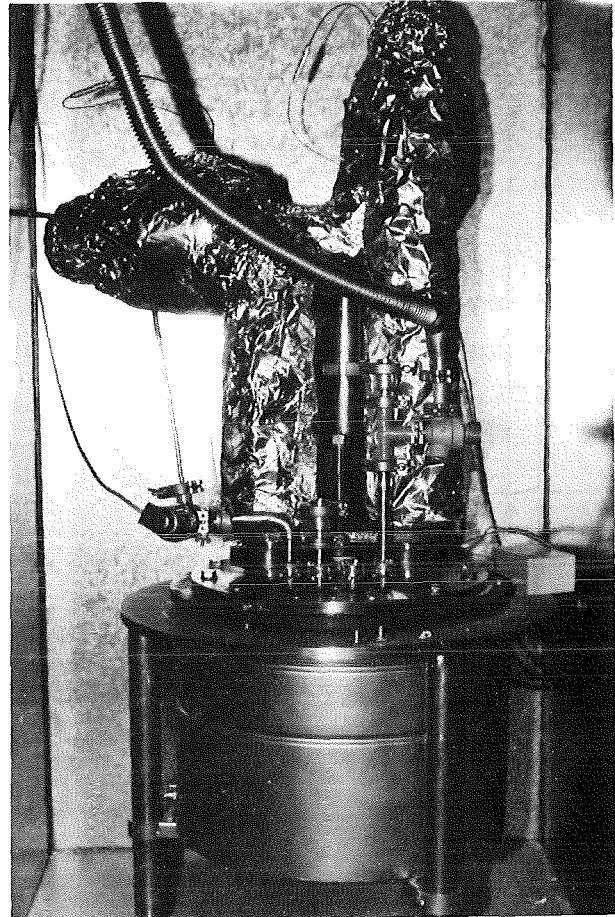
Fig. 44:   FLATEST

The objective of this sub-task is to investigate welding and cutting as potential techniques for joining, pipes, vacuum ducts and closures of the vacuum vessel.

In the period under review, the test rig FEROS was completed and comissioned, fabrication of the lip welding and cutting unit was continued, and the manufacturing drawing of a pipe welding unit for pipes of 100 - 200 mm diameter completed.

5.   Qualification of Cryogenic Connections

Within the framework of this sub-task KfK will investigate connecting techniques for cryo pipes. Work has been started with an inquiry about the state of the art regarding cryogenic connectors and design of cryogenic pipes.

The planning status of the cryosystem and the NET requirements for cryo pipes have been analyzed in cooperation with NET. Results will be presented in a study mid 1989. The draft of the study has been discussed with NET.

6.   Demonstration of Connecting Techniques

The remote handling of pipe connectors and also remote cutting and leaktight rejoining of individual blanket

segments as well as of the complete module can be tested in the BERT test facility erected at KfK.

In the period under review the remotely controlled overhead crane has been commissioned and the pipe-work has been completed.

The handling test started with the crane as a remote handling tool for assembly and disassembly of the pipe intersections in the supply lines of the individual blanket segments (Figure 45).

Staff:

L. Gumb
U. Kirchenbauer
A. Schäf
M. Selig
M. Trettin
R. Ullrich
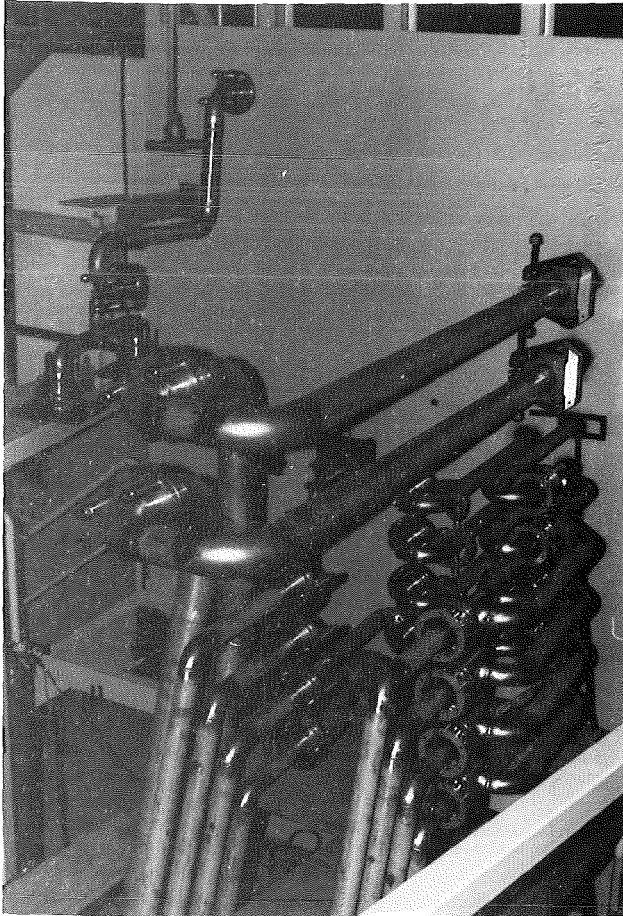
Fig. 45:   BERT

RM 2   Mechanical Component Assembly

In order to provide designers and contractors with information KfK cooperates with the NET team in the preparation of a Remote Handling Manual. It contains a set of General Rules and Design Standards for components and units of the NET device which require remote handling, and settles guidelines for handling equipment design.

Within the frame of the RM2 contract the work was continued with:

- Definition of design standards which have to be taken into account at the design of the device and epuipment

- Proposal of standards for fasteners

- The final report is in preparation

Staff:
B. Haferkamp
A. Suppan

RM 3 Handling Equipment for In-Vessel Components

The investigation of an In-Vessel Handling Unit (IVHU) for inspection, repair and replacement of NET in-vessel components was continued. CEA, CEN/SCK, ENEA, JET, SPAR and KfK cooperate in the development of such equipment. It consists of

- a contained transfer unit (CTU).

- a transport unit based on an articulated boom or an in-vessel vehicle movable on telescopically inserted rails,

- various work units with end-effectors attachable to the transporter, and

- the control system.

Out of the 9 sub-items of the RM3 technology programme the following tasks were carried out.

Sub-task 1: Development of a Conceptual Design

In-vessel handling unit - mechanical design

In agreement with the NET Team and based on the decision of the RM3 workshop in April 1988, KfK has taken charge to develop an in-vessel handling unit (IVHU) up to a prototype based on the system of an articulated boom. The work was continued with the predesign of the IVHU components, as boom, actuators, cabling, transport carrier and end-effector attachment. According to the original NET requirement to minimize the volume for the folded boom the boom design was based on scissor links combined with linear actuators arranged at the upper part of the links [1] and [2]. Always two drive units were actuating in series one link joint.

Within a design review meeting in March 1989 the requirement of minimizing the volume for the folded boom was officially supressed by the NET-Team which offers the possibility to design the boom with symmetrical links, thus increasing the boom stiffness by enlarging the link box cross section, especially the width. Therefore it was decided to re-design the IVHU with respect to the following issues:

- Use of symmetrical links with maximum stiffness.

- Minimization of the number of links.

- Investigation to apply the changed harmonic drive actuators with mechanical and electrical backlash removal which were developed during the last year by JET for their articulated boom.

- Investigation to arrange electrical wiring and cabling in the vertical axis of the boom.

- Optimization of the stress analysis with the aim to increase the stiffness and to reduce dead weight.

The desirable reduction of the end-effector weight requires the investigation of the main maintenance tasks, as divertor plate and protection tile replacement. The investigation has to be based on detailed information from NET about these components and their installation at the NET device.

Structural analysis

The realization of the IVHU as an articulated boom turned out to be a difficult problem. Since most of the load is due to the dead weight, the use of materials with different densities (steel, titanium, aluminium) has been checked.

For an appropiate material selection, different criteria were considered.

One criterion was the minimization of the vertical deflection caused by bending and torsion of the link cross-sections. For a given geometry of the link (length, width, height) the deflection due to the load L (Young modulus E, wall thickness t) is proportional to L/Et. The lowest value is obtained for the material with the highest Youngs modulus which is steel.

The deflection due to the dead weight G (material density ρ) is proportional to

$$\frac{G}{Et} \sim \frac{\rho t}{Et} = \frac{\rho}{E}.$$

Again, the lowest ratio is obtained for steel.

Another criterion is the minimization of the dead weight. It is proportional to ρ/σ_{all} (allowable stress σ_{all}). Here the lowest ratio is obtained for titanium.

The investigation shows, that steel is the most favorable material. Only when a small value for the dead weight is required (small inertia forces) or when the loads of the bearings exceed the allowed limits, titanium or a combination of steel and titanium is a reasonable selection. Figure 46 shows the deflection of the boom for steel, titanium and combinations of steel and titanium.

EDITH-Experimental device for in-torus handling

In order to test IVHU components and to investigate and demonstrate in-vessel maintenance tasks, respectively, KfK has taken charge to construct EDITH. The features of this testbed were described in the last semi-annual report.

With respect to the re-design of the IVHU the specification for EDITH will be changed and a new call for tender will have to be launched.

The flexibility of the testbed EDITH will allow also the investigation of alternative solutions if necessary.

Sub-task 2: Overall Geometry Measurement

For the remote maintenance of fusion machines a surveying system will be needed for measuring the geometry of components outside (ex-vessel) as well as inside the vacuum-vessel (in-vessel).

Ex-vessel surveying

The remote-controlled and CAD-supported surveying system GMS (Geometry Measurement System), developed by KfK, is equipped with two digital theodolites, a laser- and a camera-theodolite, completely controlled by a computer [3]. To show the feasibility of the GMS-draft a prototype system, equipped with a single camera-theodolite is built up presently (Fig. 47). The software needed for the data transfer CAD → GMS and the software for the control of the surveying process is already implemented and successfully tested. During the whole surveying process the operator is guided interactively by the GMS-software.

To support the operator a computer graphic can be selectively superimposed to the TV-picture (Figure 47). This graphical support contains both the wire-frame model of the object and the target points of the theodolite. By this graphical support the operator can recognize easily the positions of the target points.

Up to now the operator has to align the theodolite exactly to the target points using a joystick. To speed up the surveying process the operator can pick the target points with mouse-driven cross-hair lines and the theodolite angles are corrected by the picked pixle coordinates.
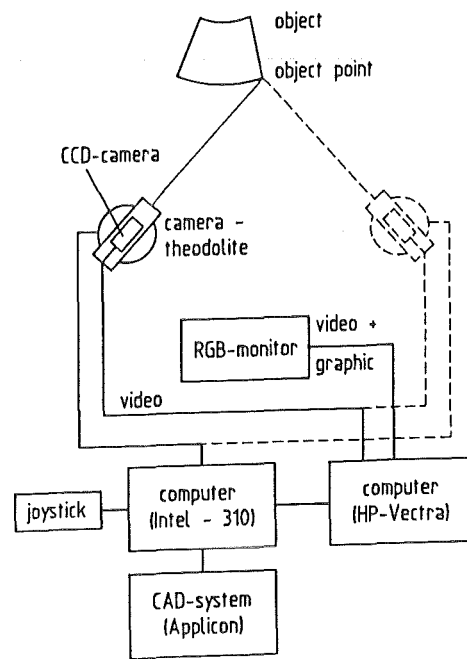
Fig. 47:   GMS-Prototype (Febr. 89)

In-vessel surveying

In order not to break the vacuum, periscopes have to be used for the in-vessel surveying. Based on the experiences with the ex-vessel surveying a first design concept for a theodolite periscope has been outlined [3]; for building up detailed
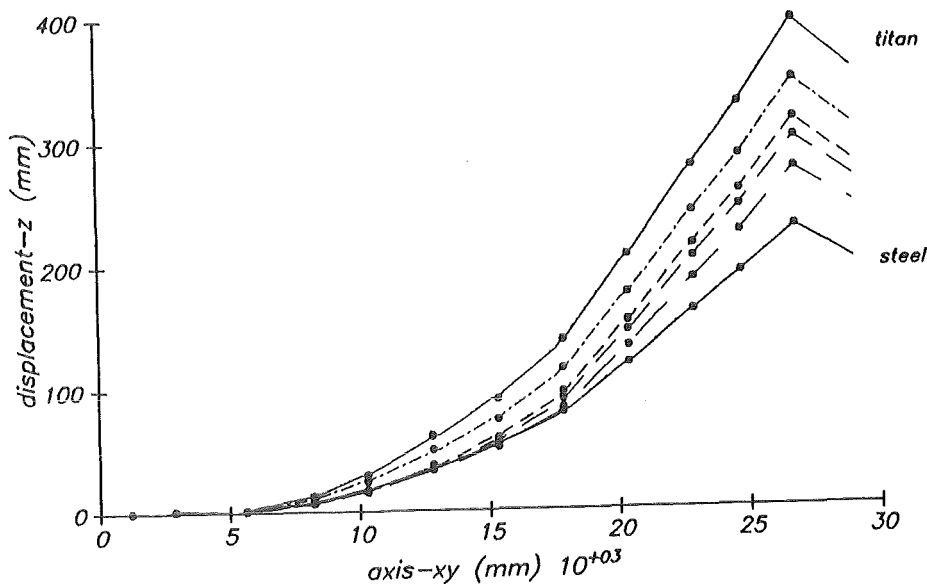
Fig. 46:   Deflection of the boom: Steel, titanium and combinations of steel and titanium

designs definite informations about the in-vessel surveying processes are needed.

Sub-task 3: Boom Position Monitoring

The development of the supervisory control system for NET [4] is concentrated on the detailed design and prototypic implementations of a remote handling workstation (RHWS) as the central tool for the operator. Four subsystems of a RHWS were identified: (1) man-machine interface, (2) spatial simulator, (3) functional simulator, (4) advisor. The RHWSs will be supported by central utilities providing (1) CAD for generation and update of simulation models, (2) model management, (3) resource management, (4) communications, (5) databases for various purposes.

KISMET (KInematic Simulation, progamming and Monitoring Environment for Tele-manipulation) the prototype of a spatial simulation subsystem, was enhanced by special off-line programming features (off-line teaching/simulation and subsequent monitored execution) which were demonstrated in the CATROB experimental site.

Critical work sequences which have to be controlled are the load transfer (e.g.divertor) between carrier and fixture, between carriers or the general procedure of docking. To investigate these problems special experiments with EDITH and in the CATROB test site were planned (EDITH/LT, TELDOCK). The experiments are dedicated to monitoring problems and possible sensor support.

The adaption of the general purpose graphic simulator KISMET to JET ex-vessel remote handling control system is going on. Processors for transfer of CAD-models from the CAD system used at JET (CATIA) to KISMET were successfully implemented and tested. Modelling of the ex-vessel working environment was started by defining the required structure of the model.

The program ROBOT, running in the APPLICON-BRAVO-CAD environment for kinematic design studies and model generation for real-time simulations, is being enhanced to cope with new KISMET features. ROBOT was used for various design studies to support especially the mechanical layout of EDITH.

Dynamic simulations

For the dynamic simulation of the NET-IVHU the dynamic analysis software ADAMS is used. This software has been embedded into the AMBOSS environment containing ADAMS itself, the APPLICON BRAVO3 CAD system and supporting software for pre and post processing of needed data.

The ADAMS code reads a text file describing the kinematic and dynamic properties of the mechanism. These are mass properties of the parts, joint and force data and data to control simulation and out put. The equations of motion are set up using the Lagrange formalism. Constraint equations,

user defined forces and differential equations are added. The solution steps forward with finite differences. Each time step the equations are solved by a Newton-Raphson iteration.

The MECHANISM subsystem inside the CAD system serves for editing the kinematics of the manipulator for ADAMS. Mass properties and inertia data are taken from solids modelling and analysis. The AMBOSS preprocessor assembles the simulation data. Modules containing detailed models of the actuator and deflection behaviour are put together. ADAMS user subroutins are compiled and linked. After the simulation run the AMBOSS post-processor prepares the results to be read by the CAD-System. Inside CAD result configurations and animated pictures are drawn.

A simple simulation of the JET boom was done to verify the method and to learn the program's behaviour. Data and modelling were taken from JET.

Rigid links are connected by revolute joints. The actuators are modelled with a motor part coupled to the link by a spring (gear stiffness). Between the motor and the other link the actuating torque acts. The joints are controlled by a PD-controller. In Fig. 48 the joint angle at joint A1 is compared
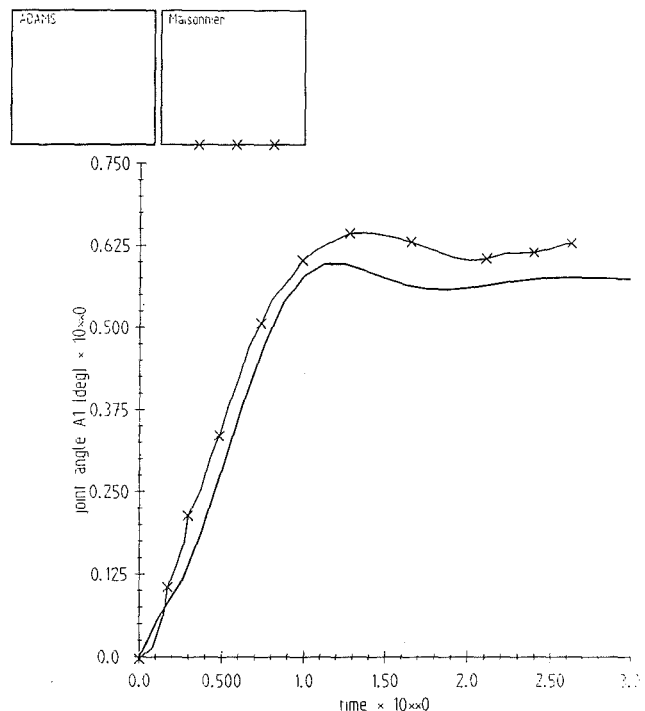
joint A1 PD-controller. A2. A3 not actuated

Fig. 48:   Comparison with JET-simulation

with results by JET. Simulation was done for a step change of the rated joint angle at joint A1, while the other joints are not actuated.

The dynamic simulation of the IVHU has been started modelling EDITH. This model will be verified by

experiments and can give precise results for the NET-IVHU. During the first phase some details were examined and written into modules called by the preprocessor. These details are backlash and gear elasticity, static and load dependent friction inside the worm gears and deflection of the links concentrated in Finite Element beams at both ends of the link.

Geometrical data was put into CAD. The mass properties were computed and the mechanism was edited in the MECHANISMs interface. Figure 49 shows the configured model in the mechanisms interface. The edited data is joined with the modules containing simulation details.

Three parts belong to the actuator model. These are the motor fixed to the link by a joint, the nut of the linear actuator driven by the motor, and the spindle of the actuator fixed at the joint lever. The detailed actuator model for one actuator is shown in Figure 50. The friction torque in the actuator acts as payload on the motorshaft. The work ist transmitted to the joint by the axial force in the linear actuator. This force takes into account the backlash and electicity of the gears.

Position and servo control are realised with differential equations representing a PI respectively PD-Controller. Further a feed-forward algorithm is planned.

This mechanism has been tested at a single joint model with test data describing backdrivability and non-backdrivability. The EDITH model with four actuated links and control algorithms are just in the test phase.

Sub-task 8 & 9: Environmental Conditions

The activities in this area were concentrated on the preparation of the radiation hardening tests with commercially available sensors which may be applied to the NET-IVHU. Based on the expected severe temperature and radiation environment conditions a restricted number of resolvers and inclinometers was selected and ordered. The design for an irradiation test-rig equipped with two multi-turn resolvers presently being acquired uses a pneumatic drive in order to set the resolvers on two pre-defined angular positions, allowing on-line measurements during the irradiation campaign up to one Giga-rad total gamma dose. All irradiation tests will be performed at the BR-2 reactor starting within the second half-year 1989. Moreover, the objective is to verify the gamma compatibility of multi-wire cables and connectors to be used ascontrol and signal cables for all resolvers and further sensors for the remote maintenance task.

References:

[1] Suppan, A., Hübener, J.: Investigations of In-Vessel Handling Concepts for NET, IAEA Technical Committee Meeting on Robotics and Remote Maintenance Concepts for Fusion Machines, Karlsruhe, 22.-24.2.1988

[2] Suppan, A., Hübener, J.: In-Vessel Handling Unit Concept for NET, 15th SOFT, Utrecht, 19.-23.9.1988

[3] Köhler, B.: GMS - a high-precision Geometry Measurement System for large fusion reactor components, and Remote Maintenance Concepts for Fusion Machines, Karlsruhe, 22.-24.2.1988

[4] Leinemann, K.: Supervisory Control System for NET: Remote Handling Workstation, Motion Controller, Central Utilities. Unpublished Report of KfK, November 1988.

Staff:
I. Aberle
B. Bartholomay
H. Breitwieser
E. Holler
B. Haferkamp
J. Hübener
D. Klein
H. Knüppel
B. Köhler
I. Kornelson
R. Krieg
U. Kühnapfel
K.H. Lang
W. Link
K. Leinemann
A. Ludwig
M. Mittelstaedt
G. Müller
S. Müller
J. Reim
W. Pleschounig
H.A. Rohrbacher
E.G. Schlechtendahl
P. Schultheiß
U. Süss
A. Suppan

universal joint

loc. axis

center of
gravity and
inertia symbol

marker to
define the
reference frame
of the link's
stiffness matrix

worm gear screw

joint lever

worm gear nut

motor

link
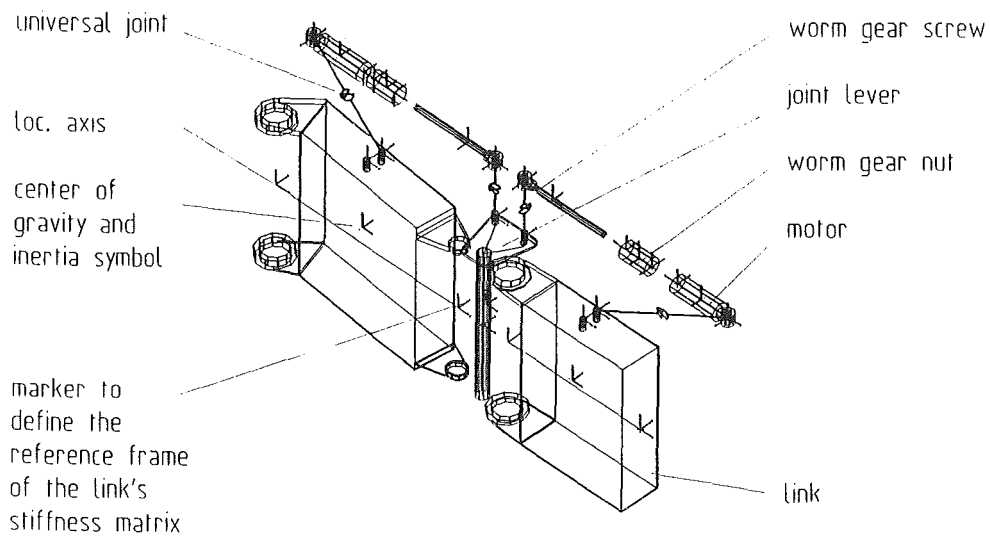
Fig. 49: IVHU joint edited with MECHANISMs interface

Symbols

Im	Inertia of the Motor Shaft	Tm	Motor Torque	Vl	Angular Velocity of the Link
Il	Inertia of the Link	Tl(i)	Torque at this joint	Al	Joint Angle
s	Length of the Wormdrives' Lever	Tl(i-1)	Torque at the next Joint	W	Debit Joint angle
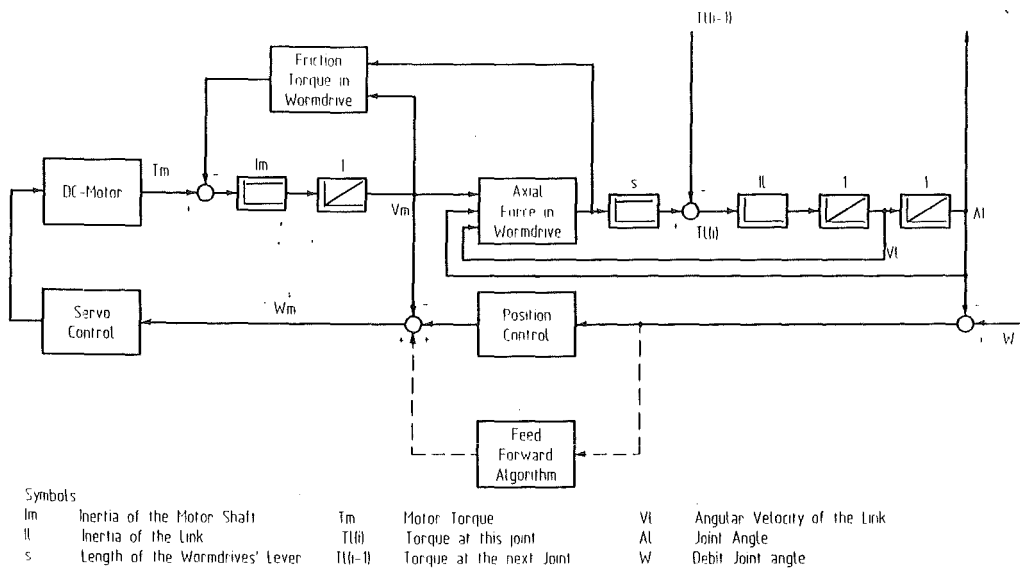
Fig. 50: Dynamic simulation of IVHU with linear actuator

4 Pneumatic Pipes
for Resolver Drive

Signal - and
Control Cables

Resolver Drive

160

Resolver „1"

110

400

Resolver „2"

110

Resolver Drive

190

[Mrad/h]

Gamma Flux
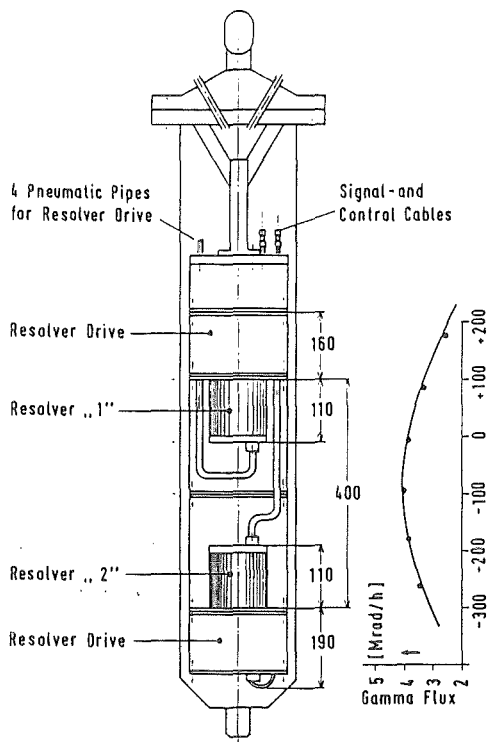
Gamma Irradiation Test rig for NET IVHU Resolvers

Fig. 51: Gamma irradiation test

S + E 4.1.2   Safety Aspects of the
                Cryosystem

Under this task safety aspects of the cryostat of NET are investigated. The cryostat surrounds the toroidal plasma vessel and all superconducting coils as well. It has to maintain high vacuum conditions. The cryostat vessel considered here is the original version of a thin shell structure under outer pressure loading. To guarantee the integrity of this vessel its complicated buckling behaviour has to be studied for normal and accident conditions.

In order to facilitate this investigation a simplified strategy [1] to calculate the buckling loads has been developed. To assess the calculational results buckling experiments for cylinders under outer pressure load have been performed. For practical reasons the first experimental and calculational results reported earlier [2] have been gained from long cylinders (h/d = 1.37; h = cylinder height, d = diameter) where the influence of imperfections is relatively low.

Then in a second step short cylinders with an h/d ratio of 0.36 characteristic for the NET-2-2a cryostat design have been investigated. Tab. 11 gives measured and calculated results for a cylinder whose buckling behaviour had been investigated several times using an internal mandrel to prevent buckling damage. Nevertheless the gap width of 0.5 mm between the shell and mandrel could not avoid a certain amount of plastic deformation leading to increased imperfections for the following experiments. Owing to this different imperfection values a part of the imperfection sensitivity curve could be experimentally determined. The calculated effective imperfection values of Tab. 11 are the amplitudes of those modes which turn out to become buckling modes.

Fig. 52 shows the imperfection sensitivity curves calculated by the simplified strategy for the long and short cylinders together with the measured values of short ones. The imperfection sensitivity of the short cylinder turns out to be rough-
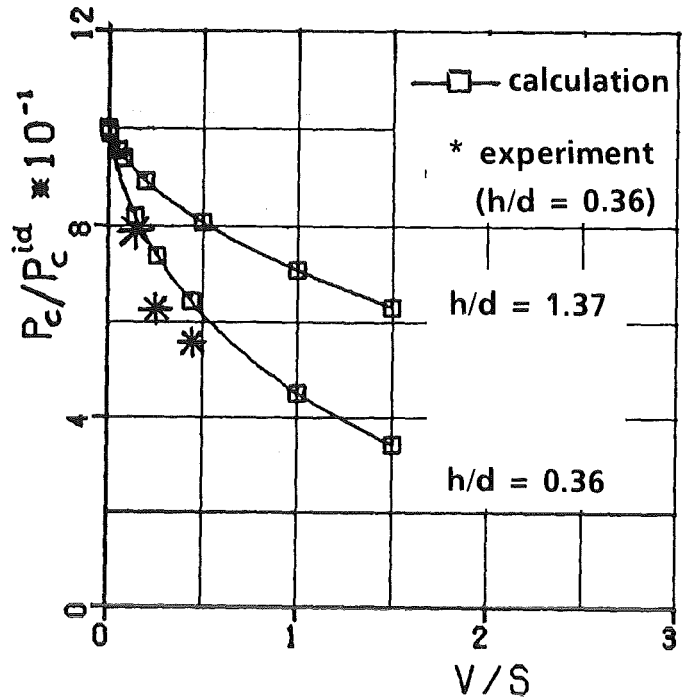
Fig. 52: Imperfection sensitivity of cylinders of different
          length under outer pressure load
          (height/diameter ratios h/d = 1.37 and 0.36)

ly twice that of a long cylinder. An imperfection amplitude of half the wall thickness will reduce the buckling load of a short cylinder by nearly 50 %. The deviations between measurement and calculations are in the order of 10 to 20 % which is a quite satisfactory result.

For the buckling behaviour of the cryostat design the cutouts will have some importance. Therefore long and short cylinders with different numbers of cutouts have been experimentally investigated. Fig. 53 shows the buckled shapes of long cylinders with two and eight cutouts compared to one cylinder without cutouts. One interesting result has been that for these tests there is a strong correlation between the positions of the cutouts and the outer buckles: the cutouts

Tab. 11   Measured and calculated buckling load values for short imperfect cylinders under outer pressure load
           (cylinder BZ21, diameter = 255 mm, length = 93 mm, wall thickness = 0.265 mm)

number of measurement	measured buckling load P_c^m [bar]	rel. imperfection amplitude v/s*		calculated buckling load P_c^{cai} [bar]	$(P_c^{cai} - P_c^m) / P_c^m$ [%]
		total	effective		
4.11.88	0.62	0.25	0.14	0.64	3
15.11.88a	0.48	0.30	0.26	0.57	19
15.11.88b	0.43	0.45	0.44	0.50	16

* v = imperfection amplitude
   s = wall thickness
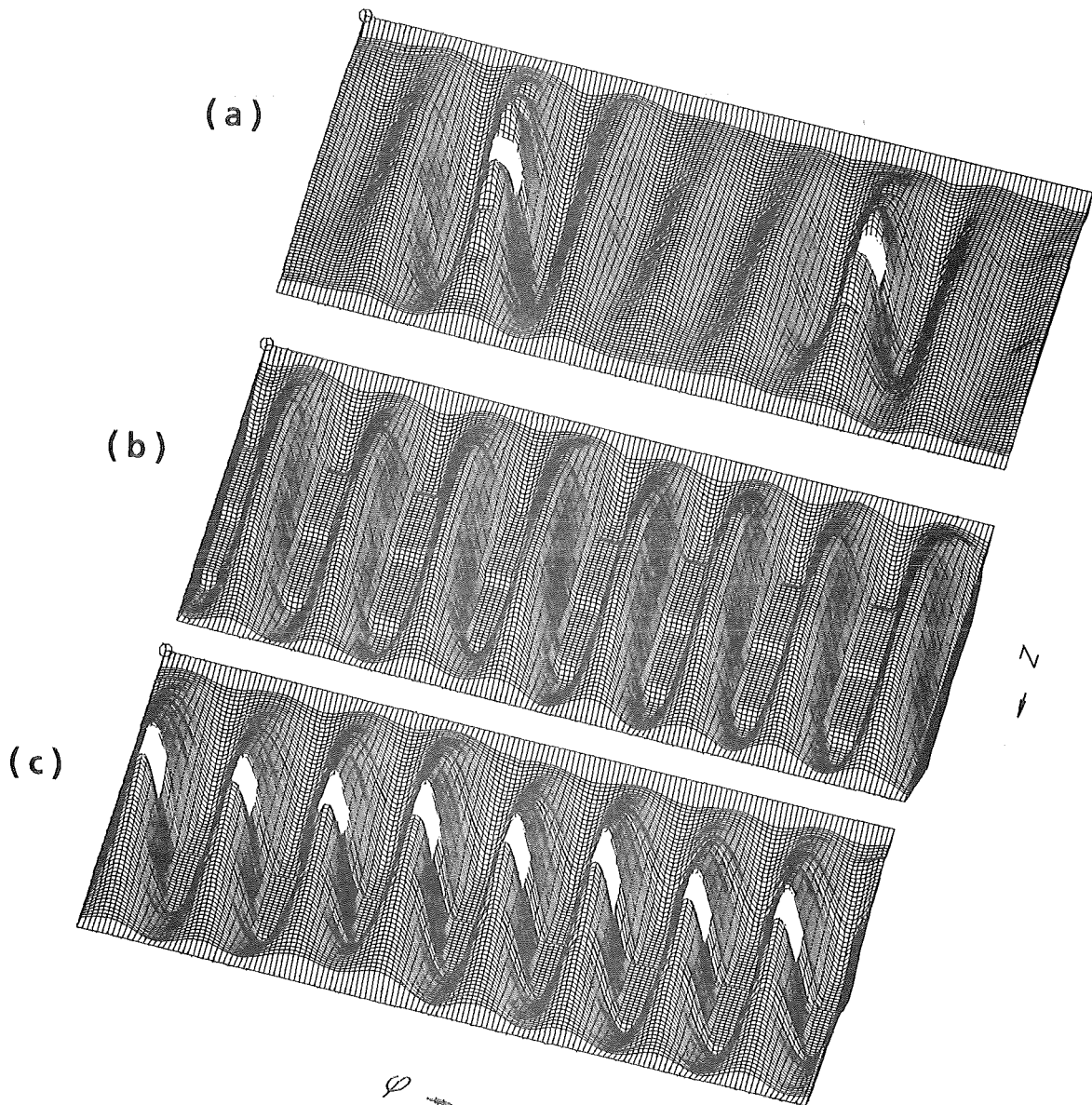
Fig. 53: The influence of rectangular cutouts (a: two, b: no, c: eight cutouts) on the buckling behaviour (long cylinder)

always are on the outer buckles, although they had been cut at circumferential positions where the cylinder formerly had inner buckles. Therefore it can be concluded that the cutouts have a stronger influence on the positioning of the buckles than the geometrical imperfections.

Fig. 54 shows the results of a similar study for short cylinders. In the case with only two cutouts, the same effect of buckle positioning is observed as above. But contrary to the long cylinders with several holes it was taken care to avoid a cutout number correlated to the mode number of the circumferential critical buckling mode. Therefore instead of eight the cylinder had only six cutouts and the question was whether this number would influence the buckling mode and where the buckles would find their positions. The result can be seen in Fig. 54. The cutouts could not change the critical mode number. But they did disturb slightly the regularity of the buckling pattern just to find a position on an outer buckle.

An important consequence of this behaviour is that properties of symmetry for the buckling behaviour are not governed in any case by the regularity of cutouts but rather by the critical buckling mode. This has to be taken into account in buckling calculations for complex geometries like the cryostat vessel where symmetry conditions are used in order to reduce the high amount of degrees of freedom.

Since a new cryostat design using a massive concrete vessel is recently favoured by the NET Team the buckling investigations for a shell type cryostat will not be continued. However, the general simplified procedure for elastic buckling analysis may be applied to other buckling problems, e.g. the central vault of the toroidal coils.
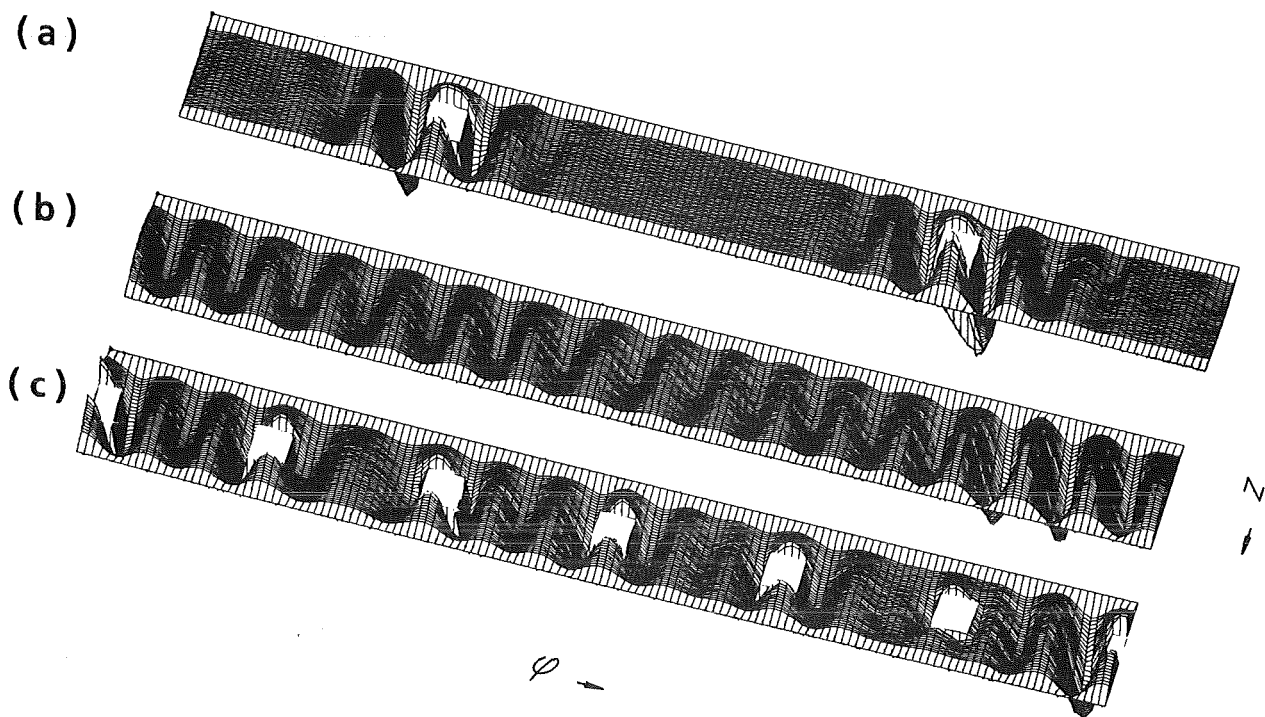
Fig. 54: The influence of rectangular cutouts (a: two, b: no, c: six cutouts) on the buckling behaviour (short cylinder)

References:

[1] S. Raff, B. Dolensky, R. Krieg 'A simpliefied procedure
for elastic buckling analysis'
Transactions of the 9th SMIRT, Vol. B, p. 569-574,
Balkema Rotterdam, Boston 1987

[2] Nuclear Fusion Project, Semi-Report of the Association
KfK/EURATOM, April 1988 - October 1988, p. 62
Staff:

B. Dolensky
R. Krieg
T. Malmberg
S. Raff
E. Wolf

S + E 4.1.3   Safety Aspects of Superconducting Magnets

During operation of superconducting magnet systems disturbances are conceivable which could finally result in the destruction of a magnet. The energy discharged thereby into an electric arc may lead to damage of the surroundings of the magnet. Cause and course of the disturbances, their detection and identification as well as their possibly destructive consequences are to be investigated using the superconducting torus arrangement TESPE-S. Through development of codes and their verification on the TESPE-S experiment an attempt will be made to transform the results to larger magnet systems.

The investigations of arcs supplied by the magnet's energy were continued concentrating on arcing under spatial restrictions like in magnet windings. The earlier experiments with arcs burning within confining chambers, thereby simulating the conditions inside a coil, were continued with a chamber which simulates forced flow windings still closer: Pieces of the LCT-superconductor were used for arc electrodes inside the chamber, the massive copper wall of the chamber was to represent heat capacity of the winding pack, and inserted sheets of stainless steel act as the conductor case material. The influence of the actual helium volume inside windings on pressures increase and arc behaviour was investigated by applying various lengthes of conductor or attached tubes. Arcs with initial currents between 500 and 2000 A were studied. The limitation of 2 kA, which is much lower than the coil operating currents used in the LCT experiment of more than 10 kA, was chosen because the essential properties of the arc can be studied while the destruction remains moderate enough to allow the required conclusions. Burning voltages were found to appear near 80 V, typically. The maximum pressure build-up reached 20 MPa and occurred when both conductor ends were closed by melting. The pure pressure influence on the burning voltage is estimated with 20 V. The observed transient voltage increases up to 200 V are attributed to a lengthening of the arc which results from the expanding gas flow during pressure rise.

In case of vertical arrangement of the chamber, simulating the vertical part of a coil, and for high arc currents a shift of electrode material occurs. Molten metal from the upper pole accumulates on the lower pole and may block the cooling channels of the superconductor. By a coil wound around the arc chamber a magnetic field of 0.1 T was applied transverse to the burning arc. Even this rather small field moves the arc against one chamber wall and produces a considerable asymmetry of the melting process. These results led to the decision to add an experiment with higher field of 3 - 4 T. The corresponding arrangement is under construction. Further it is planned to include experimental and theoretical magnet safety investigations in future magnet test arrangements of the institute (POLO, TOSKA-U).

In continuation of safety and reliability related analyses of superconducting magnet systems two lines were followed: system analyses were performed and the required data base has been improved. The first activity was a contribution to the extension and completion of the reliability data base. As a large variety of data in the field of fusion reliability is not available yet, data from other sources have to be taken as a basis for the reliability analyses. The second activity was a first assessment of the switch down mechanisms of the POLO test arrangement. As a consequence of different operation conditions and operation modes several switch down mechanisms of POLO are available. For the interactions of the switching mechanisms and for the reliability and safety of the switch down functions, first estimations have been started.

Reference:

J.S.Herring, K.P.Jüngst, J.L.Jones and H.G.Kraus:'MSCAP Simulations of TESPE Magnet Safety Transients', 8th Topical Meeting on Technology of Fusion Energy, Salt Lake City, Utah, 9-13 October 1988

Staff:
P. Duelli
K.P. Jüngst
H. Kiesel
H. Kronhardt
G. Obermaier
M. Oehmann
H. Schnauder
J. Seibert
E. Süss
A. Wickenhäuser

S + E 5.5 Development of Safety Guidelines for the Design of NET

Within the frame of a working group safety related re-commendations for the design are elaborated. The aim of these recommendations is to ensure advice to the NET Team on safety and environmental questions. The members of the working group stem from CEA, ECN, JRC-Ispra, KfK, RisØ National Laboratory, The NET Team and UKAEA.

During an informal meeting together with the chairman of the S + E-Expert Group in September 1988, the following was concluded:

Two draft documents on Confinement and on Non-Ionizing Radiation should be reviewed and issued as soon as possible. The discussion how to procede with the future work of the group should be interrupted by a pause of about half a year. This time could be used by a new safety liaison engineer within The NET Team to identify the designers' interest and the need for new tasks. Probably, these tasks will focus on specific guidance for the design of different systems of the plant.

Staff:
W. Kramer

**S + E 7   Generic Environmental Impact
               Assessment for a Fusion Facility**

The atmospheric dispersion model for tritium transport in
the environment (MOTTE) has been completed and applied
for first assessments within an ITER benchmark exercise.
Releases of HT and HTO, their deposition and the reemission
of HTO are considered in the calculations. The dispersion of
HTO after reemission is modelled by a multi-source
approximation. The present work concentrates on the
coupling of MOTTE to the tritium foodchain model COMA to
allow dose assessment including ingestion pathway.

In parallel, the program system UFOMOD has been used
within the ITER activation product dose benchmark
proposed by Y. Seki. Deterministic as well as probabilistic
calculations have been performed. Future work has to extend
the nuclide list of the ingestion module of UFOMOD to
consider all relevant activation products.

Staff:
J. Ehrhardt
I. Hasemann
W. Raskob (DTI)

T 6   Industrial development of large components for plasma exhaust pumping

On behalf of the Commission of the European Communities (CEC) a working group of CEA and KfK staff members are elaborating the specifications and are conducting development work on large vacuum components for NET. Two alternative solutions for plasma exhaust gas pumping are being pursued in parallel: mechanical pumps and cryopumps. The large components required (high vacuum pumps, forepumps, and valves) are not commercially available at present. They must be developed for operation in a fusion machine. Since January 1989 work on this subject has no longer been continued under task T6 but under individual NET contracts.

Gate valve ND 1500 mm

The results of the feasibility study on an all-metal valve satisfying the requirements of NET operation have been compiled in a final report prepared by VAT, Haag. The technical concept for isolating the divertor channel with respect to the vacuum evacuation system provides for a swinging gate with double sealing (see Fig. 56). The valve, ND 1500 mm, is made as an all-metal valve.

After analysing the various sealing systems the VAT ring concept was selected as the optimum solution. It comprises a metallic sealing ring arranged between the conical surfaces of valve disc and compression element. While the valve is closed the ring contacts the conical surfaces and generates circular sealing lines. The sealing ring is so flexible, that it compensates the deformation caused by the sealing force and thermal expansion . It rolls on the sealing surfaces without producing wear and plastic deformation. The sealing ring is coated with noble metal in order to inhibit cold welding with contact surfaces made of stainless steel. The valves previously built with VAT ring seals attain leak rates < 5 x 10^{-10} mbarl/s. Therefore, it can be anticipated that the specified single leak rate of 10^{-6} mbarl/s does not constitute any problem for the 1500 mm ND valve after 1000 closing cycles under clean conditions.

A drawback of the sealing system is its sensitivity toward dust particles. To protect the sealing surfaces a dust protection device has been integrated in the compression elements. It closes the opening giving acces to the valve disc while the valve is open and covers, at the same time, the sealing surfaces. The change of the leak rate in the valve sealing under the influence of dust particles can not be predicted without extensive field tests. Should the single leak rates diminish as a result of dust impact the volume between the valve sealings can be exhausted through two 400 mm diameter flanges. A volume rate of 500 l/s can be pumped through each flange.

Valve opening and closing are done pneumatically by a pendulum movement around a pivot pin. The valve disc is hinged to a fork at three points. After introduction into the closing position the conical sealing surfaces of the external compression elements are pressed from both sides to the valve disc using metal bellows. To open the valve the compression cylinders are exposed to compressed air in direction of the opening. After returning of the two compression elements the valve disc can be swung out. The compression cylinders are so dimensioned that opening is possible against a differential pressure of 1 bar. Both compression elements are moved by 24 compression cylinders distributed along the perimeter. The compression cylinders made as all-metal cylinders are a novel development. . A cylinder which was coated with Molykote R321 attained 60,000 cycles in the test run without remarkable wear on the sliding surfaces.

The hybrid bearing in the pivot point of the pendulum consists of dry running radial and axial bearings which are compatible with the UHV. Stainless steel is the material envisaged for the bushings of the bearings. The roll bodies are made of Si_3N_4 balls. In trials with a dry running axial bearing guided on three Si_3N_4 balls 5000 cycles of movements were attained without noticeable failures in performance. The bearing was exposed to an axial load of 1500 N and heated twice to 250 °C over 12 hours.

The time required for opening and closure, respectively, is 60 seconds. The valve can be baked up to 250 °C both in the closed and opened positions. The lifetime of 1000 cycles is limited by the metal bellows. Making these metal bellows longer could allow a greater number of closure cycles to be attained.

Practical experiences have been accumulated with variants of up to ND 400 mm. The strength analysis involving the finite element programme FLASH shows that this system can be applied to ND 1500 mm as well. The individual network zones of the valve housing are evident from Figure 55.
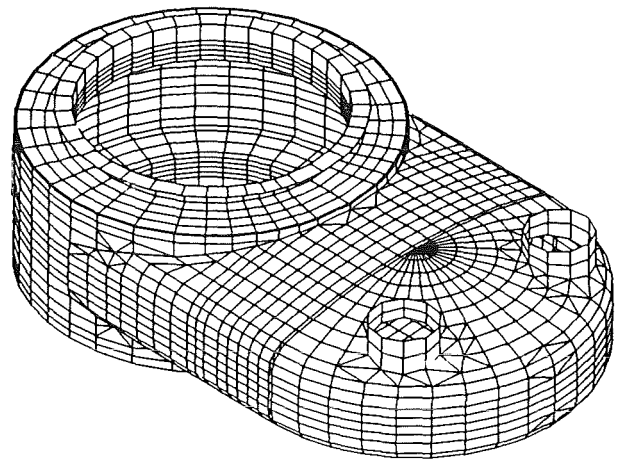
Fig. 55: Finite element net configuration of the valve housing

The analysis was made on the following assumptions of load impact:

- Valve closed, 1 bar differential pressure on the valve disc, housing evacuated,temperature 250 °C.

-Valve closed, 2 bar differential pressure on the valve disc, housing evacuated, temperature 250 °C.

-Valve closed, 1 bar differential pressure on the valve disc, housing at 1 bar absolute pressure, temperature 250 °C.

-Valve open, housing at 1 bar external or internal differential pressure, temperature 250 °C.

The computations were made referring to the guidelines applicable to pressure vessel equipment (German vessel code). In none of the load cases indicated before the admissible stress was exceeded.

The result of the feasibility study is that an all-metall valve, 1500 ND, can be technically implemented under the NET conditions. In the finalizing comments of the study a prototype is offered which could be built within 2 3/4 years and be available afterwards for test runs under NET-conditions.

Staff:
A. Mack
D. Perinić
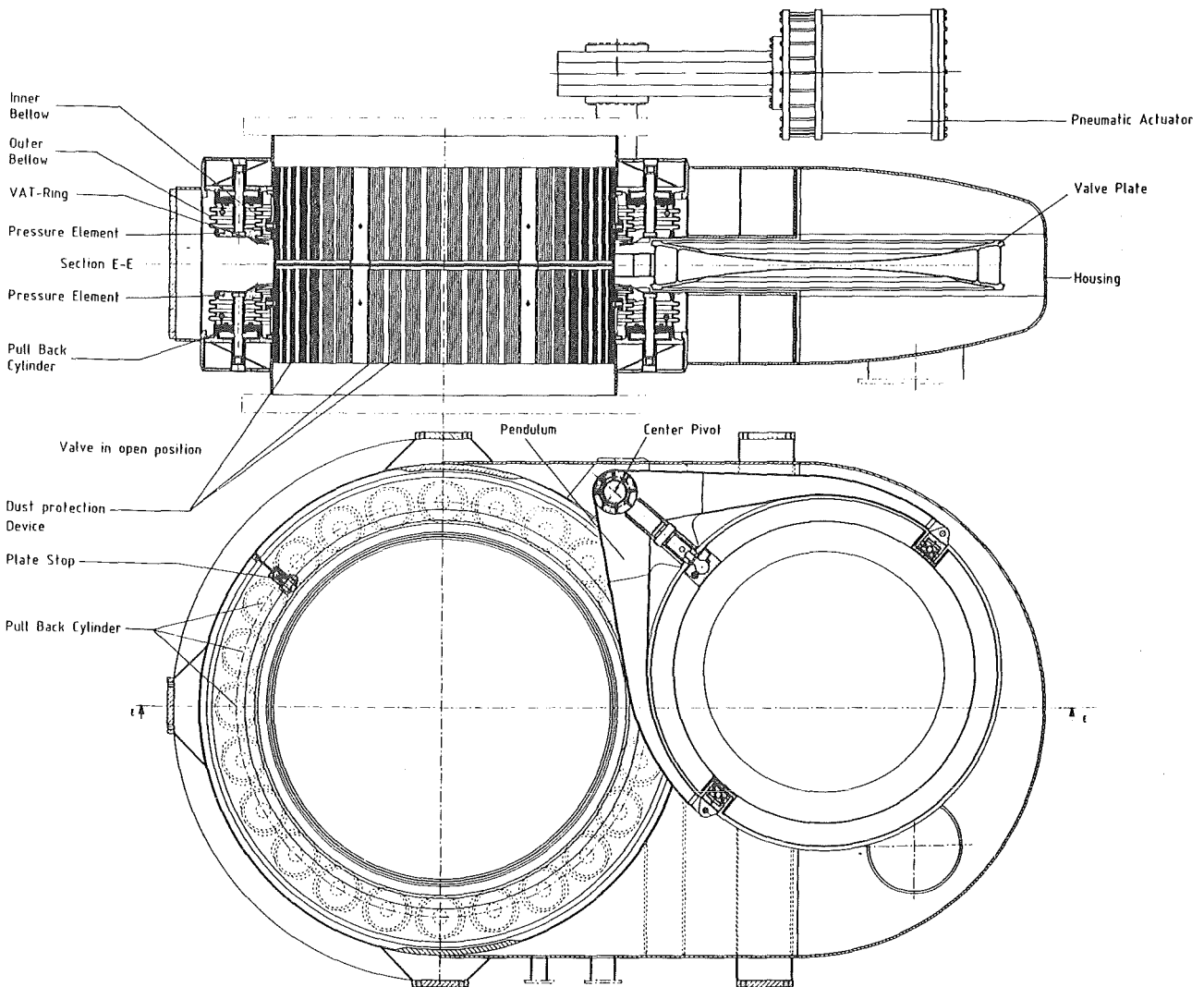
Fig. 56: Cross - sections of the all-metal gate valve ND 1500 mm

T 7   Optimization of cryogenic vacuum pumping of helium

The objective of this task is the development and optimization of cryogenic vacuum pumping of plasma exhaust including helium. To develop cryosorption panels a variety of eligible material combinations for helium cryosoption will be tested on a reduced scale. The best suited technical solutions will be optimized on a technical scale under simulated NET operation conditions. The result of the investigations will be design data and operation requirements for the compound cryopumps to be used in the plasma exhaust pumping system of a fusion machine.

Results of the capacity measurements with the C25 activated carbon at the HELENE testing facility

In the HELENE testing facility for sorption capacity tests, degassed sorption specimens of 50 mm diameter are exposed to gaseous helium at 4.2K. The adsorbed volume of helium (the helium capacity) can be determined with the help of pressure measurements performed at 4.2 and 300 K above the sorption specimen. The general layout of the facility is visible from Figure 57. After completion of the zero measurements for the two specimen holders (AR I and   AR II) a test series was carried out during which the influence was to be studied of the most different bonding materials on the capacity of one single sorbent.

Legend:
GS Gas supply
HK Helium cryostat
HP High vacuum pump
LHA Helium removal
LHe Liquid helium
LHV Liquid helium supply
LN Liquid nitrogen
LNA Nitrogen removal
LNV Liquid nitrogen supply
P   Pressure measuremen
SH Specimen holder
T   Temperature
VP Vacuum pump
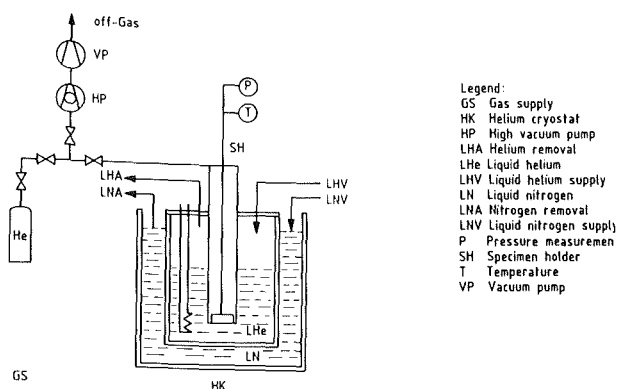
Fig.57: HELENE testing facility

The sorbent material was an activated carbon (denoted C25) supplied by Degussa. This sorbent was fixed to the specimen plate using different bonding materials. For 17 specimens of the total number of 20 the sorbent was fixed to the plate with cements and for three specimens by plasma spraying. Four different cements were used (Table 12).

Table 12: List of cements used

Cement	Manufacturer	Number of specimens
Thermoguß 2000	Klebchemie	6
Cerastil C10 or C3	Dostmann	5
Fortafix mittel	Detakta	3
Cotronics 930	Karger	3

In the course of the measurements the capacities C_A, related to the surface, and the capacities C_m, related to the mass, were determined which occurred in the following ranges:

$$20.86 > C_A(\text{mbarl/cm}^2) > 4.6, \text{ and}$$

$$330.69 > C_m(\text{mbarl/g}) > 50.5, \text{ resp.}$$

Table 13 presents a survey of the capacities measured.

To obtain more information as to which of the bonding techniques applied produced the best results, the capacities achieved (C_m and C_A, resp.) as well as the mixing ratios of both the bonding material (cement : water : copper) and of the bonding material to the sorbent (bonding material : sorbent) have been listed for all specimens investigated, grouped by the cements used and the plasma bonds applied, respectively.

The best results have been obtained with the "Thermoguß 2000" cement supplied by the Klebchemie company. The Figure 58 shows specimen prepared with this cement.
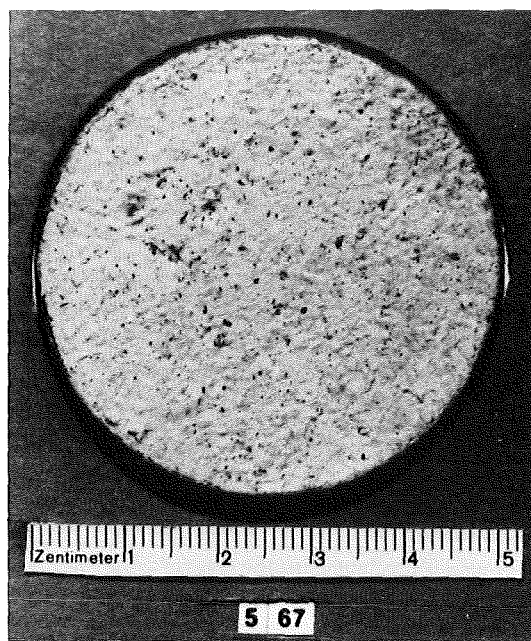
Fig.58: Sorbent test specimen no. 567.
Sorbent: activated carbon C 25, Degussa.
Bonding: adhesive Thermoguß 2000, Klebchemie.
Substrate: copper.
Helium capacity: $C_A = 20.86$ mbarl/cm^2.

Except for cementing with "Cerastil" cement supplied by Dostmann, better values have been measured of the mass related capacities on other specimens without copper powder added. It is also visible from Table 13 that these additions have neither a positive nor a negative effect on the results of measurement.

A further effect can be recognised in the comparison of the data of specimens 567 with 604 and 585 with 593 and 574 as well as 580 with 548, respectively. With approximately

Table 13: List of manufacturing and measuring data for the specimens

Specimen no.	Cement / Manufacturer and plasma bond, resp.	Mixing ratio of binding material cement : water : copper A : B : C			Mixing ratio binding material : sorbent BM : SM		C_m (mbarl/g)	C_A (mbarl/cm^2)
649	Cerastil C 10/ Dostmann	10	4	7	3,50	1	311,06	24,58
585	" C 10/ "	8	3	-	5,88	1	298,36	19,56
593	" C-3 / "	8	3	-	4,13	1	293,42	21,01
654	" C-3 / "	4	2	3	3,53	1	236,72	14,15
574	" C 10/ "	10	3	-	2,04	1	175,2	11,75
580	Cotronics 930 / Kager	25	9	-	4,59	1	299,47	19,09
630	" / "	40	26	23	6,27	1	263,32	19,21
548	" / "	5	2	-	1,99	1	219,44	13,32
558	Fortafix mittel / Detakta	1	-	-	4,89	1	310,08	25,11
681	" / "	7	1	4	4,88	1	296,11	22,40
680	" / "	7	1	4	236	1	201,05	15,56
567	Thermoguß 2000 / Klebchemie	2	1	-	5,33	1	330,69	20,86
635	" / "	40	46	43	6,81	1	314,36	20,67
607	" / "	40	46	43	5,40	1	305,62	20,06
604	" / "	2	1	-	2,83	1	281,77	17,28
616	" / "	1	1	1	3,77	1	246,26	15,50
508	" / "	1	-	-	3	1	245,14	9,94
433	Plasma bond / Memminger						~78,34	5,90
431	" / "						~50,50	4,60
432	" / "						-	15,45

identical ratios of the cement and water mixing components (Thermoguß 2000 - A : B ~ 2 : 1, Cerastil - A : B ~ 3 : 1; Cotronies - A : B ~ 3 : 1) smaller capacities C are obtained with the mixing ratios between the bonding material and the sorbent (BM : SM) becoming smaller. This result indicates an influence of the sorbent enclosing bonding paste.

Manufacturing of the three plasma sprayed specimens has not been reproducible. Due to the manufacturing process it was not possible to determine the mass of the sorbent applied on all specimens.

Staff:
H. Haas
J. Hanauer
W. Höhn
B. Kammerer
U. Kirchhof
H. Lukitsch
A. Mack
D. Perinić
D. Zimmerlin

Characterization of the adsorber

In the course of acceptance testing with the OMNISORP pore size analyser supplied by the Omicron Technology Corporation the results of measurement were confirmed which had been obtained on behalf of KfK at the Erlangen university in a similar facility. The specimens involved were activated carbon specimens (denoted C-25 and AS 16-450, resp. supplied by Degussa).

TITAN testing facility

The TITAN facility presently undergoes acceptance testing. Pressure testing of the cryopump pressure vessel designed for a maximum overpressure in operation of 10 bar to withstand potential hydrogen explosions was performed by the German Technical Inspectorate (TÜV) at 13 bar pressure without giving rise to complaints. Functioning testing is underway.

TPV 1 Development of solid particle separators for plasma exhaust

Solid particles generated during plasma/wall interaction can be transported into the plasma exhaust pumping system where they can influence the operation of the vacuum components (valves, pumps). The objectives of the task are to investigate the transport of solid particles during normal operation and during accidents and to develop solid particles separators for installation in front of the plasma exhaust pumping system.

This task was included in the Fusion Technology Programme in January 1989.

Work programme

During the first phase of the test programme it is envisaged to verify in experiments the possibility of modifying similarity laws governing particle transport at ambient pressure by the effects occurring with increasing rarefaction of the gas [1], [2]. Considering the similarity of gas flows, a model equipment will be conceived on a 1:15 scale which simulates the horizontal section of the exhaust line between the torus and the plasma exhaust pumping system of NET.

It is planned to study the transport of solid particles at gas pressures between 10^{-3} and 1 mbar and under steady-state flow conditions.

In the second phase of the test programme the transport will be studied of solid particles plated out during a sudden pressure rise accident (rupture of a water coolant pipe or of a window). The target will be to determine experimentally the maximum horizontal transport path of the solid particles as a function of their grain size along a horizontal flow channel in simulated accidents of the type described before.

The lower range of grain sizes of 1 μm which is proposed for the studies has been chosen on the basis of measurements performed by JET [3]. The upper grain size will initially be limited to 1 mm.

During the last phase of the work programme a concept of solid particle separation in NET will be elaborated. In cooperation with industry a particle separator will be developed and tested.

First results

As no metering equipment for solid particles at low gas pressures is available on the market, a suitable metering instrument must be developed for that purpose. The RBG 1000 metering equipment of the PALAS company, suitable for operation with dispersing gas, was tested at an air pressure of 10^{-3} to 10^{-4} mbar with lime particles between 10 and 20 μm in size during short-term operation of up to 24 minutes at the maximum. Also in the absence of the dispersing medium this instrument is capable of generating a particle stream (Fig. 59). The equipment will have to be

modified to adapt it to our application while the principle of operation, namely mechanical brushing of a slightly precompressed column of prefabricated solid particles, will be
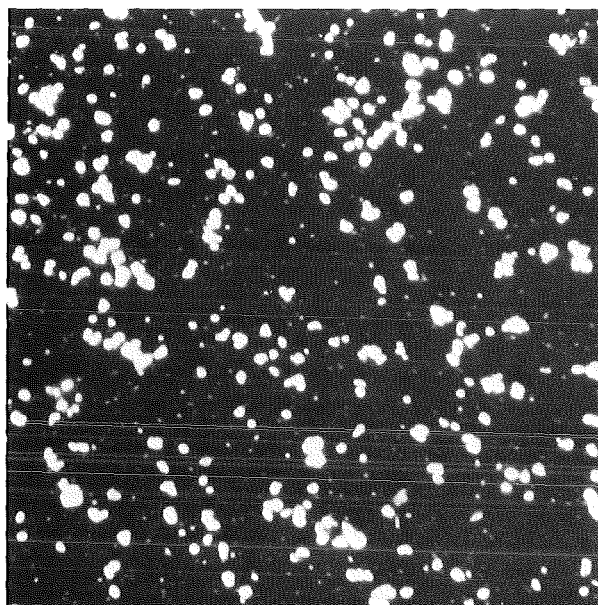
Fig. 59:   Lime particles of 10 to 20 μm grain size, metered onto a horizontal support at 10^{-3} mbar air pressure.

In a first provisional test particle transport was studied while gas was supplied into the vacuum. A multi-layered bed of lime particles, 10 to 20 μm grain size, was placed into a horizontal straight pipe of circular cross-section (150 mm inner diameter, 300 mm length) which was attached as a nozzle to a tank of about 500 l volume. After evacuation of the tank to 4 x 10^{-3} mbar air pressure an air stream was supplied to the pipe at ~ 2300 mbarl/s. Removal of the solid particles was observed. The finely dispersed particles plated out over a wide area.

Staff:
W. Höhn
B. Kammerer
M. Lieberknecht
D. Perinić

References
[1]   R.A. Millikan
       The general law of fall at a small spherical body through a gas, and its bearing upon the nature of molecular reflection from surface
       Physical Review, Vol. 22, Second Series July-Dec. 1923.
[2]   M. Knudsen
       Die Gesetze der Molekularströmung und der inneren Reibungsströmung der Gase durch Röhren
       Annalen der Physik 4. Folge Band 28, 1909.
[3]   J. Charuau, H., Djerassi
       First experiment on erosion dust measurement in a tokamak
       Paper presented at 15th Soft in Utrecht 1988.

T 10 A   **Plasma Exhaust Purification by Means of Cryosorption on Molecular-Sieves or Alternative Adsorbents**

The fuel cycle of a fusion reactor requires simple processes for the removal of impurities from gaseous streams such as the plasma exhaust gas, the solid blanket coolant, the blanket purge gas etc. One such process is cryoadsorption on molecular sieves or activated charcoal. To evaluate these alternatives quantitative information is needed on the adsorption of typical fusion fuel cycle impurities from gaseous mixtures present in a hydrogen or a helium carrier gas.

For the analysis of the gaseous species a tritium compatible gas chromatograph designed to analyse hydrogen isotopes as well as impurities such as CO, O_2, N_2, CO_2, etc. is presently being tested. The gaseous mixture is splitted into two streams. The first stream is sent through a Porapak column at - 80°C with He as a carrier gas to separate the hydrogen isotopes from the other impurities. The hydrogen isotopes are analysed with a catharometer employing an alumina column, covered with an Fe layer, and kept at -196°C. Next, the impurities are separated on the Porapak column at higher temperatures and analysed with a highly sensitive helium detector. The second stream is sent through a molecular sieve column with nitrogen as carrier gas. After the separation of helium , the sum of the hydrogen isotopes and the impurities, the gases are analysed with a TCD. With the aim of reducing the gas chromatographic retention times of the hydrogen isotopes several copper columns of different dimensions have been compared. Best results were obtained with a 3800 mm long copper column having a diameter of 3 mm.

Presently a refrigerator/cryostat from Leybold AG, which operates in the temperature range 55 - 723 K is being installed in a glove box. Two copper adsorption chambers, both gold plated on the inside, are available: one for the investigation of loose adsorbent and the other to study adsorption on a bonded matrix. The leak rates of the chambers measured with helium are lower than 10^{-8} mb·ℓs^{-1}. First test runs indicate that the temperature can be held constant to +0.3 K over a period of at least 13 hours. The time required to cool the reaction chamber from room temperature down to 77 K is 190 min.

Staff:
H.E. Noppel
R.-D. Penzhorn

T 10 C   Plasma Exhaust Gas Purification by Use of Hot Metal Getters

1.   Objectives

Main objective is the investigation of the applicability of getter materials for gas purification processes in tritium technology. Getters can be used to recover chemically bound hydrogen isotopes by decomposition of hydrocarbons and water and to remove impurities like N_2, CO, and CO_2 from a He gas stream.

The main program steps are:

A.   Inactive tests with various getter metals and alloys (e.g. Zr-Al, Ti-V-Mn) to study sorption speeds, retention capacities and cracking capabilities as a function of temperature, flow rate, and presorption.

B.   Active tests with tritium and tritiated compounds to study the influence of β-radioactivity on the kinetics of the gettering and cracking processes.

2.   Experiments

As hydrocarbons are expected to be the most significant impurities in the plasma exhaust gas the first test series at the PEGASUS facility was carried out to study cracking and gettering effects for CH_4. Table 14 summarizes the main experimental parameters: the types of getters investigated, applied temperatures, initial and final concentrations of CH_4, times of gas circulation through the getter, and two parameters (f and $T_{\frac{1}{2}}$) derived from the results which are discussed in the next paragraph.

The carrier gas was helium in all cases; it was circulated in a closed loop with a volume of 16.1 ltrs. The usual flow rate was 1.0 ltrs/min (exept for test PV-2d) and the pressure at the getter inlet was either 1100 or 1200 mbar. A GC was used to measure the CH_4 concentration at time intervals of 10 to 20 min at the inlet and the outlet of the getter.

3.   Results

As an example, the CH_4 concentration versus time is shown in Figure 60 for different temperatures of the getter. The decrease was found to be logarithmic so that the time dependence can be described by

$$c(t) = c_0 \cdot e^{-kt}$$

with k as a temperature dependent reaction constant of the getter for a given gas component (here CH_4).

$$T_{\frac{1}{2}} = \frac{\ln 2}{k} \quad \text{and } f = c_{out}/c_{in}$$

where $T_{\frac{1}{2}}$ is the half-period for the concentration decrease in the loop and f the ratio of the outlet/inlet concentration at the getter. The numerical values of both parameters decrease with increasing temperature of the getter, see Table 1.

First results on the influence of the flow rate on the sorption speed can be derived from tests PV-2c and PV-2d: At a flow rate of 0.5 ltr/min, the purification effect was higher (smaller value of f) because of the longer residence time of a given gas volume in the getter than at a flow rate of 1.0 ltr/min. On the other hand, the concentration in the loop was found to

Table 14:   Experimental Parameters of the Getter Tests with CH_4

Test-No	Getter	T (°C)	c_0 (%)	c_e (%)	t_c (min)	f	$T_{\frac{1}{2}}$(min)
PV-2a	ST-707[a]	200	1.0	0.45	450	0.97	390
PV-2b	"	300	0.45	0.063	130	0.63	45.8
PV-2c	"	400	0.8	0.012	130	0.36	21.5
PV-2d	"	400[e]	0.6	0.055	132	0.31	38.4
PV-2e	"	600	0.5	0.014	100	0.1	19.4
PV-4	HWT[b]	400	5.0	0.115	200	0.55	37.4
PV-5	ST-101[c]	600	0.5	0.12	45	0.48	21.4
PV-8	ST-198[d]	400	0.45	0.001	300	0.7	<45.3
PV-6	"	600	0.5	0.002	110	0.26	<15.0

a) Zr-V-Fe, 700 g   b) Ti-V-Mn, 3 kg   c) Zr-Al, 700 g   d) Zr-Fe, 700 g   e) 0.5 ltr/min gas flow rate   f = c_{out}/c_{in}
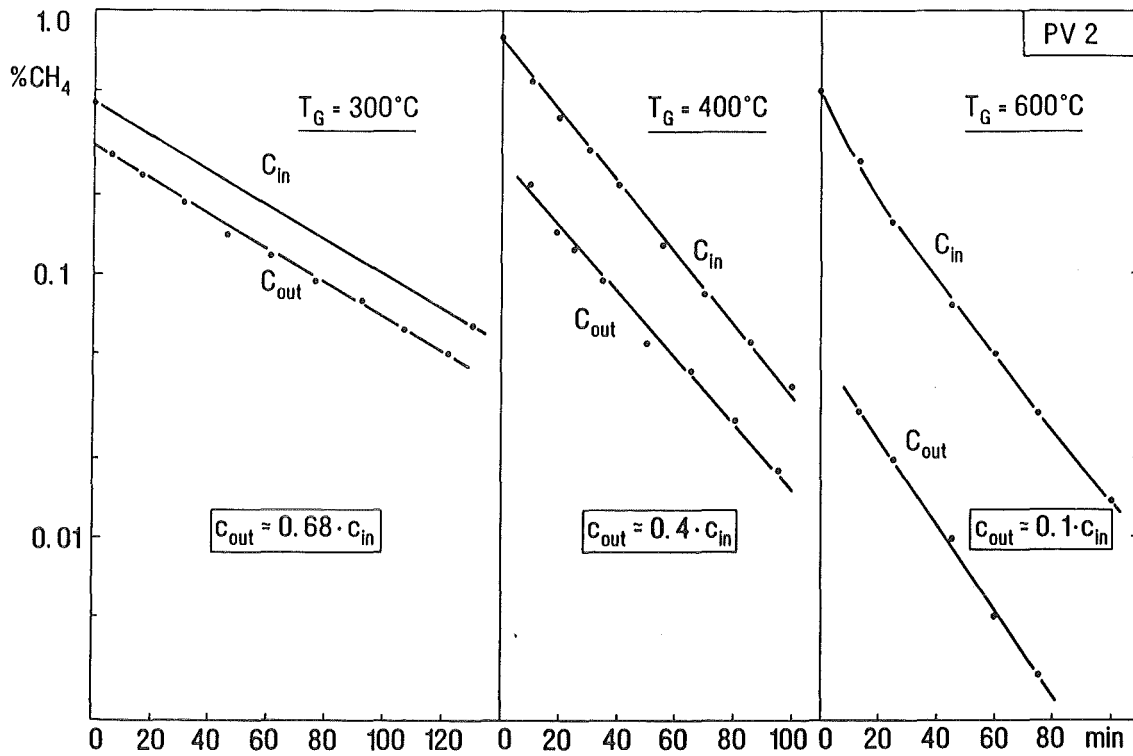
Fig. 60: Sorption of CH_4 by 700 g of Getter Material ST-707

decrease more slowly (with a longer half-period) as the gas was less frequently pumped through the getter.

In the case of the SAES getters ST-707, ST-198, and ST-101, both C and H_2 were sorbed by the getters, while 90 % of the hydrogen corresponding to the gettered CH_4 was released in the case of the HWT getter.

An additional test was performed with the result that the H_2-equilibrium pressure of the HWT getter was already 500 mb at 400 °C after an integral sorption of 3 mb · ltr per g getter material. The corresponding pressure of the SAES getters is only $< 10^{-3}$ mb. This indicates that the HWT getter is much more suitable for the recovery of tritium from tritiated methane than the three investigated SAES getters. For the latter, heating up to 500 - 800 °C is required to pump-off the hydrogen isotopes.

Staff:
H. Albrecht
W. Asel
U. Kuhnes
K. Schuster

T 10 E   Adsorption of DT on Heated Metal Beds other than Uranium

Certain metals and metal alloys, which form tritides according to the reaction

$$M(s) + x/2 Q_2 = MQ_x(s) \quad (Q = H, D, T) \qquad (1)$$
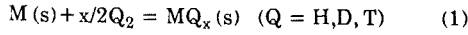
can be used to pump, store and transport tritium gas. One such getter material presently under evaluation is ZrCo. Ingots of this getter were obtained from highly pure reagents by arc melting at 1450°C. The ingot was converted into a fine powder of 0.4 [m^2/g] specific surface area by reaction with hydrogen at pressures up to 17.5 MPa and room temperatures in a 0.5 l autoclave followed by evacuation at temperatures above 500°C.

Kinetic runs at room temperature, in which hydrogen was supplied at pressures above that required to reach saturation, show that the reaction of hydrogen with ZrCo powder is fast and goes to completion ($ZrCoH_3$). As apparent from the results the rate increases with increasing p_{excess} = $((p_{H2})_0 - (p_{H2})_{sat}$ (see Table 15).

Alltogether 35 loading/deloading cycles were carried out with a single 0.01 mol ZrCo sample without observing any change in reaction rate or in maximum loading capacity. This is an indication of an unchanged matrix.

Repeated exposure of ZrCo powder to pure oxygen in steps of 13 mbar at a temperature of 275°C revealed that under these conditions a max. n_O/n_{ZrCo} ratio of 0.91 can be achieved, even when the final pressure is raised to 130 mbar. At higher temperatures, i.e. 275 < T < 310°C, a further consumption of oxygen takes place which reaches n_O/n_{ZrCo} = 2.81 when the sample is heated up to T < 645°C. These results clearly demonstrate that ZrCo powder is chemically much more stable than uranium. This observation also extends to the hydride: ZrCo powder saturated with hydrogen can be exposed to air without noticeable chemical reaction.

During the last semiannual period the effect of progressive exposure of ZrCo powder to nitrogen (550°C), oxygen (250°C) and methane (400°C) on the pc isotherms and therefore on the loading capacity was systematically investigated over a temperature range 200 - 300°C. It was found that under comparable conditions oxygen reduced the loading capacity of ZrCo least.

The reaction mechanism and the absolute rate of the reaction of gaseous hydrogen and deuterium with ZrCo powder was determined at several temperatures and constant hydrogen pressures. Evaluation of the data is in progress.

Staff:

M. Devillers
R.-D. Penzhorn
M. Sirch
E. Willin

Kinetics of hydrogen uptake by ZrCo at 25 °C.

m = 1.43 g ZrCo n_H / n_{ZrCo} = 3

$(p_{H2})_{sat}$ = 51.3 kPa $(p_{H2})_0 \gg (p_{H2})_{sat}$ $p_e \gg 0$

$(p_{H2})_0$ kPa	Time required to attain		
	$ZrCoH_{1.5}$ (50%)	$ZrCoH_{2.7}$ (90%)	$ZrCoH_{2.97}$ (99%)
99.4	3.0	30	240
99.4	3.0	25	220
86.7	3.2	36	–
77.3	3.2	37	390
66.7	3.6	35	–
66.7	3.6	35	–
55.3	4.0	37	360
51.3	4.5	49	–
	3 – 4 s	25 – 40 s	3 – 6 min

Table 15

T 10 H   Catalyst Development for the Exhaust Purification Process

In previous work - mostly carried out in a closed loop - it was shown that tritiated hydrocarbons can be decomposed catalytically into the elements on a nickel catalyst operated at < 550°C. This reaction, which under appropriate conditions proceeds up to thermodynamic equilibrium, constitutes a basic reaction step of a fuel clean-up process presently under development for NET.

To study the reaction mechanism under a variety of experimental conditions, the decomposition of methane was investigated in a flow system. Methane was selected to represent all other hydrocarbons because of its particularly high chemical stability. In most runs a He/CH_4 gas mixture with approx. NET I flow rates (v_{He} = 0.57 and v_{CH4} = 0.072 l/min) was passed over as-received Ni catalyst mixed with SS 3x3 mm helixes. Al species in the gas influent from the catalytic reactor were analysed qualitatively (H_2O) and quantitatively (CO, CO_2 and CH_4) by in-line Fourier transform infrared spectroscopy and by gas chromatography.

The results of the experiments, summarized in Table 16, allow the following conclusions:

i) As-received Ni catalyst (NiO on Al_2O_3) can be activated by reaction with hydrogen (product: H_2O) as well as by reaction with methane (products: H_2O, CO and CO_2) at 550°C. The reactivity of the catalyst does not depend upon the selected method of activation.

ii) (0.34 ± 0.08) mol_{CH4}/g catalyst can be decomposed on a nickel catalyst at < 550°C, without any regeneration step.

iii) A constant overall rate of (0.0015 ± 0.0001) mol_{CH4}/min was found for the decomposition of methane, when v_{He} = 0.57 l/min and v_{CH4} = 0.072 l/min were passed over 5.5 g Ni catalyst at a conversion of (44.7 ± 7) % up to at least 34% of the max. attainable CH_4 decomposition, i.e. 0.34 ± 0.08 mol_{CH4}/g cat.

iv) When carbon dioxide (v_{CO2} = 0.073 l/min) was passed over 0.50 g of exhausted Ni catalyst carbon monoxide was produced according to the reaction

$$Ni\,(C) + CO_2 = Ni + 2\,CO. \qquad (1)$$
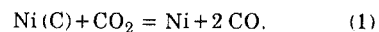
Table 16:   Decomposition of methan on a nickel catalyst at < 550°C.
V_{He} = 0.57 l/m V_{CH4} = 0.072 l/min

m_{cat} [g]	m_{helix} [g]	conv. [%]	t [min]	tot.CH_4 decomp. [mol]	mol_{CH4} g_{cat}	- r_{CH4} [mol/min]	f*
5.51	27.00	47.8	95	0.164	0.030	1.72 E-3	0.080
5.51	27.01	50.0	120	0.180	0.033	1.50 E-3	0.088
5.50	27.00	54.2	130	0.191	0.035	1.47 E-3	0.093
5.50	27.00	49.3	140	0.189	0.034	1.30 E-3	0.092
5.50	27.01	45.2	290	0.301	0.055	1.00 E-3	0.147
5.52	26.98	42.2	428	0.602	0.109	1.40 E-3	0.292
5.53	27.04	44.1	360	0.590	0.108	1.60 E-3	0.286
5.53	32.39	43.7	340	0.574	0.104	1.69 E-3	0.278
5.53	26.99	41.3	470	0.697	0.126	1.48 E-3	0.338

* f = (- $\triangle CH_4$) $_{t=t}$ / (- $\triangle CH_4$) $_{t=\infty}$

Under these conditions the catalyst is regenerated up to about 42 - 46 % (result of 2 experiments) of its original reactivity. After decomposing methane on the catalyst up to exhaustion a second time 7 - 12 % of the original reactivity can be recovered by passing CO_2 over the catalyst.

Staff:
U. Engelmann
M. Glugla
Chr. Nolte
R.-D. Penzhorn
R. Rodriguez
M. Tank

Development of ECRH Power Sources

The KfK gyrotron experiment has been continued with the test operation of a new 140 GHz modular gyrotron. The electron gun was redesigned, the outpuf rf-window became variable. The distance between the two window discs can be changed during operation to obtain the optimum transmission for the individual modes.

The 140 GHz resonator used in this experiment had a center part of 10 mm length and 3,47 mm radius; the input taper was 18,9 mm long with a 1 ° slope, the output taper was 10,1 mm in length with a 3 ° slope.

The beam position within the resonator was centered with the help of the superconducting beam steering magnets and monitored during the measurements by the body-current observation . The body-current, i. e. the spilled electron current which does not hit the collector, was thereby minimized to < 40 mA at a beam current of 14 A.

The short pulse, low average power calorimeter was used for rf-power measurements as for the previous 150 GHz experiments. The calibration of this calorimeter changed during the test period, and was carefully controlled, therefore.

The tube was assembled and integrally heat treated at 460 °C in the inertial gas furnace. The formation of the cathode was done during the heat treatment.

The experimental programme was carried out in pulsed operation, mainly with 0,5 msec pulselength and 0,5 Hz repetition rate. During the test series the pulse length was increased up to 14 msec without significant changes in the results.

In agreement with the calculations the following oscillation frequencies were found:

$$TE_{231} \quad 137,61 \text{ GHz}$$

$$TE_{031} \quad 140,37 \text{ GHz}$$

$$TE_{521} \quad 145,15 \text{ GHz}$$

For window optimization, the distance between the ceramic discs was changed between 3 and 5 mm. The maximum rf power for the TE_{031}-mode was found at a distance of 3,75 ±0,055 mm. A typical transmission curve is shown in Fig.61:

The parameter optimisation started by changing the modulation voltage for given beam current and magnetic field. At the end of this procedure the optimum magnetic field, beam voltage and modulation voltage for that current gave the maximum rf power and efficiency. The results are given in Fig. 62 as a function of beam current. A maximum rf output power of 214 kW at 12 A beam current gave an overall efficiency of 25 %.
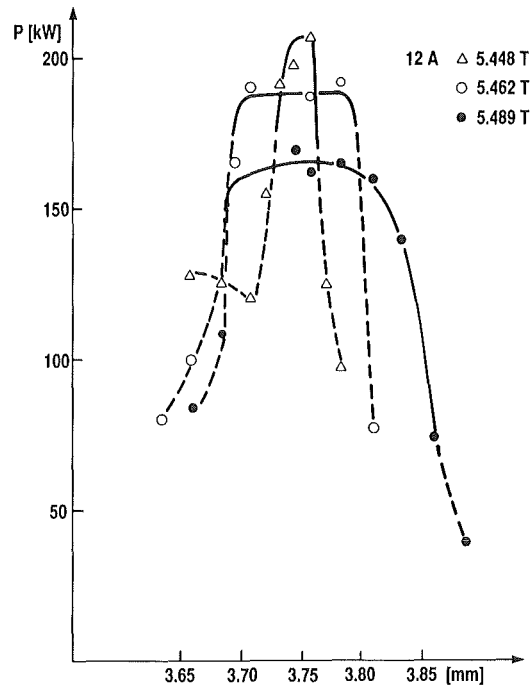
Fig. 61: Influence of the window variation on the transmission of the 140 GHz gyrotron.The tube is operated in TE_{031}-mode at different beam parameters.
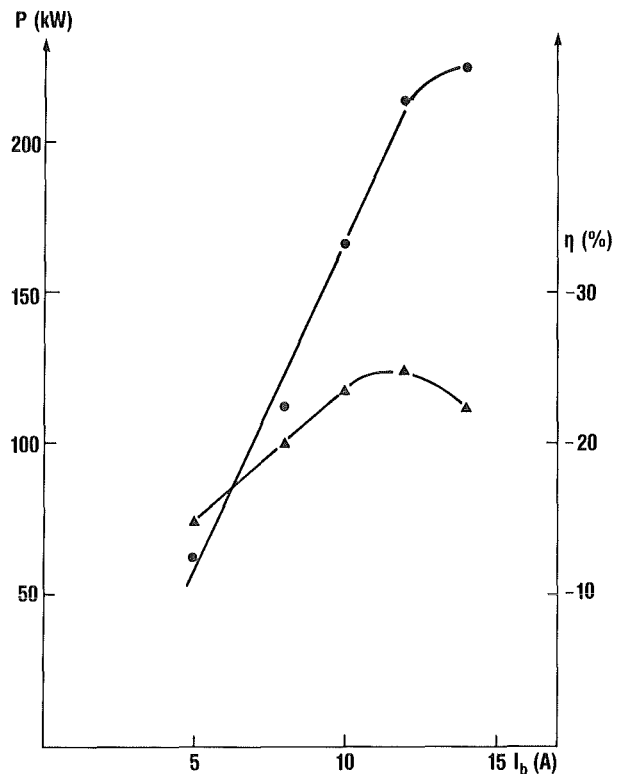
Fig. 62: Rf output power and efficiency in TE_{031}-mode as function of beam current.

The oscillation regions for the three different modes are shown in Fig. 63 as an example for I_b = 11 A and B = 5,53 T. The oscillation region for the TE_{031}-mode is clearly separated from the other modes within a broad parameter range, as can be seen from Fig. 63. A pure TE_{031}-mode is oscillating stable at optimized parameters (U_b = 71,8 kV, U_{mod} = 25,4 kV).

The short pulse operation (0,5 msec, 0,5 Hz) was followed by single pulse operation with up to 14 ms duration. The obtainable maximum rf power and efficiency did not change. The TE_{031}-mode oscillation was stable during a long pulse, but the frequency increased slightly up to 8 MHz for 14 msec pulse length due to heating of the resonator walls. Finally the resonator was overheated by increasing the repetition rate of the long pulses. The result was a permanent frequency change of 0,6 GHz in each mode and a change in oscillation properties. The parameter optimisation was repeated after the change in frequency. But the achievable output power was only half that obtained before the frequency change. The experimental programme was terminated, and the gyrotron tube was disassembled. In agreement with the above results the diameter of the resonator had changed to smaller values (-0,04... -0,05mm).

In the mean time a modified resonator was fabricated. It was carefully measured mechanically and was assembled in the tube again. The heat treatment was completed and the experimental programme was restarted.

The prototype gyrotron is in final assembly and almost ready for heat treatment. This integrally brazed tube intended for operation at the W 7 AS stellarator incorporates the advanced components pretested in the modular gyrotron. The superconducting magnet system has been finally tested and adjusted.

Theoretical work considered the influence of deviation of the operating parameters from the design values. In particular the efficiency calculations were repeated by approximating the beam parameters used for the actual operation. Complementary some investigations of the effect of deformation of the resonator geometry due to thermal stresses or manufacturing tolerances were performed. Design work for a whispering gallery mode gyrotron is going on.

Staff:
W. Baumgärnter
E. Borie
H. Budig
G. Dammertz
O Dumbrais
U. Feißt
G. Gantenbein (from 01.10.88)
T. Geist
P. Grundel
R. Hietschold (to 31.12.88)
G. Hochschild
A. Hornung
M. Kuntze
R. Lehm
N. Münch
H.U. Nickel (from 01.02.89)
H. Oppermann
B. Piosczyk
G. Redemann
R. Vincon
H. Wenzelburger
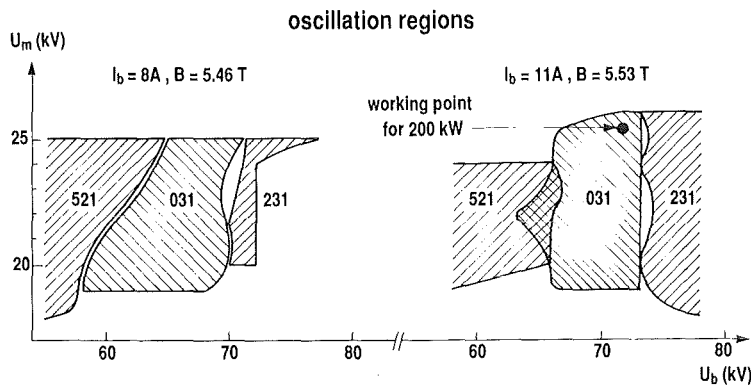
Fig. 63: Beam parameter regions for TE_{231}-, TE_{031}- and TE_{521}-mode oscillations.

NET Study Contracts

Investigation on the Vacuum and Exhaust Performance of NET

Version 1 of the the DWELLMAP-Code was implemented and tested by the NET team. It includes the plasma-wall interaction in a first simple approach. The program calculates the time dependence of key process values in four subsequent modules from burntime to dwell time pumping. At the beginning, the equilibrium conditions within the core plasma, the scape-off layer and the near-surface material layer are generated.

The results allow the determination of the exhaust performance and considerations about the amount of parasitic fuel inventory. Figure 64 shows as example the
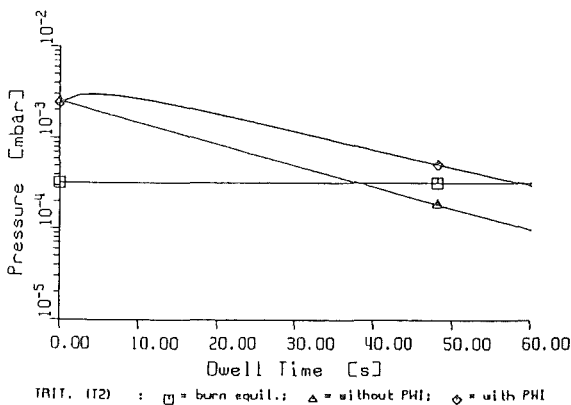
Fig. 64: Tritium pressure within the plasma chamber during the dwell time

time dependence of the tritium pressure within the plasma chamber with and without plasma-wall interaction during the dwell time. (Input: Test data, oriented on NET parameter).

Staff:
R.A. Müller

Study on NET TF Pancake Tests

The necessity of a test facility for prototype conductor testing was approved by the FTSC in Nov. 88. The task was assigned to KfK Karlsruhe by upgrading of the existing TOSKA facility.

A draft of the report about the investigations of a "TWIN" test configurations was presented to the NET-team Febr. 2, 89. The report is being open for discussion till end of February. It was agreed to start with the 1.8 K upgrading of the TOSKA facility and the EURATOM-LCT coil for the 1.8 K test. A first contract was placed for the extension of the

1.8 K subatmoshperic circuit for the TOSKA facility. The arrangement of test pancakes will be discussed and decided as soon as NET conductor concepts will have the maturaty for prototype production.

Staff:
A. Grünhagen
R. Heller
W. Herz
K.Jentzsch
H. Kapulla
B. Kneifel
W. Maurer
A. Ulbricht
A. Vogt
G. Zahn

CAD Data Exchange between NET and KfK

The design of NET is to a large degree done by means of computer aided design (CAD) systems. Since NET and KfK use dissimilar CAD systems a neutral CAD data exchange interface IGES (Initial Graphics Exchange Specification) is used for exchange of NET drawing data. Both the NET CAD system MEDUSA and the KfK CAD system BRAVO3 have IGES pre- and postprocessors which write and read the IGES file. However the IGES specification is rather ambiguous and the IGES processors are not bug free. It was the objective of the contract to improve the data exchange via IGES between NET and KfK.

The project was finished in September 1988. The final reportwas submitted to the NET team in December 1988. In the meantime the methods and tools developed were completely taken into production use. While the optimized setting of processor parameters allows to process about 90% of the NET drawings. In order to cope with the remaining 10% a new software (MODIGS) has been developed. Experience during the last few months shows, that there remain still some errors in a few IGES files which are not been taken care of by the current implementation of the MODIGS system. To overcome this problem two alternatives are currently being evaluated:

Enhancement of MODIGS to detect and remove those errors.

Purchase of a commercial product for IGES syntax analysis. This product could be used to detect the erroneous entities in the file which would subsequently be removed by the current version of MODIGS.

Independent of that evaluation the user interface and the file handling of MODIGS are currently being revised.

Staff:
U. Gengenbach
A. Ludwig

Design of a Catalytic Plasma Exhaust Gas Clean-up Facility for NET

Present efforts have concentrated on the development of basic flow sheets as well as chemical flow sheets for a NET II plasma exhaust clean-up facility based on several catalytic and permeation steps and capable of coping with the following process streams:

i)	burn and dwell (mode I: 1 mbar back-pressure)
ii)	burn and dwell (mode II: 10 mbar back-pressure)
iii)	glow discharge/deuterium
iv)	glow discharge/helium
v)	air pump down (recovery)
iv)	air pump down (freeze out)
vii)	He pump down (recovery)
viii)	He pump down (freeze out)
ix)	bake out mode

Two permeators, one to recover highly pure hydrogen isotopes (Purity < 99.9999 %) from the plasma exhaust and the other to recover hydrogen isotopes obtained from the cracking of hydrocarbons or the water gas shift reaction, are used. Extensive experiments have shown that at temperatures above 300°C palladium/silver permeators are neither poisoned by any of the potential impurities present in the plasma exhaust gas (CO_2, CO, air, CH_4 or NH_3) nor the gases used as reactants with high partial pressure (CO, CO_2). From model calculations, verified by experiments with a technical permeator having a total permeation area of 0.12 m^2 and coupled to a 500 l/s turbomolecular pumping system, it is concluded that for the processing of 20 mol/h hydrogen isotopes (NET I) with an efficiency of 99.85 % a permeation area of at least 0.35 m^2 is required. For the processing of the off-gas from carbonization or from glow discharge operation of NET I about three times as much permeation area is necessary. In the case of NET II the permeation area is determined by the burn and dwell mode and calculated to be 1.2 m^2. First estimates indicate that an oil-free pump with a capacity of the order of 600 [m^3/h] will be required at the secondary side of the main permeator of NET II (70 mol/l hydrogen isotopes).

Design calculations have been carried out for a system consisting of 10 kg Ni catalyst placed inside either a 10 or a 20 l reactor, integrated into a loop comprising a permeatur and a buffer vessel. The results show that while a large r = reactor volume/buffer volume ratio improves the overall efficiency of the catalytic loop, an increase in catalyst reactor volume is associated with a departure from plug flow behaviour and therefore with an efficiency decrease of the catalytic step.

Staff:
M. Glugla
R.D. Penzhorn
R. Rodriguez
D. Herbrechter (KAH)

NET Blanket Handling Device

Mechanical Design

Within the frame of the NET contract 282/87-10FU D NET, NET Blanket Handling Device, KfK has finished the investigation of handling concepts for blanket segments resulting in a preliminary specification and pre-design of the required equipment. The draft of the final report was finished.

The pre-design of the blanket handling device (BHD) is described in the last semi-annual report. In order to reduce the required height of the BHD two alternative options to the reference concept were investigated. Both are based on the component withdrawal in two steps instead of one. In one case the blanket segment will be withdrawn by the main lifting device until it is free from the other installed segments. Then it will be taken over by a lifting device which is integrated into the component transport flask. (Figure 65)

In the other case the segment will be taken over by an auxiliary lifting device and after further lifting it will be transferred into the transport flask (Fig. 66).

Control System

The Blanket Handling Device has to be controlled fully remotely via the general purpose NET Remote Workstation as the only interface between the operator and the device. This workstation serves as intelligent tool to support the operator in planning, executing, and monitoring the maintenance process. To cope with the restricted observability of the blanket replacement a geometric simulation system, as integral part of the NRWS, plays a central role for systems state presentation, whereby actualisation of the model is contolled by various sensors. The motion control and the control of supporting devices is done by the BRD-section/motion controller. A central feature of this controller is its problem-suited interface to the superordinated NRWS. Through this interface the NRWS and the operator have complete access to all functions and states of the section controller and the controlled process. The NET remote workstation and the BRD-section/motion controller are components of the Supervisory Control System proposed in /1/ for NET
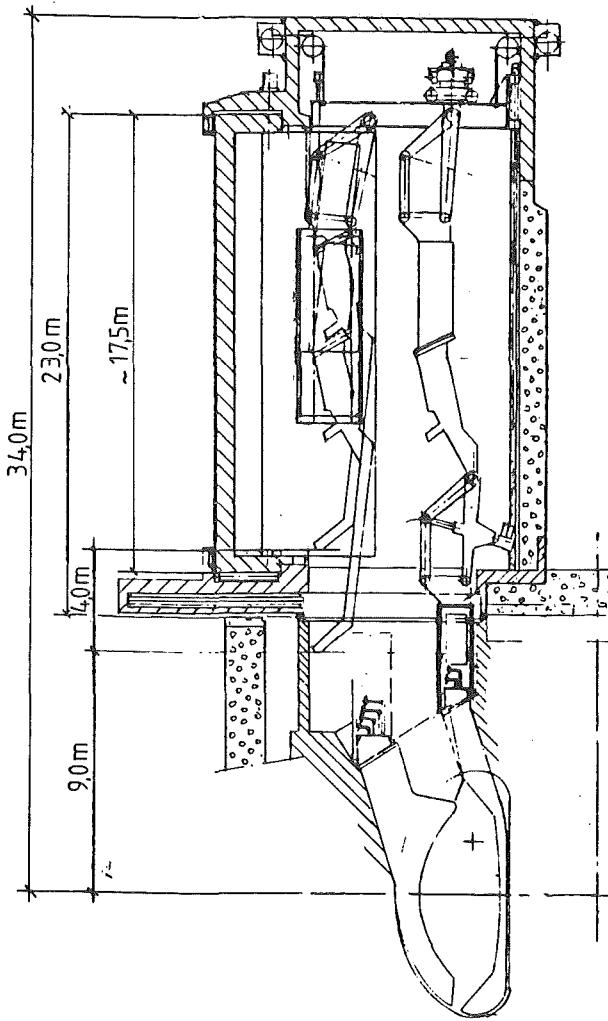
Fig. 65: BHD-Alternative
Option: Auxiliary lifting device integrated into the
transport flask
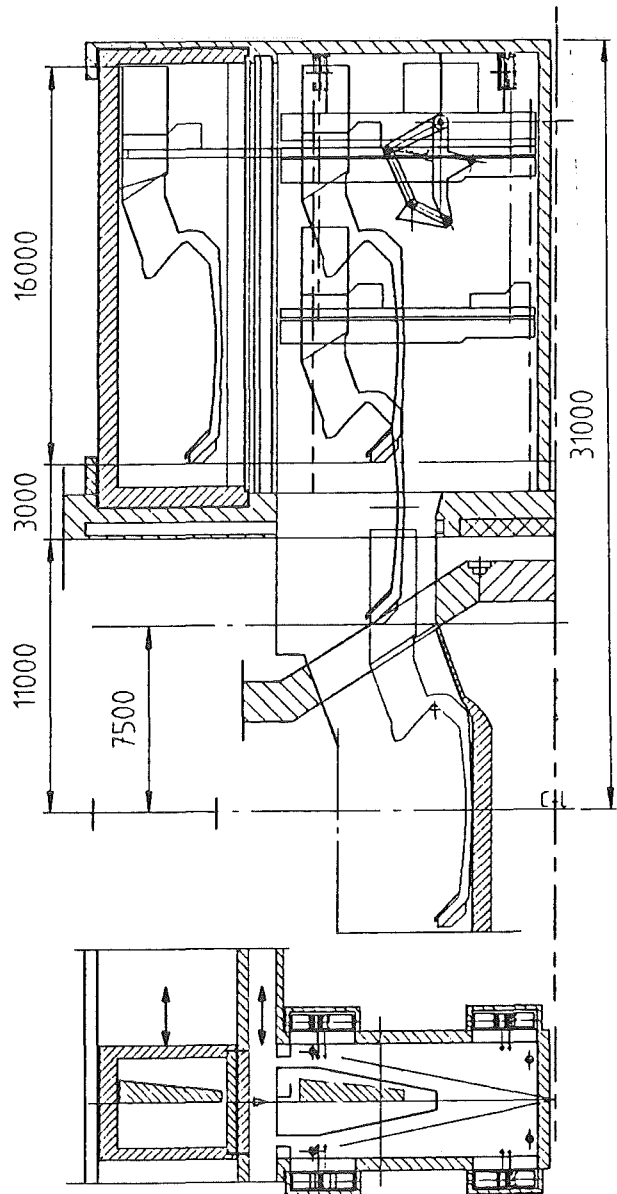
References:

Leinemann, K.: Supervisory Control System for NET:
Remote Handling Workstation, Motion Controller, Central
Utilities. unpublished report of KfK, November 1988.

Staff:
B. Haferkamp
W.E. Hörl
Hübener
I. Kornelson
K. Leinemann
W. Link
E.G. Schlechtendahl
A. Suppan

Fig. 66: BHD-Alternative
Option: Auxiliary lifting device integrated into the
tcontained transfer unit

Electrical Connectors for Remote Handling

Work has been started with the review of the NET-report
201/85. In reviewing the report it was recognized that
additional information on remotely operated connectors can
be obtained from the design work carried out for fission
projects, from results of experimental work at KfK and from
extensive inquires on fusion-related experiments.

With the additional information it will be possible to produce
the first data sheet for standard types in the 2nd quarter of
1989.

Even more information is necessary on the following items:
-    gas tight feedthroughs

- combinations of feedthroughs and electrical connectors
- connectors for control signals via fibre optics (LWL-connectors)
- multi-mix lock systems for a combination of connectors in one casing.

In parallel efforts have been put into the investigation of the different types of the screw-version of connectors. This type shows a high potential for further applications and it can be adapted to the remote handling equipment and to the NET environmental conditions.

Staff:
M. Selig

Appendix I: Table of Fusion Technology Contracts

Task Code No.	Title	KfK Departments
B1	Blanket Design Studies	IMF III, INR, IRB, IT
B 2	Development of Computational Tools for Neutronics	INR
B6	Corrosion of Structural Materials in Flowing Pb-17Li	IMF I, IMF II
B 6.3	Fatigue of Structural Material in Pb-17Li	IMF I, IMF II
B9	Tritium Extraction from Liquid Pb-17Li by the Use of Solid Getters	IT
B 11-16	Development of Ceramic Breeder Materials	IMF I, IMF III, INR, IRCH
B 15.3	End of Life of Solid Breeding Materials in Fast Neutron Flux	IMF I, IMF III, INR
M1	The Large Coil Task	ITP
M 3	Development of High Field Composite Conductors	ITP
M 4	Superconducting Poloidal Field Coil Development	ITP
M 8	Design and Construction of a Poloidal Field Coil for TORE SUPRA as NET-Prototype Coil	ITP
M 9	Structural Materials Fatigue Characterization at 4 K	ITP
M 12	Low Electrical Conductivity Structures Development	IMF IV, ITP
MAT 1.6	Development and Qualification of MANET 1	IMF II
MAT 1.9	Pre- and Post-Irradiation Fatigue Properties of 1.4914 Martensitic Steel	IMF II
MAT 1.11	Post-Irradiation Fracture Toughness of Type 1.4914 Martensitic Steel	IMF II
MAT 2.2	In-Pile Creep-Fatigue Testing of Type 316 and 1.4914 Steels	IMF II, IMF III
MAT 6/ MAT 13	Ceramics for First-Wall Protection and for RF Windows	IMF I
MAT 9.2	Investigation of Fatigue Under Dual Beam Irradiation	IMF II
MAT 18	Development of Low Activation Ferritic-Martensitic Steels	IMF II
N1	Design Study of Plasma Facing Components	INR, IRB, IRE
N2	Shield Design Studies	IMF III
N3	Development of Procedures and Tools for Structural Design Evaluation	IMF IV
N5	Development of Theory and Tools for Evaluation of Magnetic Field Effects on Liquid-Metal Breeder Blankets	IRB

N6	Studies of Pebble Beds of Ceramic Compounds	INR
RM1	Background Studies on Remote Maintenance	IT
RM2	Mechanical Components Assembly	IT
RM 3	Handling Equipment for In-Vessel Components	IDT, IRE, IT
S + E 4.1.2	Safety Aspects of the Cryosystem	IRE
S + E 4.1.3	Safety Aspects of Superconducting Magnets	IDT, IRE, ITP
S + E 5.4	Overall Plant Accident Scenarios for NET	IRE
S + E 5.5	Development of Safety Guidelines for the Design of NET	IRE
S + E 7	Generic Environmental Impact Assesssment for a Fusion Facility	INR, IMK
T 6	Industrial Development of Large Components for Plasma Exhaust Pumping	IT
T 7	Optimization of Cryogenic Vacuum Pumping of Helium	IT
TPV 1	Development of Solid Particle Separators for Plasma Exhaust	IT
T 10 A	Plasma Exhaust Purification by Means of Cyrosorption on Molecular-Sieves or Alternative Adsorbents	IRCH
T 10 C	Plasma Exhaust Gas Purification by Use of Hot-Metal Getters	IRCH
T 10 E	Adsorption of DT on Heated Metal Beds other than Uranium	IRCH
T 10 H	Catalyst Development for the Exhaust Purification Process	IRCH

Development of ECRH Power Sources (This task is part of the Fusion Physics Programme of the EC.)	IDT, ITP

Appendix II: Table of NET Contracts

Theme	Contract No.	Working Period	
Investigation of the Vacuum and Exhaust Performation of NET	254/86-11/FU-D/NET	10/86 -	12/87
Study about the NET TF Pancake Test	240/86-6 FU-D/NET	05/86 -	04/88
CAD Data Exchange between NET and KfK	265/87-3/FU-D/NET	03/87 -	09/88
Design of a Catalytic Plasma Exhaust Gas Clean-up Facility for NET	322/88-8/FU-D/NET	10/88 -	10/89
NET Blanket Handling Device	282/87-10/FU-D/NET	11/87 -	10/88
Electrical Connectors for Remote Handling	313/88-7 FU-D/NET	09/88 -	05/89

Appendix III: KfK Departments contributing to the Fusion Project

Kernforschungszentrum Karlsruhe GmbH Telephone (07247) 82-1
Postfach 3640   Telex 7 826 484
D-7500 Karlsruhe 1   Telefax/Telecopies (0) 07247/825070
Federal Republic of Germany

KfK Department	KfK Institut/Abteilung	Director	Ext.
Institute for Data Processing in Technology	Institut für Datenverarbeitung in der Technik (IDT)	Prof. Dr. H. Trauboth	5700
Institute for Materials and Solid State Research	Institut für Material- und Festkörperforschung (IMF)	I. Prof. Dr. K.-H. Zum Gahr II. Dr. K. Anderko III. Prof. Dr. K. Kummerer IV. Prof. Dr. D. Munz	3897 2902 2518 4815
Institute for Neutron Physics and Reaktor Engineering	Institut für Neutronenphysik und Reaktortechnik (INR)	Prof. Dr. G. Keßler	2440
Institute for Reactor Components	Institut für Reaktorbau-elemente (IRB)	Prof. Dr. U. Müller	3450
Institute for Radiochemistry	Institut für Radiochemie (IRCH)	Prof. Dr. H.J. Ache	3200
Institute for Reactor Development	Institut für Reaktor-entwicklung (IRE)	Prof. Dr. D. Smidt	2550
Central Engineering Department	Hauptabteilung Ingenieur-technik (IT)	Dr. H. Rininsland	3000
Institute for Technical Physics	Institut für Technische Physik (ITP)	Prof. Dr. P. Komarek	3500
Institute for Meteorology and Climate Research	Institut für Meteorologie und Klimaforschung	Prof. Dr. F. Fiedler	2093

Appendix IV: Fusion Project Management Staff

Project Manager
Dr. J. E. Vetter
5460

Secretariat:	Fr. I. Sickinger	5461
	Fr. I. Pleli	5466

Project Administration Documentation

BW G. Kast	5462

Studies NET Contacts

Dr. J.E. Vetter	5460

Blanket Development Test Facilities

DI H. Sebening	5464

Superconducting Magnets Gyrotron Development

Dr. J.E. Vetter	5460

Tritium Technology Structural Materials

Dr. H.D. Röhrig	5463

Safety and Environmental Impact, Remote Handling

DI A. Fiege	5465